NASA TECHNICAL NOTE

NASA TN D-2642

NASA TN D-2642

THE STATIONARY LAMINAR VELOCITY BOUNDARY LAYER WITH CONSTANT FLUID PROPERTIES AND ARBITRARY DISTRIBUTIONS OF PRESSURE AND MASS TRANSFER

by Ernst W. Adams and Benton K. Berry

George C. Marshall Space Flight Center
Huntsville, Ala.

NATIONAL AERONAUTICS AND SPACE ADMINISTRATION • WASHINGTON, D. C. • FEBRUARY 1965

THE STATIONARY LAMINAR VELOCITY BOUNDARY LAYER WITH CONSTANT FLUID PROPERTIES AND ARBITRARY DISTRIBUTIONS OF PRESSURE AND MASS TRANSFER

By Ernst W. Adams and Benton K. Berry

George C. Marshall Space Flight Center
Huntsville, Ala.

NATIONAL AERONAUTICS AND SPACE ADMINISTRATION

For sale by the Office of Technical Services, Department of Commerce,
Washington, D.C. 20230 -- Price $3.00

TABLE OF CONTENTS

LIST OF ILLUSTRATIONS

LIST OF ILLUSTRATIONS (Continued)

LIST OF TABLES

DEFINITION OF SYMBOLS

Symbol	Definition
A_n	coefficient in expansion (16)
a_n	coefficient in expansion (22)
B_n	coefficient in expansion (50)
$c_f = 2\bar{\tau}_w/\bar{\rho}\bar{u}_\infty^2$	wall friction coefficient
c_p	specific heat at constant pressure
F	auxiliary functions
$G = g(\emptyset, \psi_\alpha^*)$	boundary function defined in (31)
$g = p(\emptyset) + u^2(\emptyset, \psi)$	total pressure
H, H_o, $H_{o\alpha}$, H_I, H_{II}, $H_{II\alpha}$	regions defined in Section II and Figure 1
H_M, H_P	regions defined in Appendix D
L	reference length
M, N	auxiliary functions in Section XI
p	static pressure
Pr	Prandtl number
P_P	operator defined in (5)
P_M	operator defined in (D-7)
R	radius of circular cylinder
$Re = \bar{L}\bar{u}_\infty/\bar{\nu}$	Reynolds number

DEFINITION OF SYMBOLS (Continued)

Symbol	Definition
T	temperature
u	velocity component parallel to the wall
$u_\infty = \text{const.}$	free stream velocity
v	velocity component normal to the wall
x	arc length of the wall
x_o	boundary of the stagnation point vicinity
x_m	first maximum of $u_e(x)$ past the stagnation point
x_s	point of separation of the boundary layer
y	coordinate normal to the wall
Γ, Γ_o, $\Gamma_{o\alpha}$, Γ_I, Γ_{II}, $\Gamma_{II\alpha}$	boundaries of regions defined in Section II
Γ_M, Γ_P	boundaries of regions defined in Appendix D
φ	angle measuring on circumference, $\varphi = 0$ at stagnation point
$\varnothing = \int_o^x u_e(x)\, dx$	potential of velocity at the outer edge of the boundary layer
$\varnothing_\alpha$	see Figure 1
$\psi = \int_o^y u(x, y)\, dy$	stream function
$\psi^*_\alpha = \text{const.}$	stream line

DEFINITION OF SYMBOLS (Continued)

Symbol	Definition
$\psi^*(x)$	boundary of H_I and H_{II}, consisting of lines $\phi = \phi_\alpha$ and $\psi = \psi^*_\alpha$
μ	viscosity and transform for ϕ, equation (C-3)
$\nu = \mu/\rho$	kinematic viscosity
ρ	density
τ	shear stress
η	dummy variable for ϕ

SUPERSCRIPTS

-	indicates that the parameter possesses a physical dimension, e.g., $\bar{p}$; absence of bar denotes dimensionless parameters, e.g., p
*	refers to the line $\psi^*(x)$ separating H_I and H_{II}

SUBSCRIPTS

b	boundary value
e	outer edge of the boundary layer, $y = \infty$
i, j, n	summation index
L	lower bound
U	upper bound
w	wall

THE STATIONARY LAMINAR VELOCITY BOUNDARY LAYER WITH CONSTANT FLUID PROPERTIES AND ARBITRARY DISTRIBUTIONS OF PRESSURE AND MASS TRANSFER

SUMMARY

Along sections of stream lines $\psi = \psi^*_\alpha(x, y)$, series expansions representing an inner solution ($0 < y \leqq y^*$) are matched with a closed-form outer solution ($y^* \leqq y < \infty$), whose linearization error vanishes asymptotically as $y \to \infty$. This process yields a nonlinear integro-differential equation for the friction coefficient $c_f(x)\ Re^{1/2}$. The velocity distributions $u_e(x)$ at $y = \infty$ and $u_w(x)$ and $v_w(x)$ at $y = 0$ may be represented sectionally by polynomials. Comparison with other solutions shows that accurate approximations of $c_f(x)\ Re^{1/2}$ can be computed. This accuracy decreases with the number of points where $u'_e(x)$, $u'_w(x)$, and $v'_w(x)$ change their signs. Results presented show the influence of the direction of the mass transfer vector relative to the wall. Generalizations of the method are outlined with respect to compressible boundary layer flow and a special second-order boundary layer theory. Rigorously valid bounds for $c_f(x)\ Re^{1/2}$ can be calculated by use of this method and the theorem of Nagumo and Westphal.

I. INTRODUCTION

Even though Prandtl derived the boundary layer equations from the complete Navier-Stokes equations as early as 1904 [44], only a relatively small number of exact solutions have been published since that time. Separation of the variables yields the most important class of rigorous solutions, the so-called similar solutions for $u_e(x) = c\ x^m$ or $u_e(x) = \alpha\ e^{\beta x}$, where α, β, c, and m are constant numbers (see References 3, 9, 10, and Ch. VIII of Reference 48).

Under the assumption of analytical functions representing the velocity distributions $u_e(x)$, $u_w(x)$, and $v_w(x)$ at the boundaries $y = 0$ and $y = \infty$, respectively, Blasius [6, 1908] presented a series expansion for $u(x, y)$ in powers of x, whose coefficients are determined by ordinary differential equations. This expansion proceeds in odd powers of x in case of profiles whose symmetry axis is aligned with the free stream. For this case, Howarth [22, 24] and later Tifford [59] calculated "universal" functions of y which are not related to a particular body shape and represent the coefficients of the powers $x, x^3, \ldots, x^{11}$ in Blasius' expansion (see Ch. IX of Reference 48). It is shown in Appendix A that a partial sum employing the available universal coefficients yields accurate approximations to rigorous solutions for profiles with considerable bluntness only. Even for a circular cylinder, the error

is negligible only in the region where $u_e'(x) > 0$. For functions $u_e(x)$ which can be expanded in powers of $x^{m/2}$ with $m \neq -1$, Görtler [18] has presented a series expansion in powers of $\xi^{1/2}$ for the solution of Prandtl's boundary layer problem, where

$$\xi = \int_0^{\bar{x}} \bar{u}_e(\bar{x})\, d\bar{x}/\bar{\nu}.$$

Tables of universal functions have been published for the coefficients of this expansion [19]. Since the convergence is still an open issue, both Blasius' and Görtler's series could be called "formally exact."

A very large number of approximate solutions and solution methods of Prandtl's boundary layer problem has been published since 1904; convergence towards rigorous solutions has been shown only for certain types of explicit difference methods as applied to convex initial profiles and $u_e'(x) > 0$ [29, 72]. References 16, 55, and 71 present explicit difference methods. A comparison of explicit and implicit difference schemes is given in Reference 53. If the convergence problem is unresolved and error estimates are not available, the practical value of approximate solution methods can be tested by consideration of computation work and accuracy obtainable in those special cases for which rigorous solutions are available.

In 1921, von Kármán [26] and K. Pohlhausen [43] initiated the development of integral methods, e.g., Ch. XII of Reference 48. With the exception of cases where high accuracy is required as in stability analysis, integral methods are still more important than any other approximate procedure in engineering boundary layer work. Prandtl's momentum differential equation of the boundary layer is multiplied consecutively by u^0, u, u^2, u^3, ..., u^M and then integrated over y in each case from $y = 0$ to $y = \delta(x)$, where $\delta(x)$ is the "boundary layer thickness." Substitution of a polynomial

$$u = \sum_{n=1}^{N} b_n(x)\, (y/\delta(x))^n$$

with $N > M$ in these M relations yields a system of M simultaneous nonlinear ordinary differential equations for $M + 1$ unknown "form-parameters" $\Lambda_i(x)$ which depend on $u_e(x)$, $\delta(x)$, etc., and determine the friction coefficient $c_f(x)\, Re^{1/2}$. By use of boundary conditions at $y = 0$ and $y = \delta(x)$, the coefficients $b_n(x)$ are expressed in terms of the form parameters. One-parameter integral methods in general furnish fairly accurate results at relatively little computation work, provided u_e, u_w, and v_w are sufficiently smooth

functions of x. Mangler [33], Wieghardt [70], and in particular Walz [65, 66, 67, 12] have developed and applied two-parameter integral methods which in general give surprisingly accurate results. Kwan-tsu-Yang [30,31] has presented an iteratively corrected integral method. The convergence of integral methods of any type towards rigorous solutions is still an open issue.

"Locally similar solutions" have been proposed (e.g., References 34 and 50) which determine $u(x, y)$ from tables of similar solutions. To obtain the momentum thickness $\theta(x_n)$ of the boundary layer at the grid point $x = x_n$, $u_e(x)$ is approximated by $k(x - x_o)^m$ between the grid points x_n and x_{n-1}. The three free constants, k, x_o, and m are determined by requiring that $u_e(x_{n-1})$, $u_e(x_n)$, and $\theta(x_{n-1})$ are matched. Smith [50] points out that the accuracy appears to be very high in regions of decreasing pressure; however, separation is predicted somewhat early. This is readily explained by the fact that the upstream history of the boundary layer for $x < x_{n-1}$ is neglected altogether, as is also true in integral methods. The influence of this deficiency usually manifests itself strongly in a region of increasing pressure. To avoid this disadvantage, "difference-differential" methods have been presented [20, 51, 52, 57] which substitute difference expressions for the x-derivatives in the nondimensional boundary layer equation for the stream function $\psi(x, y)$. Accuracy thus is gained at the expense of computation work since tables of similar solutions cannot be used here. At every grid station $x = x_n$, a nonlinear ordinary differential equation with boundary conditions at $y = 0$ and at $y = \infty$ has to be solved iteratively. This method involves about as much computation work at any grid station as implicit difference schemes.

The approximation of local features in the boundary layer is greatly facilitated by the two independent variables, x and y, available in difference and difference-differential methods. Both the inner and the outer solution proposed in this paper also depend on x and y (or transformed variables); computation work is saved, however, as compared to difference and difference-differential methods since matching of the inner and the outer solution yields one integro-differential equation for the friction coefficient in dependence on x only. This relation accounts explicitly for the entire upstream history of the boundary layer. The inner solution employed here is represented by a series expansion in powers of y or $\psi - \psi_w$, whereas both Blasius' and Görtler's series expansions proceed in powers of x. The closed-form outer solution follows from a linearized momentum equation whose linearization error vanishes asymptotically as $y \to \infty$. This linearized relation can be transformed into the differential equation for one-dimensional transient heat conduction. Comparison with other solutions of Prandtl's boundary layer problem shows that accurate approximations of $c_f(x)\ Re^{1/2}$ can be obtained from numerical solutions of the integro-differential equation mentioned above. As is true for other approximate methods in boundary layer theory, the accuracy of the method proposed here decreases with the number of points where $u_e'(x)$, $u_w'(x)$, and $v_w'(x)$ change their signs. This restriction of the applicability refers to a wavy wall and to the concentration of mass transfer in slots, respectively. The method proposed here surpasses the capabilities of

Blasius' and Görtler's series expansions insofar as $u_e(x)$, $u_w(x)$, and $v_w(x)$ may be represented sectionally by polynomials. Results presented show the influence of the direction of the mass transfer vector relative to the wall. Generalizations of the method are outlined with respect to compressible boundary layer flow and a special second-order boundary layer theory. In particular, in these cases, the savings of computation work as compared to difference and difference-differential methods become obvious.

In view of the small number of exact solutions and solution methods which have become available so far, Prandtl's boundary layer problem was in rather unsatisfactory state from a rigorous point of view until Nickel [37, 38, 40, 41] in response to a remark by Görtler [17] published rigorously valid theorems on all the relevant general features of the velocity distribution $u(x, y)$ in the incompressible stationary boundary layer flow under discussion. Nickel obtained these theorems by a suitable modification of the lemma of Nagumo [36] and Westphal [68] as applied to Prandtl's momentum equation in von Mises or Crocco variables. Velte [62, 63, 64] later rederived the majority of Nickel's theorems by application of Nirenberg's maximum principle [42] to Prandtl's momentum equation. Recently, Nickel [39] employed his modified version of Nagumo's and Westphal's lemma to determine a rigorously valid lower bound of the friction coefficient by use of locally similar solutions. Since these solutions do not represent the upstream history of the boundary layer adequately, rather conservative lower bounds are obtained in Nickel's paper. According to the brief outline in Appendix D, rigorously valid bounds of exact boundary layer solutions can be determined by application of the method derived in this paper and Nickel's modified version of Nagumo's and Westphal's lemma. Details of this procedure will be presented in a forthcoming paper by the first author. In view of the preceding discussions on available solutions and solution methods for Prandtl's boundary layer problem, it would be quite valuable to be able to compute rigorous and, at the same time, close upper and lower bounds of the exact friction coefficient.

II. DEFINITIONS AND GENERAL PROPERTIES OF THE BOUNDARY LAYER FLOW UNDER DISCUSSION

The solution of Prandtl's boundary layer problem under discussion is to be determined in the region H of the Cartesian x-y plane (Figure 1). To facilitate the discussions, subregions H_o, etc., are introduced according to Figure 1,

$$\begin{cases} H : & 0 < x < x_s, & 0 < y < \infty, \\ H_o : & 0 < x < x_o, & 0 < y < \infty, \\ H_{o\alpha} : & 0 < x < x_o, & \psi_\alpha^* < \psi < \infty, \\ H_I : & x_o < x < x_s, & 0 < \psi < \psi^*(x) \\ H_{II} : & x_o < x < x_s, & \psi^*(x) < \psi < \infty \\ H_{II\alpha} : & x_o < x < x_{\alpha+1}, & \psi_\alpha^* < \psi < \infty. \end{cases} \tag{1a}$$

The integer number α takes the values 0, 1, ..., β, where $x_\beta = x_s$; in Figure 1, $\beta = 3$. The boundary line $\psi^*(x, y^*)$ separating H_I and H_{II} consists of stream line sections and sections $x = \text{const.}$,

$$\psi = \psi^*_\alpha, \quad x_\alpha < x < x_{\alpha+1} \text{ and } x = x_{\alpha+1}, \quad \psi^*_\alpha \leqq \psi \leqq \psi^*_{\alpha+1}. \tag{1b}$$

The parabolic boundaries of the regions listed in (1a) are represented by the following lines:

$$\left\{\begin{array}{lll}
\Gamma: & \underline{(a)}\ x = 0,\ 0 < y < \infty; & \underline{(b)}\ y = 0,\ 0 \leqq x < x_s, \\
 & & \underline{(c)}\ y = \infty,\ 0 \leqq x < x_s; \\
\Gamma_o: & \underline{(a)}\ x = 0,\ 0 < y < \infty; & \underline{(b)}\ y = 0,\ 0 \leqq x < x_o, \\
 & & \underline{(c)}\ y = \infty,\ 0 \leqq x < x_o; \\
\Gamma_{o\alpha}: & \underline{(a)}\ x = 0,\ \psi^*_\alpha < \psi < \infty; & \underline{(b)}\ \psi = \psi^*_\alpha,\ 0 < x < x_o, \\
 & & \underline{(c)}\ \psi = \infty,\ 0 \leqq x < x_o; \\
\Gamma_I: & \underline{(a)}\ x = x_o,\ \psi_w < \psi < \psi^*_o; & \underline{(b)}\ y = 0,\ x_o \leqq x < x_s, \\
 & & \underline{(c)}\ \psi = \psi^*(x),\ x_o \leqq x < x_s; \\
\Gamma_{II}: & \underline{(a)}\ x = x_o,\ \psi^*_o < \psi < \infty; & \underline{(b)}\ \psi = \psi^*(x),\ x_o \leqq x < x_s, \\
 & & \underline{(c)}\ \psi = \infty,\ x_o \leqq x < x_s; \\
\Gamma_{II\alpha}: & \underline{(a)}\ x = x_o,\ \psi^*_\alpha < \psi < \infty; & \underline{(b)}\ \psi = \psi^*_\alpha,\ x_o \leqq x < x_{\alpha+1}, \\
 & & \underline{(c)}\ \psi = \infty,\ x_o \leqq x < x_{\alpha+1}.
\end{array}\right. \tag{1c}$$

In H_o, the rigorous stagnation point solution of both the Navier-Stokes equations and Prandtl's boundary layer equations is employed. This solution (e.g., Ch. V of Reference 48) yields $u(x_o, y) > 0$ for $0 < y < \infty$ and $\partial u(x_o, y)/\partial y > 0$ for $0 \leqq y < \infty$. By definition, $u(x, y) > 0$ in H. The separation point $x = x_s$ is determined by the condition that $u(x_s, y) = 0$ at least at one point (x_s, y) of the line $x = x_s$, $0 < y < \infty$. The theorem

(I) "$\partial u(x, y)/\partial y$ takes its maximum and its minimum values on Γ" has been derived by Nickel [37] under the assumption $u_w(x) \equiv 0$ and by Velte [62, 64] under the assumption $u_w(\xi) \neq u_e(\xi)$ at any point $x = \xi$ in $0 < x < x_s$. Under the assumptions $u_w(x) \equiv v_w(x) \equiv 0$, Nickel [37] has derived theorem II.

(II) If $u_e'(x)$ changes its sign j times in $x_o < x \leq \xi$, the velocity component $u(\xi, y)$ possesses at most j points of inflection on the line $x = \xi$, $0 < y < \infty$.

Theorems (I) and (II) are valid if certain conditions on differentiability and continuity of $u(x, y)$ are satisfied. Theorem (II) as it is presented here is correct under the condition of the boundary layer beginning at a stagnation point. The following theorems can be derived immediately from (I) and (II):

(Ia) If $\partial u(x, 0)/\partial y > 0$ for $x_o \leq x < x_s$, $u(x, y)$ must increase monotonically as a function of y in sections x = const., i.e., $u(\xi, y) < u_e(\xi)$ on lines $x = \xi$, $0 \leq y < \infty$.

(Ib) Because of theorem (Ia) and the definition of x_s given above, $\partial u(x_s, 0)/\partial y = 0$ at the separation point.

(IIa) Since the boundary layer supposedly begins at a stagnation point, a point of inflection of $u(x, y)$ in sections x = const. does not exist in $0 \leq x \leq x_m$, $0 < y < \infty$, where $u_e'(x) > 0$ for $0 \leq x \leq x_m$.

III. DIFFERENTIAL EQUATIONS, BOUNDARY CONDITIONS, AND INITIAL CONDITIONS

Nondimensional quantities are introduced as follows:

$$x = \frac{\bar{x}}{\bar{L}}, \quad y = \frac{\bar{y}}{\bar{L}}\sqrt{Re}, \quad u = \frac{\bar{u}}{\bar{u}_\infty}, \quad v = \frac{\bar{v}}{\bar{u}_\infty}\sqrt{Re}, \quad p = \frac{\bar{p}}{\bar{p}_o},$$

$$\varphi = \frac{\bar{\varphi}}{\bar{u}_\infty \bar{L}}, \quad \psi = \frac{\bar{\psi}}{\bar{u}_\infty \bar{L}}\sqrt{Re}, \quad \text{and} \quad \nu = \frac{\bar{\nu}}{\bar{u}_\infty \bar{L}} = \frac{1}{Re}. \tag{2}$$

Bars refer to values with physical dimensions. For simplicity, the static pressure $\bar{p}_\infty$ of the uniform flow at sufficiently large distance ahead of the obstacle under consideration is supposed to be zero. According to Bernoulli's theorem, therefore, $\bar{p}_o = (\bar{\rho}/2)\bar{u}_\infty^2$ and $p(x, y) + u^2(x, y) = 1$. The stream function, which is defined by

$$u = \frac{\partial \psi}{\partial y} \quad \text{and} \quad v = -\frac{\partial \psi}{\partial x}, \tag{3}$$

satisfies the continuity equation identically,

$$\frac{\partial u}{\partial x} + \frac{\partial v}{\partial y} = 0. \tag{4}$$

Prandtl's momentum equation of the boundary layer,

$$P_p u = u \frac{\partial u}{\partial x} + v \frac{\partial}{\partial y} - u_e u_e' - \frac{\partial^2 u}{\partial y^2} = 0, \tag{5}$$

Ch. VII of Reference 48, is written in terms of the operator P_p. Streamline coordinates of the boundary layer

$$\varphi(x) = \int_o^x u_e(x)\, dx, \quad \psi(x, y) = \int_o^y u(x, y)\, dy, \quad \text{and} \quad \psi_w(x) = -\int_o^x v_w(x)\, dx. \tag{6}$$

are introduced by the von Mises transformation,

$$\left(\frac{\partial}{\partial x}\right)_y = \left(\frac{\partial}{\partial x}\right)_\psi - v \left(\frac{\partial}{\partial \psi}\right)_x \quad \text{and} \quad \left(\frac{\partial}{\partial y}\right)_x = u \left(\frac{\partial}{\partial \psi}\right)_x, \tag{7}$$

e.g., Reference 15 or Reference 24, where $(\partial/\partial x)_y$ denotes the derivative with respect to x when y is constant, etc. The stream function $\psi(x, y)$ is constant along stream lines and the velocity potential $\varphi(x)$ is a transform of the geometric arc length x of the wall. The Jakobian of the transformation (7) is given by

$$\frac{\partial(\varphi, \psi)}{\partial(x, y)} = u_e(x)\, u(x, y). \tag{8}$$

The transformations (6) and (7) are uniquely reversible in H according to theorem (Ia) in Section II. Because $v^2 \ll u^2$ and $p(\varphi, \psi) = p_e(\varphi) = 1 - u_e^2(\varphi)$ in boundary layer flow, the total pressure $g = \bar{g}/\bar{p}_o$ is defined as

$$g(\varphi, \psi) = p(\varphi) + u^2(\varphi, \psi) = 1 + u^2(\varphi, \psi) - u_e^2(\varphi). \tag{9}$$

This expression takes negative values at the wall if $u_e^2 - u^2 > 1$, as is true in general in the vicinity of a maximum of $u_e(\emptyset)$. Von Mises' coordinates (6) satisfy the continuity equation (4) identically and transform Prandtl's momentum equation (5) as follows:

$$\frac{\partial g}{\partial x} = u \frac{\partial^2 g}{\partial \psi^2} \tag{10a}$$

or

$$\frac{\partial g}{\partial \emptyset} = \frac{u}{u_e} \frac{\partial^2 g}{\partial \psi^2} . \tag{10b}$$

Prandtl's boundary layer equations (4) and (5) or von Mises' boundary layer equations (10) are to be solved by use of the following initial and boundary conditions prescribed on the parabolic boundary Γ:

$$u(x_o, y) = F(x_o, y), \tag{11a}$$

or

$$u(\emptyset_o, \psi) = F(\emptyset_o, \psi). \tag{11b}$$

$$u(x, 0) = u_w(x) \geq 0, \tag{12a}$$

or

$$u(\emptyset, \psi_w) \equiv 0. \tag{12b}$$

$$v(x, 0) = v_w(x), \tag{13a}$$

or

$$\psi_{wall} = \psi_w(\emptyset(x)). \tag{13b}$$

$$\lim_{y \to \infty} u(x, y) = u_e(x), \tag{14a}$$

or

$$\lim_{\psi \to \infty} u(\emptyset, \psi) = u_e(\emptyset). \tag{14b}$$

The functions $F(x_o, y)$, $u_w(x)$, $v_w(x)$, $u_e(x)$, $F(\emptyset_o, \psi)$, $\psi_w(\emptyset)$, and $u_e(\emptyset)$ are supposed to be given boundary functions which satisfy certain conditions on differentiability and continuity. Owing to the continuity of the flow problem, the relations

$$F(x_o, y) = u_w(x)$$

and

$$\lim_{y \to \infty} F(x_o, y) = u_e(x)$$

hold true, with corresponding relations valid in $\emptyset$-ψ coordinates. Rheinboldt [47] has shown that (14a) is automatically satisfied by $u(x, y)$ provided u is analytic with respect to x; also $F(x_o, y)$ is assumed to be analytic in y and to possess a suitable asymptotic expansion as $y \to \infty$. The boundary layer is assumed to begin at a stagnation point, i.e., $u(0, y) \equiv 0$. Because of (9) and (14b), therefore,

$$g(0, \psi) = \lim_{\psi \to \infty} g(\emptyset, \psi) = 1. \tag{15}$$

IV. THE INNER SOLUTION

Within a certain vicinity of the wall, the solution of equations (4) and (5) is expanded as follows:

$$u = \sum_{n=0}^{\infty} A_n(x) \frac{y^n}{n!} \tag{16a}$$

and

$$v = - \sum_{n=0}^{\infty} A'_{n-1}(x) \frac{y^n}{n!} . \tag{16b}$$

Because of the boundary conditions (12a) and (13a), the coefficients $A_0(x)$ and $A_{-1}(x)$ are known,

$$A_0(x) = u_w(x) \quad \text{and} \quad A'_{-1}(x) = - v_w(x), \tag{17}$$

where $A_{-1}(x) = + \psi_w(x)$ appears only in (16b). The relations (2) yield

$$A_1(x) = \frac{1}{2} c_f(x) \, Re^{1/2} \tag{18}$$

where

$$c_f = \frac{2}{\bar{\rho} \, \bar{u}_\infty^2} \bar{\mu} \frac{\partial \bar{u}}{\partial \bar{y}} .$$

Substitution of (16) in (5) gives

$$A_2(x) = A_0(x) \, A'_0(x) - A'_{-1}(x) \, A_1(x) - u_e(x) \, u'_e(x) \tag{19}$$

and, if $n > 0$,

$$\frac{A_{n+2}(x)}{n!} = \sum_{i=0}^{n} \left[\frac{A_i(x)}{i!} \frac{A'_{n-i}(x)}{(n-i)!} - \frac{A'_{i-1}(x)}{i!} \frac{A_{n-i+1}(x)}{(n-i)!} \right]. \tag{20}$$

The coefficients $A_i(x)$, $i \geq 2$, depend on the given velocity distributions (12a), (13a), and (14a) at the boundaries and on the friction coefficient $c_f(x)$. For $u_w(x) = v_w(x) \equiv 0$, equations (20) have been rearranged to represent the coefficients $A_i(x)$, $2 \leq i \leq 11$, as functions of $f(x) = - u_e(x) \, u'_e(x)$ and $A_1(x)$,

$$
\begin{cases}
A_2(x) = f(x), \\
A_3(x) = 0, \\
A_4(x) = A_1(x)\, A_1'(x), \\
A_5(x) = 2A_1(x)\, f'(x), \\
A_6(x) = 2f(x)\, f'(x), \\
A_7(x) = 4A_1^2(x)\, A_1''(x) - A_1(x)\, A_1'^2(x), \\
A_8(x) = 10A_1^2(x)\, f''(x) - 13A_1(x)\, A_1'(x)\, f'(x) + 9f(x) \left[A_1(x)\, A_1''(x) + A_1'^2(x) \right], \\
A_9(x) = 40A_1(x)\, f(x)\, f''(x) - 16A_1(x)\, f'^2(x), \\
A_{10}(x) = -24A_1^2(x)\, A_1'(x)\, A_1''(x) + 27A_1(x)\, A_1'^3(x) + 28A_1^3(x)\, A_1'''(x) \\
\qquad - 16f(x)\, f'^2(x) + 40f^2(x)\, f''(x), \\
A_{11}(x) = 135fA_1\, A_1'\, A_1'' + 451A_1\, A_1'^2 f' - 130A_1^2\, A_1' f'' - 224f'\, A_1^2\, A_1'' \\
\qquad - 270\, f\, A_1'^3 + 180f\, A_1^2\, A_1''' + 80A_1^3\, f''', \\
A_{12}(x) = -510A_1^2\, f'\, f_2'' - 615A_1\, A_1'\, ff'' + 710A_1^2\, ff''' - 1739A_1\, A_1'\, f'^2 \\
\qquad - 899ff'\, A_1'^2 - 899ff'\, A_1\, A_1'' + 945f^2\, A_1'\, A_1'' + 315f^2\, A_1\, A_1'''.
\end{cases}
\tag{21}
$$

The expressions (21) for $A_m(x)$, $3 \leq m \leq 9$, are listed in Ch. VIII of Reference 48.

Under the assumption $u_w(x) \equiv 0$, the solution of equations (10a) or (10b) is expanded as follows within a certain vicinity of the wall:

$$
u(x, \psi) = \sum_{n=0}^{\infty} a_n(x) \left[\psi - \psi_w(x) \right]^{\frac{n+1}{2}}, \tag{22}
$$

where $\phi(x)$ may be substituted for x by use of (6). The expansion (22) satisfies the boundary condition (13b). The relations (2) yield

$$a_o^2(\phi(x)) = c_f(\phi(x))\ Re^{1/2}. \tag{23}$$

Substitution of (22) in (10a) gives

$$a_1(x) = \frac{2}{3}\left[\frac{-\,2u_e(x)\,u_e'(x)}{a_o^2(x)} - \frac{d\psi_w(x)}{dx}\right], \tag{24}$$

$$a_2(x) = -\frac{7}{8}\frac{a_1^2(x)}{a_o(x)} - \frac{3}{4}\frac{a_1(x)}{a_o(x)}\frac{d\psi_w(x)}{dx} \tag{25}$$

and, if $n \geq 3$,

$$a_n(x) = -\frac{1}{2a_o(x)}\sum_{i=1}^{n-1} a_i(x)\,a_{n-i}(x)$$

$$-\frac{2}{n(n+2)\,a_o^2(x)}\left[\sum_{i=0}^{n-2} a_{n-i-1}(x)\left(\frac{i+2}{2}\right)\frac{i}{2}\left(\sum_{j=0}^{i} a_j(x)\,a_{i-1}(x)\right)\right.$$

$$-\sum_{j=0}^{n-3}\left(a_j'(x)\,a_{n-j-3}(x) + a_j(x)\,a_{n-3-j}'(x)\right)$$

$$\left.+\frac{n+1}{2}\frac{d\psi_w(x)}{dx}\sum_{j=1}^{n-1} a_j(x)\,a_{n-j-1}(x)\right]. \tag{26}$$

The coefficients $a_i(x)$, $i \geq 1$, depend on the given boundary functions $\psi_w(x)$ and $u_e(x)$ and on the friction coefficient $c_f(x)\,Re^{1/2}$. Because of

$$a_o^2(0) = a_o^2(x_s) = 0,$$

the coefficients $a_i(x)$, $i \geq 1$, do not exist both at the stagnation point, $x = 0$, and at the point of separation of the laminar boundary layer, $x = x_s$.

The problem of the convergence and thus existence of the infinite series (16) and (22) is too involved to be treated here. Since partial sums of the expansions (16) and (22) will be used subsequently, the convergence and existence problem is superseded by the question of the accuracy of these polynomial representations.

This accuracy question will be discussed now employing the example of the impermeable circular cylinder ($u_w = v_w \equiv 0$) with $u_e = 2 \sin \varphi = 2 \sin 2x$ as given by potential flow theory, Ch. IX of Reference 48. In order to have unified treatment of arbitrary cylindrical profiles, the diameter $2\bar{R}$ of the circular cylinder represents the reference length $\bar{L}$. The velocity profiles marked "B" at stations $x = \text{const.}$ in Figures 2-9 are results of evaluating the six available terms ($n = 1, \ldots, 6$) in Blasius' series expansion

$$\frac{\bar{u}(\bar{x}, \bar{y})}{\bar{u}_\infty} = 2 \sum_{n=1}^{\infty} (-1)^{n+1} \frac{2n}{(2n-1)!} f'_{2n-1}(\eta) \left(\frac{\bar{x}}{\bar{R}}\right)^{2n-1} - 2f'_1(\eta)\,\frac{\bar{x}}{\bar{R}}, \qquad (27)$$

see Appendix A. According to Ch. IX of Reference 48, the available terms in (27) yield

$$c_f(x)\sqrt{Re} = \sqrt{2}\left[6.973\,\frac{\bar{x}}{\bar{R}} - 2.732\left(\frac{\bar{x}}{\bar{R}}\right)^3 + 0.292\left(\frac{\bar{x}}{\bar{R}}\right)^5 - 1.83 \times 10^{-2}\left(\frac{\bar{x}}{\bar{R}}\right)^7 + 0.43 \times 10^{-4}\left(\frac{\bar{x}}{\bar{R}}\right)^9 - 1.15 \times 10^{-4}\left(\frac{\bar{x}}{\bar{R}}\right)^{11}\right]. \qquad (28)$$

Since it is intended to study in sections $x = \text{const.}$ the approximation of the supposedly exact (u/u_e)-profiles as following from (27) while $u_e(x)$ and $c_f(x)$ are given, (28) has been used to evaluate partial sums of (16) (Figures 2-6) and (22) (Figures 7-9) with the number N of terms marked at the curves in

Figures 2-9. The general expressions (20) and (26) for the coefficients have been used to calculate the partial sums of u/u_e shown in Figures 2-4 and 7-9, respectively. The derivatives of A_i and a_i have been obtained from first backward difference quotients, e.g., $A_i'(x) \equiv dA_i(x)/dx = [A_i(x) - A_i(x-\Delta x)]/\Delta x$. The number of decimals of the coefficients in expression (28) for $2A_1(x) = a_0^2(x)$ indicates a rapid decrease of accuracy in approximating the derivatives of A_i or a_i as i increases. The partial sums of u/u_e shown in Figures 5 and 6 have been determined by use of the special formulas (21) for the coefficients A_n. Here the derivatives of A_1 have been computed more reliably from the unsymmetric finite expressions (37) in Section VII with h = 0.02.

Figures 2 and 7 show that about seven terms suffice at x = 0.1, i.e., $\varphi = 11.5°$, to approximate Blasius' (u/u_e)-profile from zero up to $u/u_e = 0.95$. At x = 0.5, i.e., $\varphi = 57.2°$, ten terms are sufficient for this approximation as seen in Figures 3, 5, and 8. Even though the (u/u_e)-profiles following from (16) or (22) have been calculated by use of Blasius' expression (28) for $2A_1(x) = a_0^2(x)$, Blasius' curve "B" in Figure 6 deviates at y as low as one from the nearly coincident curves representing partial sums with 7, 9, 10, and 11 terms. Since Figure 6 refers to x = 0.85, i.e., $\varphi = 97.4°$, close to the separation point, this deviation is explained by the shortcomings of Blasius' expansion in the region where $u_e'(x) < 0$.

Even at x = 0.5, the higher-order terms must still have such small contribution to the numerical values of the partial sums of (16) and (22) that it does not make any noticeable difference whether the more accurate coefficients A_n are used in Figure 5 or the less reliable coefficients A_n and a_n in Figures 3 and 8, respectively. At x = 0.85, however, the more reliable coefficients yield a more regular pattern of curves, Figure 6, as compared to Figures 4 and 9. Computed results not presented here show that the way of determining the coefficients just begins to manifest itself at x = 0.8.

V. THE OUTER SOLUTION

The asymptotic approach $u \to u_e$ as $y \to \infty$ can be studied to a first approximation if u/u_e in (10b) is replaced by one. The resulting relation

$$\frac{\partial g}{\partial \varphi} = \frac{\partial^2 g}{\partial \psi^2} \tag{29}$$

has the form of the differential equation

$$\frac{\partial T}{\partial t} = A \frac{\partial^2 T}{\partial y^2} \tag{30}$$

for the one-dimensional transient distribution of temperature T(y, t) in a slab possessing thermal diffusivity A = 1, e.g., Ch. II of Reference 7. Because of its asymptotic validity, the differential equation (29) will be considered in the following only for the regions $H_{o\alpha}$, $H_{II\alpha}$, and their common boundary line $\phi_o = \phi(x_o)$, $\psi_\alpha^* < \psi < \infty$; see (1a), (1c), and Figure 1. Here $\phi_{\alpha+1} = \phi(x_{\alpha+1})$ is a given constant number and $\psi = \psi_\alpha^*$ represents any stream line in H. According to (15), the initial and the boundary conditions for the solution of (29) in $H_{o\alpha} + H_{II\alpha}$ are given as follows:

$$g(0, \psi) = 1, \quad g(\phi, \psi_\alpha^*) = G(\phi), \quad \text{and} \quad \lim_{\psi \to \infty} g(\phi, \psi) = 1; \tag{31}$$

here $G(\phi)$ is supposed to be a given function of ϕ. Evidently, $G(\phi) \leqq 1$ because of (9) and theorem (Ia) in Section II.

The solution of equations (29) and (31) for the regions $H_{o\alpha} + H_{II\alpha}$ is derived in Appendix C.

$$\frac{\partial g(\phi, \psi)}{\partial \psi} = -\frac{2}{\sqrt{\pi}} \int_{\eta=0}^{\eta=\phi} \frac{dG(\eta)}{d\eta} \frac{\exp\left[-(\psi - \psi_\alpha^*)^2/4(\phi - \eta)\right]}{2\sqrt{\phi - \eta}}\, d\eta \text{ in } H_{o\alpha} + H_{II\alpha}. \tag{32}$$

This relation expresses the solution $\partial g(\phi, \psi)/\partial\psi = 2\partial u(\phi, \psi)/\partial y$ of equations (29) and (31) in $H_{o\alpha} + H_{II\alpha}$ as a function of the boundary parameter $dG(\phi)/d\phi$. As $\psi \to \infty$, the right-hand side of (32) is determined by the values of $G'(\phi)$ as $\phi \to 0$. This conclusion is closely related to Rheinboldt's theorem [47] quoted at the end of Section III. This theorem may be interpreted as follows: As $y \to \infty$, the influence of vorticity, which is generated at the wall and diffuses across the boundary layer, tends to zero as compared to the influence of the initial velocity distribution. A transformation of (30) (see Appendix C) yields the following convolution-type expression on the boundary-line $\psi = \psi_\alpha^*$ of $H_{o\alpha} + H_{II\alpha}$:

$$-\sqrt{\pi}\left[g(\phi, \psi_\alpha^*) - 1\right] = \int_{\eta=0}^{\eta=\phi} \frac{\partial g(\eta, \psi_\alpha^*)}{\partial \psi} \frac{d\eta}{\sqrt{\phi - \eta}}. \tag{33}$$

It is shown in Appendix D that the solution of the linearized differential equation (29) furnishes a lower bound with respect to the solution of the rigorous differential equation (10a) if the same initial and boundary conditions (31) are used in both cases. A pertinent upper bound is also derived in Appendix D. The gradient

$$\frac{\partial g(\varnothing,\ \psi_\alpha^*)}{\partial \psi} = \frac{2\partial u(\varnothing,\ \psi_\alpha^*)}{\partial y}$$

can be enclosed by these upper and lower bounds; see equation (D-28). The constant number U_2 in (D-28) can be specified a priori; see equation (39). Equation (D-28), therefore, furnishes an estimate for the linearization error of the outer solution, which is only asymptotically valid as y or ψ tend to infinity.

As a first rough approximation, expression (32) may be used to represent the wall friction coefficient according to the relation

$$\frac{\partial g(\varnothing,\ \psi_w)}{\partial \psi} = \frac{2\partial u(\varnothing,\ \psi_w)}{\partial y} = c_f(x)\sqrt{\mathrm{Re}}\ .$$

This procedure has been employed in References 1 and 2 in case of heat transfer in laminar boundary layer flow. Equation (9) shows that $G(\varnothing) = p(\varnothing)$ when $u_w(\varnothing) \equiv 0$. Accordingly, equation (32) yields

$$c_{fa}(x)\sqrt{\mathrm{Re}} = -\frac{2}{\sqrt{\pi}} \int_{\eta=0}^{\eta=\varnothing} \frac{dp(\eta)}{d\eta} \frac{d\eta}{\sqrt{\varnothing - \eta}}\ . \tag{34}$$

The subscript a refers to "approximate." For the potential velocity distribution $u_e(x) = 2 \sin \varphi$ past the circular cylinder, Figure 10 presents both $c_f(x)\ \mathrm{Re}^{1/2}$ from (28), solid line, and $c_{fa}(x)\ \mathrm{Re}^{1/2}$ from (34), dashed line. As in References 1 and 2, the agreement between the solutions being compared is considerably improved when $c_{fa}(x)/c_{fa}(x_o)$ and $c_f(x)/c_f(x_o)$ are plotted (see Figure 11). Here x_o is any arbitrary point within the range of the x-axis where $u_e(x)$ may be replaced with sufficient accuracy by its initial tangent, $u_e'(0)\ x$. When $\bar{a}$ is determined from $u_e'(0)\ x = (\bar{a}\bar{L}/\bar{u}_\infty)x$, the rigorous stagnation point solution of both the Navier-Stokes equations and Prandtl's boundary layer equations yields, according to Ch. V of Reference 48,

$$c_f(x)\sqrt{Re} = 2.4652\,\frac{\bar{a}\bar{L}}{\bar{u}_\infty}\,x. \tag{35}$$

The parameter $c_{fa}(x)\,Re^{1/2}$ to be determined may be obtained from $c_{fa}(x)/c_{fa}(x_o)$ by multiplication of this ratio by the exact expression (35). According to References 1 and 2, better agreement of the curves presented in each one of Figures 10 and 11 would obtain if a slender profile were studied instead of the circular cylinder. It is seen that equation (34) yields a rough "engineering-type" approximation of $c_f(x)\,Re^{1/2}$ whose evaluation requires very little computation work. While (34) is a result of replacing u/u_e in von Mises' boundary layer equation (10b) by one, Lighthill [32] linearized (10a) in a different way; he substituted

$$\bar{u} = \bar{y}\,\frac{\partial\bar{u}(x,\,0)}{\partial\bar{y}} = \sqrt{(2\bar{\psi}/\bar{\rho})\,(\partial\bar{u}(x,\,0)/\partial\bar{y})}$$

for $\bar{u}$ and obtained a nonlinear integral equation for $c_f(x)\,Re^{1/2}$.

VI. THE MATCHING PROCEDURE OF THE INNER AND THE OUTER SOLUTION

As has been mentioned before, the coefficients of the series expansions (16) and (22) depend on the friction coefficient $c_f(x)$ in addition to their dependence on the given initial and boundary conditions (11) - (14). Under consideration of equation (9) between g and u, either expansion (16) or expansion (22) is now substituted into the expressions $g(\emptyset,\,\psi^*_\alpha)$ and $\partial g(\emptyset,\,\psi^*_\alpha)/\partial\psi$ appearing in the boundary relation (33) of the outer solution, which thus becomes a nonlinear ordinary integro-differential equation for $c_f(x)$,

$$-\sqrt{\pi}\left[g(\emptyset,\,c_f(\emptyset),\,c_f'(\emptyset),\,\ldots) - 1\right] = \int_{\eta=0}^{\eta=\emptyset} \frac{\partial g(\eta,\,c_f(\eta),\,c_f'(\eta),\,\ldots)}{\partial\psi}\,\frac{d\eta}{\sqrt{\emptyset - \eta}}\,. \tag{36}$$

It is remarkable that equation (33), which is part of the outer solution, depends only on the parameters $A_1(x) = 0.5\,c_f(x)\,Re^{1/2}$ or $a_o(x) = c_f^{1/2}(x)\,Re^{1/4}$ of the inner solution after the said substitution has been carried out. Solution of the resulting integro-differential equation for $A_1(x)$ or $a_o(x)$ determines the partial sums of the expansions (16) and (22) completely. Expression of

$dG(\emptyset)/d\emptyset = \partial g(\emptyset, \psi^*_\alpha)/\partial\psi$ by partial sums of either expansion then enables one to evaluate the outer solution completely in the range $\psi^*_\alpha < \psi < \infty$ by use of equation (32). For both the inner and the outer solution, the outlined matching process renders the values of $g(\emptyset, \psi^*_\alpha)$ coincident and also the values of $\partial g(\emptyset, \psi^*_\alpha)/\partial\psi$. The values of $\partial^2 g(\emptyset, \psi^*_\alpha)/\partial\psi^2$, however, as determined from these two solutions are different as is seen by comparison of the pertinent differential equations (10b) and (29).

By the outlined matching procedure, Prandtl's boundary layer problem has been reduced to the solution of one approximately valid integro-differential equation which replaces the partial differential equations (4) and (5), or (10), plus the pertinent initial and boundary conditions (11) - (15). This reduction is representative of a class of hereditary-type problems which are equivalent to integro-differential equations depending on one variable.

Numerical solutions of Prandtl's boundary layer problem are greatly facilitated by use of the integro-differential equation (36) for $c_f(x)$, whose derivation has been possible because the coefficients of the expansions (16) and (22) are given by closed-form expressions, (19) - (21) or (24) - (26). The coefficients of both Blasius' and Görtler's series expansions, though, are determined by ordinary differential equations. In addition, these expansions require analytical expressions for the velocity distributions $u_e(x)$, $u_w(x)$, and $v_w(x)$ at the boundaries, whereas the method presented here is applicable under less stringent conditions (see Section X).

VII. THE NUMERICAL SOLUTION PROCEDURE

A grid of not necessarily constant unit length $\Delta\emptyset$ is introduced along the $\emptyset(x)$-axis to solve equation (36) for $A_1(\emptyset) = 1/2\ c_f(\emptyset)\ Re^{1/2}$ or $a_o^2(\emptyset) = c_f(\emptyset)\ Re^{1/2}$. Suppose this solution has already been obtained stepwise in the range $0 < \emptyset \leq \emptyset_{N-1}$. The right-hand side of equation (36) then can be approximated by Lagrangian integration methods for $0 < \emptyset \leq \emptyset_{N-1}$. The function $\partial g(\emptyset, \psi^*_\alpha)/\partial\psi$ is unknown between $\emptyset_{N-1}$ and $\emptyset_N$; it is approximated in this section of the $\emptyset$-axis by a polynomial whose coefficients depend on the numerical values which $\partial g/\partial\psi$ takes at the points $\emptyset_N$, $\emptyset_{N-1}$, $\emptyset_{N-2}$, ..., on the stream line $\psi = \psi^*_\alpha$. The right-hand side of equation (36) then can be evaluated in closed form between $\emptyset_{N-1}$ and $\emptyset_N$. This procedure removes the singularity of the integrand at the upper limit $\emptyset = \emptyset_N$ of the integral.

By use of (9), both $g(\emptyset_N, \psi^*_\alpha)$ and $\partial g(\emptyset, \psi^*_\alpha)/\partial\psi$ in equation (36) are expressed in terms of the expansions (16) or (22). According to the recursion formulas (20) or (26), the coefficients A_n and a_n in these expansions depend on the intermediate coefficients, i.e., $A_n = A_n(\emptyset, A_{-1}, \ldots, A_{n-1}, A'_{-1}, \ldots, A'_{n-2})$ and $a_n = a_n(\emptyset, a_o, \ldots, a_{n-1}, a'_o, \ldots, a'_{n-3})$. With the exception of the dashed lines in Figures 5 and 6, the numerical solutions presented in this paper have been obtained by replacing the first-order derivatives in these recursion

formulas for A_n and a_n by backward difference quotients, $A'_j(\phi_N) \equiv dA_j(\phi_N)/dx = [A_j(\phi_N) - A_j(\phi_{N-1})]\, u_e(\phi_N)/\Delta\phi$. The accuracy of this representation could be improved by use of unsymmetric finite expressions for $A'_j(\phi)$. In any case, however, if a prescribed round-off error is not to be exceeded, the number of digits carried in the computations must increase with the number of terms in the partial sums of (16) or (22). This evidently is a disadvantage since partial sums of (16) or (22) with at least 10 terms have to be used as $x \to x_s$ according to Figures 4, 6, and 9. Whereas A_n depends on A'_{-1}, ..., A'_{n-2} according to the recursion formulas (20), the special expressions (21) for the coefficients A_n show that the order of the highest derivative of A_1 in the equation for A_n increases considerably slower than n. The recursion formulas (26) for the coefficients a_n can be solved stepwise to give special expressions for the coefficients a_n comparable to the relations (21). Forthcoming applications of the solution method presented here will be carried out by use of the special expressions (21) for the coefficients A_n and by use of generalized versions of (21) to account for mass transfer at the wall which is supposed to be zero in the relations (21). The derivatives of A_1 in the expression (21) are replaced by the following unsymmetric finite formulas, Ch. III of Reference 8:

$$
\begin{aligned}
A'_1(\phi_N) &= -\frac{A_1(\phi_{N-5})}{5\Delta\phi} + 5\frac{A_1(\phi_{N-4})}{4\Delta\phi} - 10\frac{A_1(\phi_{N-3})}{3\Delta\phi} + 5\frac{A_1(\phi_{N-2})}{\Delta\phi} - 5\frac{A_1(\phi_{N-1})}{\Delta\phi} \\
&\quad + \frac{137}{60}\frac{A_1(\phi_N)}{\Delta\phi} - \frac{(\Delta\phi)^5}{6} A_1^{VI}(\phi_N), \\
A''_1(\phi_N) &= -5\frac{A_1(\phi_{N-5})}{6(\Delta\phi)^2} + 61\frac{A_1(\phi_{N-4})}{12(\Delta\phi)^2} - 13\frac{A_1(\phi_{N-3})}{(\Delta\phi)^2} + 107\frac{A_1(\phi_{N-2})}{6(\Delta\phi)^2} \\
&\quad - 77\frac{A_1(\phi_{N-1})}{6(\Delta\phi)^2} + 15\frac{A_1(\phi_N)}{4(\Delta\phi)^2} - \frac{137}{180}(\Delta\phi)^4 A_1^{VI}(\phi_N), \\
A'''_1(\phi_N) &= -7\frac{A_1(\phi_{N-5})}{4(\Delta\phi)^3} + 41\frac{A_1(\phi_{N-4})}{4(\Delta\phi)^3} - 49\frac{A_1(\phi_{N-3})}{2(\Delta\phi)^3} + 59\frac{A_1(\phi_{N-2})}{2(\Delta\phi)^3} \\
&\quad - 71\frac{A_1(\phi_{N-1})}{4(\Delta\phi)^3} + 17\frac{A_1(\phi_N)}{4(\Delta\phi)^3} - \frac{5}{8}(\Delta\phi)^3 A_1^{VI}(\phi_N), \\
A''''_1(\phi_N) &= -2\frac{A_1(\phi_{N-5})}{(\Delta\phi)^4} + 11\frac{A_1(\phi_{N-4})}{(\Delta\phi)^4} - 24\frac{A_1(\phi_{N-3})}{(\Delta\phi)^4} + 26\frac{A_1(\phi_{N-2})}{(\Delta\phi)^4} \\
&\quad - 14\frac{A_1(\phi_{N-1})}{(\Delta\phi)^4} + 3\frac{A_1(\phi_N)}{(\Delta\phi)^4} - \frac{17}{6}(\Delta\phi)^2 A_1^{VI}(\phi_N).
\end{aligned}
\tag{37}
$$

The last term in each one of these relations indicates the next nonvanishing term of the Taylor expansion at $\varnothing_N$.

It has been shown in the preceding paragraph that both $g(\varnothing_N, \psi_\alpha^*)$ and $\partial g(\varnothing_N, \psi_\alpha^*)/\partial\psi$ can be expressed as functions of the unknown numbers $A_1(\varnothing_N)$ or $a_o(\varnothing_N)$ when the method under discussion is applied to determine the solution at the point $\varnothing = \varnothing_N$. In this way, the integro-differential equation (36) with the upper limit $\varnothing_N$ of the integral becomes a nonlinear ordinary equation for $A_1(\varnothing_N)$ or $a_o(\varnothing_N)$, provided (36) has already been solved in $0 < \varnothing \leqq \varnothing_{N-1}$. This ordinary equation can be solved iteratively, starting from a straight-line continuation of the numerical values of A_1 or a_o at the grid points $\varnothing_{N-2}$ and $\varnothing_{N-1}$. The results presented in this paper have been computed by use of a tolerance of 0.01 percent in the iterations for $A_1(\varnothing_N)$ or $a_o(\varnothing_N)$.

When partial sums of expansion (22) are used to express $g(\varnothing_N, \psi_\alpha^*)$ and $\partial g(\varnothing_N, \psi_\alpha^*)/\partial\psi$ in (36) as functions of $\varnothing_N$ and $a_o(\varnothing_N)$, the powers $[\psi - \psi_w(\varnothing_N)]^{1/2}$ in (22) can be evaluated directly since $\psi = \psi_\alpha^* = \text{const}$. However, when partial sums of (16) are employed to determine $A_1(\varnothing_N)$, the powers of y in (16) cannot be obtained directly since the intersection of the stream line $\psi = \psi_\alpha^*$ with the grid line $\varnothing = \varnothing_N$ depends on $u(\varnothing_N, \psi_\alpha^*)$ and thus on $A_1(\varnothing_N)$. The results presented in this paper by use of expansion (16) have been obtained by employing the relation

$$y_N^* = y_{N-1}^* + \frac{\Delta\varnothing}{u_e(\varnothing_N)} \frac{v(\varnothing_{N-1}, \psi_\alpha^*)}{u(\varnothing_{N-1}, \psi_\alpha^*)} \tag{38}$$

which represents the tangent to the stream line $\psi = \psi_\alpha^*$ at the point $\varnothing_{N-1}$, ψ_α^*. A better value for y_N^* could be obtained by use of a quadratic equation for $\psi = \psi_\alpha^*$ between $\varnothing_{N-1}$ and $\varnothing_N$ which employs the already known values of $\partial u/\partial x$, $\partial u/\partial y$, $\partial v/\partial x$, and $\partial v/\partial y$ at the point $\varnothing_{N-1}$, ψ_α^*.

The differential equation (29) for the outer solution has been obtained by substituting one for u/u_e in the rigorous differential equation (10b). In general, u/u_e decreases as $\varnothing$ increases along any given stream line $\psi = \psi_\alpha^*$ in the boundary layer; i.e., the linearization error of the outer solution increases with the coordinate $\varnothing$ which measures along the stream line $\psi = \psi_\alpha^*$. It is specified, therefore, that u/u_e along any given stream line changes only within the arbitrarily prescribed bounds U_1 and U_2,

$$0 < U_2 < u(\varnothing, \psi_\alpha^*)/u_e(\varnothing) \leqq U_1 < 1. \tag{39}$$

The inequalities $0 < U_2$ and $U_1 < 1$ are a consequence of Section II. When, for the first time, $u(\emptyset, \psi^*_\alpha)/u_e(\emptyset)$ gets smaller than U_2 at the grid point $\emptyset_{\alpha+1}$ (see Figure 1), the employed partial sum of expansion (16) or (22) is evaluated on the line $\emptyset = \emptyset_{\alpha+1}$, $\psi > \psi^*_\alpha$ to determine by trial and error a point $\emptyset_{\alpha+1}$, $\psi^*_{\alpha+1}$ at which

$$\frac{u(\emptyset_{\alpha+1}, \psi^*_{\alpha+1})}{u_e(\emptyset_{\alpha+1})}$$

is approximately equal to U_1. This fixes a new stream line $\psi = \psi^*_{\alpha+1}$ which serves as the boundary of H_I and $H_{II,\alpha+1}$. In general

$$\lim_{\emptyset \to \emptyset_{\alpha+1} - 0} g(\emptyset, \psi) \neq \lim_{\emptyset \to \emptyset_{\alpha+1} + 0} g(\emptyset, \psi)$$

within the section $\psi^*_\alpha < \psi < \psi^*_{\alpha+1}$ of the line $\emptyset = \emptyset_{\alpha+1}$. The same type of discontinuity affects $\partial g(\emptyset, \psi)/\partial\emptyset$ in this section. These discontinuities do not have any consequences with respect to the approximate calculation procedure being presented. The function $\partial g(\emptyset, \psi^*_{\alpha+1})/\partial\psi$ is needed to evaluate the right-hand side of (36) in the range $0 < \emptyset \leq \emptyset_{\alpha+1}$. This function can be determined along the new stream line $\psi = \psi^*_{\alpha+1}$ by employing (32).

The start of the numerical solution procedure is now considered. Available standard quadrature formulas require a sufficient number of grid points $\emptyset_i$ between $\emptyset = 0$ and $\emptyset = \emptyset_{N-1}$ to evaluate the integral in the right-hand side of (36). Because of this reason, it is advisable to employ the rigorous stagnation point solution in a sufficiently small neighborhood H_o (Figure 1) of the stagnation point before the outlined numerical solution procedure of equation (36) is applied beginning at the grid point $\emptyset(x_o) + \Delta\emptyset$. The station $x = x_o$ is determined so that $u_e(x)$ can be approximated in H_o with sufficient accuracy by the straight line expression $u_e = (\bar{a}\bar{L}/\bar{u}_\infty)x$ of the stagnation point solution, see Ch. V of Reference 48. Tables of this solution present the function $(\partial u/\partial y)/x = (\partial g/\partial\psi)/2x$ which appears in the integrand of equation (36). The portion between $\emptyset = 0$ and $\emptyset = \emptyset(x_o)$ of this integral then can be evaluated by use of standard quadrature formulas and interpolation of the tables. The numerical evaluation of the integro-differential equation (36) begins at the point $\emptyset(x_o) + \Delta\emptyset$, ψ^*_o, whose coordinate ψ^*_o is selected so that the stagnation point solution gives $u(x_o, \psi^*_o)/u_e(x_o) \cong U_1$; see (39).

According to the preceding paragraph, the numerical solution procedure of equation (36) starts with a relatively small increment $\Delta\emptyset$ in order to have a sufficient number of grid points $\emptyset_i$ in the range $0 < \emptyset_i < \emptyset(x_o)$ to be handled

by use of the stagnation point solution. This step size $\Delta\phi$ may be increased several times during any particular boundary layer evaluation to save computation time. In case of a perforated wall with suction or blowing, $\Delta\phi$ must be small enough as compared to the width of the slots in the wall. Evidently, significant round-off errors are incurred if $\Delta\phi$ is too small as compared to the number of digits carried in the computation scheme. The numerical results presented in this paper have been obtained by use of an IBM 1620 digital computer with 40,000 data storage spaces. Seven digit numbers (and two digit powers of ten) have been used in the computation program.

VIII. ERROR ANALYSIS

Witting [72] has shown that Prandtl's boundary layer equations (4) and (5) are stable with respect to the propagation of small errors ("disturbances" of the velocity profile) if $Du/Dt \equiv u(\partial u/\partial x) + v(\partial u/\partial y) \geq 0$. The "stability boundary" $Du/Dt = 0$ begins at the point of maximum shear stress at the wall and approaches asymptotically the line $x = x_m$ which is defined by $dp(x_m)/dx = 0$. In the vicinity of any point (x_1, y_1) where $Du(x_1, y_1)/Dt < 0$, disturbances exist which increase at least locally with $x > x_1$. It is mentioned without proof in Reference 72 that von Mises' boundary layer equation (10) is stable with respect to the propagation of errors in the region of decreasing pressure.

The numerical solution procedure presented in this paper employs equations which are closely related to, but nevertheless different from Prandtl's original boundary layer equations. While instability of the presented method with respect to the propagation of errors then is possible even in the boundary layer region where $Du/Dt \geq 0$, this type of instability has not been observed so far in any numerical application of the method. Difference methods are stable in this respect if a certain step size ratio is not exceeded [29, 71].

The derived method is subjected to the unresolved convergence (and thus existence) problem of the expansions (16) and (22). In addition, the following sources of error can be listed:

(a) A sufficiently large number of terms has to be evaluated in the partial sums of (16) or (22) to represent u accurately in sections $x = \text{const.}$, $0 \leq y \leq y^*(x)$. Since $y^*(x)$ in general increases with x, the number of terms available for evaluation may be too small as $x \to x_s$.

(b) The outer solution, which asymptotically tends towards the rigorous solution as y (or ψ) goes to infinity, is used at at relatively small values of y (or ψ).

(c) Linearization errors, round-off errors, etc., are incurred in the numerical solution procedure.

The influence of error sources (a) and (b) may be diminished if partial sums of (16) or (22) are used for a subregion of H_I adjacent to the wall only. For the remainder of H_I, solutions of a linearized version (C-13) of von Mises' boundary layer equation (10b) are employed according to Appendix C.

The discussions of this section indicate that both the validity and the accuracy of the derived method are rather questionable, as is true for the majority of approximate methods in boundary layer theory. These shortcomings of the derived method can be overcome if the method is employed together with the lemma of Nagumo and Westphal to determine rigorously valid bounds of exact solutions. The calculation procedure for these bounds is outlined briefly in Appendix D.

IX. APPLICATION OF THE METHOD TO THE CIRCULAR CYLINDER

The method as derived in this paper requires the boundary layer to begin at a forward stagnation point. This condition is satisfied by the vast majority of flows past profiles in engineering fluid dynamics. With slight modifications referring to the initial condition (11), the method can be adapted to profiles with a sharp leading edge. The desirable test of the accuracy of the method, however, has to be carried out here by use of boundary layer solutions beginning at a stagnation point. The most important test solution of this type is Blasius' series expansion for profiles symmetric with respect to the free stream. The shortcomings of the available partial sums of Blasius' expansion are outlined in Appendix A. These deficiencies have already been discussed in Section IV with reference to the (u/u_e)-profiles in the boundary layer past the circular cylinder with $u_e = 2 \sin \varphi$ and $u_w = v_w = 0$ (see Figures 2-9). For these velocity distributions at the boundaries, Figures 12 and 13 present $c_f(x)\, Re^{1/2}$ as following from the partial sum (28) of Blasius' expansion (27) and from the derived method. The dashed lines in both figures have been obtained by employing the stagnation point solution for $0 < x \leqq 0.077$, i.e., $0 < \varphi \leqq 8.75°$ (see Section VII). The dashed line in Figure 12 has been computed by use of expansion (16) for $x > 0.077$, whereas the dashed line in Figure 13 is a result of employing (22) for $0.077 < x \leqq 0.459$ and expansion (16) for $x > 0.459$. This procedure is explained by the singularity of expansion (22) at the separation point $x = x_s$.

Figures 12 and 13 exhibit satisfactory agreement between Blasius' expansion and the derived method in the range $0 \leqq x < 0.785$ of decreasing pressure. Since Blasius' expansion is reliable in this region according to Appendix A, the error sources listed in Section VIII have only negligible influence for $x < 0.785$. This is not necessarily true as $x \to x_s$. Owing in particular to the increase of the displacement thickness, the maximum ordinates $y^*(x)$ or $\psi^*(x)$ of the partial sums of (16) or (22), respectively, increase considerably.

To clarify this situation, Table 1 presents at several stations x = const. numerical values of the individual terms in the partial sums of expansions (16) and (22) as employed to obtain the circular cylinder results in Figure 13. Table 1 lists these terms at the boundary lines $\psi = \psi_\alpha^*(x, y^*)$ = const. of H_I where $|A_n\, y^n/n!|$ and $|a_n\, \psi^n|$ take their maximum values. As exemplified by the column for x = 0.4586 in Table 1, the numerical values of $|A_n\, y^{*n}/n!|$ and $|a_n\, \psi^{*n}|$ decrease rapidly with increasing index n if only small and medium values of x are considered in the range $0 < x < x_s$. As $x \to x_s$, however, the decrease of $|A_n\, y^{*n}/n!|$ becomes slower and slower as has been explained above. Since the higher order terms have an appreciable influence on the numerical values of the partial sums as $x \to x_s$, the data presented must become somewhat unreliable because the coefficients A_n and a_n have been computed by use of backward difference quotients for the derivatives rather than by the more accurate unsymmetric finite expressions (37) (see Section VII). Even though the individual terms $|A_n\, y^{*n}/n!|$ listed in Table 1 do not decrease fast enough at x = 0.7974 as n increases, quite satisfactory results for the point of separation are obtained as shown in the following.

Table 2 compares results for the point of separation, $x = x_s$ and $\varphi = \varphi_s$, of the boundary layer flow past the circular cylinder with $u_e = 2 \sin \varphi$ and $u_w = v_w = 0$. According to Ch. IX of Reference 48, Blasius' expansion (28) gives separation at $\varphi_s = 108.8°$; this value is unreliable according to Appendix A and as seen by comparison to all the other data listed in Table 2. According to Ch. XII of Reference 48, a one-parameter Kármán-Pohlhausen integral method gave separation at the same point as Blasius' expansion (28). Kosson's method [28], see Appendix B, yields separation at $\varphi_s = 102.45°$ which is considerably lower than the other data listed in Table 2. Terrill's difference-differential method [57, 58] gives separation at $\varphi_s = 104.45°$. Witting [71] determined $\varphi_s = 105.1°$ by application of Blasius' expansion for $0 < x \leq 0.75$ and a certain explicit difference scheme for $x > 0.75$. Four results of Schönauer's implicit difference method [54] employing Crocco variables are listed, where h represents the increment of x, and n the number of grid points in the other direction. The approach towards $x_s = 0.9117$ is seen as h and n^{-1} decrease. With regard to the derived method, the computer run underlying the dashed line in Figure 13 indicates a change of sign of $c_f(x)\, Re^{1/2}$ between the neighboring grid points 0.894 and 0.906. In the column pertaining to the derived method, therefore, separation is indicated at $x_s = 0.90$.

Even though error estimates are not available for any one of the data listed in Table 2, inspection of the various separation points renders $x_s = 0.911$, i.e., $\varphi_s = 104.4°$, the most likely answer. It is expected that the results of the derived method will approach this value as the stepsize Δx is decreased and as the calculation method becomes more accurate in the vicinity of the separation point due to employing the special formulas (21) for the coefficients in connection with expressions (37) for the derivatives. Even now, the results of the derived method look quite promising in view of the amount of evaluation work involved: they have been computed by solving an integro-differential equation depending on one variable only, whereas Schönauer's, Terrill's, and Witting's results follow from difference and difference-differential methods with two independent variables.

X. APPLICATION OF THE METHOD TO GENERAL CYLINDERS

The application of the derived method to arbitrary smooth profiles can be explained appropriately by discussion of the following special case: the flow past an impermeable cylinder with elliptic cross section having a ratio $\lambda = b/a = 0.25$ of minor axis b to major axis a and the major axis aligned with the free stream.

At first, the potential flow distribution $u_e(x_E)$ is determined by conformal representation of the ellipse (subscript E) on the circle (subscript C). The conformal representation relates the sinusoidal $u_e(x_C)$-distribution to

$$u_e(x_E)/u_\infty = \frac{1 + \lambda}{\sqrt{1 + \lambda^2 \operatorname{ctg}^2 \varphi_C}}$$

(Ch. II of Reference 49) where the polar angle φ_C measures from the stagnation point. The conformal representation gives the following relations between φ_C and the Cartesian coordinates ξ and η of the plane of the ellipse: $\xi = a \cos\varphi_C$ and $\eta = b \sin \varphi_C$. The arc length x_E is determined as a function of ξ (and thus φ_C) by use of elliptic integral tables. To facilitate the computer evaluations, $u_e(x_E)$ and its pertinent derivatives are represented by polynomials

$$\left.\begin{aligned} x_E &= \sum_{n=0}^{4} \alpha_{\sigma,n} \varnothing_E^n \\ \text{and} \qquad u_e &= \sum_{n=0}^{5} \beta_{\sigma,n} x_E^n \end{aligned}\right\} \quad \text{for } \varnothing_{\sigma,E} \leqq \varnothing \leqq \varnothing_{\sigma+1,E}, \quad \sigma = 0, 1, \ldots$$

(40)

(41)

Each pair of these polynomials is valid for a suitably selected section of $\varnothing_E$-scale between $\varnothing_{\sigma,E}$ and $\varnothing_{\sigma+1,E}$. For the ellipse under discussion, Table 3 presents the coefficients $\alpha_{\sigma,n}$ and $\beta_{\sigma,n}$ and also their ranges of validity, $\varnothing_{\sigma,E}$ to $\varnothing_{\sigma+1,E}$. The following expressions have been used in H_o:

$$u_e = 39.8\, x_E \qquad 0 \leqq x_E \leqq 0.00313$$

and for and (42)

$$x_E = \sqrt{2\phi_E/39.8}, \qquad 0 \leqq \phi_E \leqq 0.1948 \times 10^{-3}.$$

For the ellipse, Figure 14 compares results of the derived method by use of expansion (16), solid line, and expansion (22), dashed line, both with 9 terms evaluated. It is remarkable that expansion (22) yields good results quite close to its singularity at the separation point. Table 4 presents the numerical values of the individual terms $A_n\, y^n/n!$ at station $x = 0.7151$ and $y^* = 1.830$. It is seen that the terms decrease fairly rapidly with increasing index n, even though y^* exceeds one considerably and even though the u-profile in sections x = const. has acquired a point of inflection at x = 0.53, i.e., a considerable distance upstream of x = 0.7151.

Unfortunately, no accurate data were available to check the curves presented in Figure 14. Results of a Kármán-Pohlhausen integral method for the ellipse under discussion are given in a very small graph in Ch. XII of Reference 48. Since this graph can be read only with considerable error, a comparison to the results derived here is rather questionable. It should be mentioned only that the point of separation is estimated at $x \equiv \bar{x}/\bar{L} = 0.86$ from the graph in Reference 48, whereas the solid line in Figure 14 indicates separation at x = 0.86.

It is quite remarkable that the derived method gives satisfactory results for the ellipse under discussion even though equations (40) and (41) approximate $u_e(\phi_E)$ by polynomials whose derivatives possess at least one discontinuity at each transition point between neighboring polynomials. It may be concluded that the derived method is applicable if $u_e(x)$ is represented by a function with piecewise continuous derivatives provided the discontinuities are sufficiently small. This consideration should also apply to $u_w(x)$ and $v_w(x)$. Both Blasius' and Görtler's expansions (see Introduction) require an analytical function for $u_e(x)$ or the representation of $u_e(x)$ by <u>one</u> polynomial for the entire x-range to be covered by the series solution.

XI. APPLICATION OF THE METHOD TO BOUNDARY LAYER FLOWS WITH MASS TRANSFER

It is known that the separation point of a laminar boundary layer can be influenced by mass transfer across the wall, e.g., Ch. XIII of Reference 48. Both blowing and suction demand a wall with pores or slots and a suitable plumbing system. The local inclination $\theta = tg^{-1}(v_w/u_w)$ of the mass transfer vector with components $\rho u_w(x)$ and $\rho v_w(x)$ is determined by the angle θ which

these channels make relative to the wall's outer tangent plane at station $x = \text{const}$. Design considerations require $|\theta|$ to exceed a certain minimum value. The case $\theta = 0$ represents a moving wall without mass transfer. The case $u_{w,j-1}(x) = c_{j-1} = \text{const.}$ for $x_{j-1} \leqq x \leqq x_j$ and $v_w(x) \equiv 0$ can be realized by placing a conveyor belt of speed c_{j-1} in the segment $x_{j-1} \leqq x \leqq x_j$ of the wall. If the pores and/or slots are sufficiently densely distributed over a region of the wall, the rapidly fluctuating functions $\rho u_w(x)$ and $\rho v_w(x)$ may be averaged, i.e., replaced by smoother or even constant functions $\rho u_w(x)$ and $\rho v_w(x)$.

The derived method has been applied to study the boundary layer on a circular cylinder by use of expansion (16) for the five mass transfer situations listed as cases 2 - 6 in Table 5. The function M(x) in Table 5 is defined as follows:

$$M(x) = \begin{cases} 0 & \text{for} \quad 0 \leqq x \leqq 0.08, \\ N(x) & \text{for} \quad 0.08 \leqq x \leqq 0.12, \text{ and} \\ 0.2 & \text{for} \quad 0.12 \leqq x \leqq x_s. \end{cases} \tag{43}$$

The continuous transition function N(x) satisfies the conditions $N(0.08) = 0$ and $N(0.12) = 0.2$. For simplicity, mass transfer is assumed to be zero for $x \leqq 0.08$ so that the tables given in Ch. V of Reference 48 can be used for the stagnation point solution in H_o. It is possible, though, to solve the pertinent ordinary differential equation in a vicinity of the stagnation point if both $u_w(x)$ and $v_w(x)$ are constant there.

Figure 15 presents $c_f(x)\, Re^{1/2}$ as following from the derived method for cases 1 - 3 in Table 5. In these three cases, $u_w(x) \equiv 0$. As compared to a zero mass transfer situation, normal suction raises the $c_f(x)\, Re^{1/2}$-curve and delays separation at the same time. Normal blowing has the opposite effect. Figure 16 shows $c_f(x)\, Re^{1/2}$ for cases 4 - 6 in Table 5 which pertain to positive tangential velocity components at the wall. The normal mass transfer component $\rho v_w(x)$ exerts the same qualitative effect on the separation point regardless of whether $\rho u_w(x)$ is positive or zero. Comparison of Figures 15 and 16 shows that the application of a positive tangential mass transfer component $\rho u_w(x)$ diminishes $c_f(x)\, Re^{1/2}$ and shifts x_s in the downstream direction. Figure 17 presents $c_f(x)\, Re^{1/2}$ for cases 1, 2, and 4 of Table 5. This figure demonstrates that the application of the tangential mass transfer component $M(x) \geqq 0$, case 4, more than compensates for the shift of x_s in upstream direction when a normal blowing situation, $M(x) \geqq 0$, case 2, is compared to zero mass transfer, case 1. With regard to transpiration cooling of a wall, it may be concluded that the undesirable influence which normal blowing exerts on the location of the separation point can be avoided by inclining the jets emitted from the slots or holes in the downstream direction.

Figure 18 presents $c_f(x)\ Re^{1/2}$ as following from the derived method by use of expansion (16) for a cylinder with the elliptic cross section employed in Section X: ratio $\lambda = b/a = 0.25$ of minor axis b to major axis a, and major axis aligned with the free stream. The solid line represents the zero mass transfer case of Figure 14. The dashed line stands for the mass transfer situation defined in equation (43) when $N(0.12) = 0.2$, $u_w(x) \equiv 0$, and $v_w(x) = - M(x)$. It is seen in Figure 18 that this distribution of suction, $-0.2 \leqq v_w(x) \equiv Re^{1/2}\ \bar{v}_w(x)/\bar{u}_\infty \leqq 0$, has negligible influence on $c_f(x)\ Re^{1/2}$ in the region of accelerated boundary layer flow, except at the peak of the wall friction.

The derived method has been applied by use of expansion (16) to calculate the boundary layer past a circular cylinder with $u_e(x) = 2 \sin \varphi$ and suction through a sequence of slots in the cylinder wall. A continuous distribution $v_w(x) = - 0.2 \sin^2 [(x - x_\beta)/(x_{\beta+1} - x_\beta)]$ was assumed over the width $x_\beta \leqq x \leqq x_{\beta+1}$ of each slot. The smooth curve representing $c_f(x)\ Re^{1/2}$ for the circular cylinder without mass transfer becomes wavy due to the presence of slots. Numerical results are not presented here because of a still unresolved stability phenomenon: the magnitude of the terms $A_n\ y^n/n!$ in expansion (16) decreases rapidly with increasing n provided the slots are restricted to a region where $c_f'(x)\ Re^{1/2}$ exceeds a small negative number; the presence of slots in the region of strongly decreasing wall friction, though, causes the computation procedure to become unstable. This failure of the derived method may very well disappear if special formulas for the coefficients are employed, similar to (21), in connection with the expressions (37) for the derivatives of $A_1(x)$. Necessarily, however, the accuracy of approximating the inner solution by polynomials with a given number of terms must decrease as $c_f(x)\ Re^{1/2}$ becomes wavy due to the concentration of mass transfer in narrow slots. A comparable influence on the accuracy is to be expected for wavy functions $u_e(x)$; in particular, theorem (IIa) in Section II indicates that the number of points of inflection of u(x, y) in sections x = const. increases together with the changes of sign of $u_e'(x)$. These considerations show that the accuracy of the derived method depends on the smoothness of u(x, y) in H.

XII. COMPARISON WITH KÁRMÁN-POHLHAUSEN INTEGRAL METHODS

As is exemplified by the separation data listed in Table 2, the accuracy of one-parameter integral methods is rather unsatisfactory in the region of increasing pressure. This is mainly due to the fact that the upstream history is neglected in the calculations at any grid point. At the expense of computation work, the accuracy of integral methods can be increased by use of two form parameters. At every grid point, a double iteration is required to determine these two parameters, whereas the method derived in this paper requires only a single iteration for $2A_1(x) = a_0^2(x) = c_f(x)\ Re^{1/2}$. In addition, however, the derived method involves a reevaluation of the integral in (36) at every grid point. Both the derived method and integral methods are applicable when the velocity distributions $u_e(x)$, $u_w(x)$ and $v_w(x)$ at the boundaries possess piecewise continuous derivatives as discussed in Section X.

As compared to integral methods of any type, the derived method possesses the following advantages in accounting for the physical characteristics of boundary layer flow:

(1) The integral in the right-hand side of equation (36) represents explicitly the entire upstream history of the boundary layer, whereas the ordinary differential equations of integral methods depend explicitly only on an infinitesimal neighborhood in flow direction. The importance of accounting for the entire history of the boundary layer is discussed in the Introduction in connection with References 39 and 50.

(2) The derived method represents the asymptotic transition $u(x, y) \to u_e(x)$ as $y \to \infty$ in a rigorous way, whereas this process in integral methods can be approximated only by use of special functions.

(3) The series expansions (16) and (22) satisfy an infinite number of compatibility conditions at the wall (see Ch. VIII of Reference 48) whereas integral methods in general fulfill only the first one of these conditions. Partial sums of (16) or (22) with n terms still satisfy (n-1) compatibility conditions.

XIII. GENERALIZATIONS OF THE DERIVED METHOD

A given axisymmetric boundary layer problem may be solved by applying the derived method to the planar boundary layer related by Mangler's transformation, e.g., Ch. X of Reference 48. By use of assumptions as Prandtl number one and linear viscosity-temperature relationship, Howarth [23], Illingworth [25], and Stewartson [56] have presented transformations which give compressible boundary layer solutions in terms of incompressible solutions of the type discussed in this paper. In addition to these rather trivial extensions of the range of applicability of the derived method, two genuine generalizations are discussed in the following.

According to p. 152 of Reference 15, von Mises' transformation (6) and (7) yields the following differential equations for stationary laminar compressible boundary layer flow of a perfect gas with constant Prandtl number:

$$\bar{\rho}\bar{u}\,\frac{\partial \bar{u}}{\partial \bar{x}} - \bar{\rho}_e\,\bar{u}_e\,\frac{d\bar{u}_e}{d\bar{x}} = \bar{\rho}\bar{u}\,\frac{\partial}{\partial \bar{\psi}}\left(\bar{\mu}\bar{\rho}\bar{u}\,\frac{\partial \bar{u}}{\partial \bar{\psi}}\right) \tag{44}$$

and

$$\bar{\rho}\bar{c}_p\bar{u}\,\frac{\partial \bar{T}}{\partial \bar{x}} - \bar{\rho}_e\,\bar{c}_{pe}\,\bar{u}_e\,\frac{d\bar{T}_e}{d\bar{x}} = \frac{\bar{\rho}\bar{u}}{Pr}\,\frac{\partial}{\partial \bar{\psi}}\left(\bar{\mu}\bar{\rho}\bar{c}_p\,\frac{\partial \bar{T}}{\partial \bar{\psi}}\,\bar{u}\right) + \bar{\mu}\left(\bar{\rho}\bar{u}\,\frac{\partial \bar{u}}{\partial \bar{\psi}}\right)^2. \tag{45}$$

The thickness of the velocity and the temperature boundary layer are proportional to $Re^{1/2}$ and $Re^{1/2}\ Pr^{1/2}$, respectively, according to Ch. XIV of Reference 48. Since $Pr \cong 1$ in general for one-component gas flow, inner and outer solutions of both the velocity and the temperature boundary layer, respectively, may be matched to each other along one and the same curve $\psi^*(x, y)$, separating the region H_I of the inner solutions from the region H_{II} of the outer solutions. The parameter

$$\bar{\Omega} = \int_0^{\bar{x}} \bar{\mu}_e\ \bar{\rho}_e\ \bar{u}_e\ d\bar{x} \tag{46}$$

is introduced to replace x or $\varnothing$. The outer solutions are defined by initial and boundary conditions of the type (31) and by the following linearized and asymptotically rigorous forms of the differential equations (44) and (45):

$$\frac{\partial(u^2 - u_e^2)}{\partial\Omega} = \frac{\partial^2(u^2 - u_e^2)}{\partial\psi^2} \tag{47}$$

and

$$\frac{\partial(T - T_e)}{\partial\Omega} = \frac{1}{Pr}\frac{\partial^2(T - T_e)}{\partial\psi^2}\ . \tag{48}$$

After suitable changes of notation, the closed-form expressions derived in Appendix C represent the outer solutions of (47) and (48). In particular, along the stream line sections $\psi = \psi_\alpha^*$ of the boundary $\psi^*(x, y^*)$, the outer solutions take the form of (36). The inner solutions of the velocity and the temperature boundary layer can be expanded in series of the type (16) or (22). Substitution of partial sums into the said boundary relations of the outer solution yields two simultaneous integro-differential equations of the type (36) for the friction coefficient $c_f(x)$ and the heat transfer coefficient $c_h(x)$. In analogy to Sections VI and VII, this system can be solved in a stepwise way by use of a double iteration process at each step. The interrelationship between u and T in compressible flow causes u(x, y) and T(x, y) to possess maxima, minima, points of inflection, etc., for initial and boundary distributions which exclude these complicating features in constant-property flow, [4]. In view of discussions at the end of Section XI, this situation requires careful application of the derived method to compressible boundary layer flow.

Because of the underlying assumption $Re \to \infty$, Prandtl's boundary layer theory implies $u = 0(Re^{0})$ and $v = 0(Re^{-1/2})$, i.e., $|v| \ll u$, e.g., Ch. VII of Reference 48. These implications of $Re \to \infty$ are violated in a certain vicinity of the wall if normal mass transfer is prescribed, $u_w(x) \equiv 0$ and $v_w(x) \not\equiv 0$. Provided $Re \gg 1$ and $Re^{1/2} |\bar{v}_w| \ll \bar{u}_\infty$, however, this vicinity is restricted to a narrow subregion of H_I adjacent to the wall. Under the same conditions, the thickness of the boundary layer is sufficiently small so that potential flow past the given profile determines $u_e(x)$ with the required accuracy. To check the validity of boundary layer solutions with normal mass transfer, a special second-order boundary layer theory is proposed which in H_I employs the complete Navier-Stokes equations (e.g., Ch. V of Reference 48),

$$u \frac{\partial u}{\partial x} + v \frac{\partial u}{\partial y} = - \frac{\partial p}{\partial x} + \frac{1}{Re} \left(\frac{\partial^2 u}{\partial x^2} + \frac{\partial^2 u}{\partial y^2} \right)$$

and (49)

$$u \frac{\partial v}{\partial x} + v \frac{\partial v}{\partial y} = - \frac{\partial p}{\partial y} + \frac{1}{Re} \left(\frac{\partial^2 v}{\partial x^2} + \frac{\partial^2 v}{\partial y^2} \right),$$

and in H_{II} the linearized version (29) of von Mises' boundary layer equation (10). In H_I, the expansions (16) are assumed for $u(x, y)$ and $v(x, y)$ which satisfy the continuity equation (4) identically. The corresponding expansion

$$p = \sum_{n=0}^{\infty} B_n(x) \frac{y^n}{n!} \tag{50}$$

for the pressure $p(x, y)$ in H_I has to satisfy the condition

$$\sum_{n=0}^{\infty} B_n(x) \frac{y^{*n}(x)}{n!} = p(x, y^*(x)) = P_e(x) = \text{given} \tag{51}$$

since $p(x, y) \equiv p_e(x)$ in H_{II} and on the boundary line $\psi^*(x)$ separating H_I and H_{II}. Substitution of (16a), (16b), and (50) in (49) yields the coefficients as follows:

$$A_2 = \mathrm{Re}\, B_0', \qquad B_1 = -A_1' \mathrm{Re}^{-1},$$

$$A_3 = -2A_1'', \qquad B_2 = -B_0'' \tag{52}$$

$$A_4 = \mathrm{Re}\, A_1 A_1' - \mathrm{Re}\, B_0''' - B_0'',$$

$$\vdots$$

The coefficients $A_n(x)$, $n \geq 2$, and $B_n(x)$, $n \geq 1$, depend on $A_1(x)$ and $B_0(x)$ only. The expansions (16) and (50) with the coefficients given by (52) are substituted in the boundary relation (33) of the outer solution. A system is obtained consisting of the integro-differential equation (36) and the ordinary equation (51). After appropriate modifications have been made to account for (51), this system can be solved in a stepwise way according to the procedure outlined in Section VII.

XIV. CONCLUSIONS

Prandtl's boundary layer problem is solved by matching outer and inner solutions along the stream line segments $\psi = \psi_\alpha^*$ of the curve $\psi^*(x)$ shown in Figure 1. The closed-form outer solution is obtained from a linearized version of von Mises' boundary layer equation; the linearization error tends to zero as $y \to \infty$. The outer solution yields a relation between $g(\emptyset, \psi_\alpha^*)$ and $\partial g(\emptyset, \psi_\alpha^*)/\partial\psi$. With very little evaluation work, a rough approximation of $c_f(x)\,\mathrm{Re}^{1/2}$ is obtained by evaluating this relation at the wall, i.e., for $\psi_\alpha^* = \psi_w$. This approximation yields a lower bound of the exact friction coefficient if $u_e'(x) > 0$.

The inner solution is represented by expansion (16) in powers of y or by expansion (22) in powers of $(\psi - \psi_w)^{1/2}$. The coefficients of these expansions depend on $c_f(x)\,\mathrm{Re}^{1/2}$ and on the given velocity distributions $u_e(x)$, $u_w(x)$, and $v_w(x)$ at the boundaries. The majority of the numerical results presented in this paper has been computed by use of general expressions for the coefficients and backward difference quotients for their derivatives. According to Section IV, higher order terms cannot be determined with sufficient accuracy in this way. Special formulas for the coefficients and unsymmetric finite expressions for their derivatives are proposed because of this situation.

In case of the circular cylinder with $u_e = 2 \sin\varphi$ and $u_w = v_w \equiv 0$ the accuracy of partial sums of (16) or (22) is tested by use of the available partial sum of Blasius' series expansion. The said deficiency in computing the coefficients manifests itself only in a small vicinity of the separation point. Except for this vicinity, a ten-term partial sum of (16) is sufficient to represent Blasius' u-profile up to $u/u_e = 0.8$. Even at $x/x_s = 0.85/0.90$, the curves representing partial sums with 9, 10, and 11 terms differ very little

up to $u/u_e = 0.9$ if certain shortcomings of Blasius' expansion as $x \to x_s$ are taken into account. Therefore, a negligible error of the inner solution is to be expected in case of the circular cylinder if 11-term partial sums are matched to the outer solution in a range of u/u_e values between $U_2 = 0.7$ and $U_1 = 0.85$. According to Section VII, U_1 and U_2 determine the choice and length of the stream line segments $\psi = \psi_\alpha^*$ of the curve $\psi^*(x)$ separating the regions of the inner and the outer solutions.

Even though $c_f(x)\ Re^{1/2}$ has been computed by use of the said inadequate higher order coefficients, the results for the circular cylinder yield separation quite close ($\delta(x_s)/x_s = 0.01$) to the most likely location as given by other methods. Still better results are expected as the stepsize Δx is decreased and as the more adequate way of calculating the coefficients is employed. Even now, however, the results of the derived method, as compared to difference and difference-differential methods, look quite promising in view of the computation work involved.

The accuracy of approximating the inner solution by polynomials with a given number of terms must decrease as $c_f(x)\ Re^{1/2}$ becomes wavy due to the concentration of mass transfer in narrow slots. A comparable influence on the accuracy is to be expected for a wavy function $u_e(x)$. The derived method is applicable if $u_e(x)$, $u_w(x)$, and $v_w(x)$ are represented by functions with piecewise continuous derivatives, provided the discontinuities are sufficiently small. As compared to integral methods with any number of form parameters, the derived method possesses distinct advantages in accounting for the physical characteristics of the boundary layer flow. About as much numerical work is involved as in two-parameter integral methods. The method as derived requires the boundary layer to begin at a stagnation point. The method can be adapted to profiles with a wedge-type nose.

By use of Mangler's transformation, the derived method is immediately applicable to axisymmetric boundary layer flow. If Howarth's, Illingworth's, or Stewartson's transformations are considered to be valid, the derived method applies to compressible boundary layer flow. The outlined generalization of the method to compressible boundary layer flow with arbitrary property laws requires careful application because of the complexities of possible velocity and temperature profiles. The other generalization, a special second order boundary layer theory, demands very little extra work as compared to the presented version of the method.

As is true for the vast majority of other approximate methods in boundary layer theory, no general error estimate is available for the derived method. For the outer solution, though, an estimate of this type is derived by use of the lemma of Nagumo and Westphal. According to the brief outline given in Appendix D, this lemma may be employed in conjunction with the derived method to determine rigorously valid bounds of exact boundary layer solutions.

TABLE 1. NUMERICAL VALUES OF THE INDIVIDUAL TERMS IN PARTIAL SUMS OF (16) AND (22) FOR THE CIRCULAR CYLINDER (FIGURE 13)

	Expansion (22)		Expansion (16)	
	$x = 0.4586$ $\varphi = 52.6$		$x = 0.7010$ $\varphi = 80.3$	$x = 0.7974$ $\varphi = 91.4$
	$\psi^* = 0.4812$		$y^* = 0.9670$	$y^* = 1.063$
$a_0\ \psi^{*1/2}$	1.7378	$A_1\ y^*$	2.4064	1.8705
$a_1\ \psi^*$	-0.39470	$A_2\ y^{*2}/2!$	-0.61951	0.10843
$a_2\ \psi^{*3/2}$	-0.07844	$A_3\ y^{*3}/3!$	0	0
$a_3\ \psi^{*2}$	-0.01866	$A_4\ y^{*4}/4!$	-0.58465	-0.91655
$a_4\ \psi^{*5/2}$	0.71788×10^{-2}	$A_5\ y^{*5}/5!$	0.53899	0.63629
$a_5\ \psi^{*3}$	0.47181×10^{-2}	$A_6\ y^{*6}/6!$	-0.045237	0.012295
$a_6\ \psi^{*7/2}$	-8.1764×10^{-4}	$A_7\ y^{*7}/7!$	-0.15632	-0.21017
$a_7\ \psi^{*4}$	1.8440×10^{-4}	$A_8\ y^{*8}/8!$	0.099186	0.14460
$a_8\ \psi^{*9\ 2}$	-3.4179×10^{-5}	$A_9\ y^{*9}/9!$	-0.025330	-0.034425
		$A_{10}\ y^{*10}/10!$		-0.053514
		$A_{11}\ y^{*11}/11!$		0.077657
		$A_{12}\ y^{*12}/12!$		-0.036679
$u(x, \psi^*)/u_e(x)$	0.7967	$u(x, y^*)/u_e(x)$	0.8458	0.8009

TABLE 2. SEPARATION POINT x_s OF THE BOUNDARY LAYER AT THE CIRCULAR CYLINDER

Author	Blasius		Kosson	Witting	Terrill	Schönauer				Adams/Berry
Reference	48, Ch. IX	48, Ch. XII	28	71	57	54				
Comments	Partial sum (28) of series expansion	One parameter integral method	Matching method, approximation	Difference method in continuation of (28)	Difference-differential method	Difference Method h=0.1 n=10	Difference Method 0.1 100	Difference Method 0.005 100	Difference Method 0.005 300	Matching Method, preliminary results
Separation Point $x = \bar{x}/2\bar{R}$	0.9495	0.9495	0.8943	0.917	0.9115	0.898	0.9015	0.911	0.9117	0.90
Separation Angle φ	108.8°	108.8°	102.45°	105.08°	104.45°	102.90°	103.30°	104.39°	104.47°	103.13°

TABLE 3. COEFFICIENTS IN THE POLYNOMIAL EXPRESSIONS (40) AND (41) PERTAINING TO THE ELLIPSE 1:14

x-range	$\emptyset$-range	α_0	α_1	α_2	α_3	α_4
$0.00313 \leqq x \leqq 0.01975$	$0.0001948 \leqq \emptyset \leqq 0.0070142$	1.8818843×10^{-3}	6.7492604	-1822.5411	305990.15	-18754890.
$0.01975 \leqq x \leqq 0.0603$	$0.0070142 \leqq \emptyset \leqq 0.043883$	.0074851	2.020792	-45.024752	944.09701	-7800.1065
$0.0603 \leqq x \leqq 0.1268$	$0.043883 \leqq \emptyset \leqq 0.115$	.01973704	.94900275	-.59872593	1.0791514	-.77037815
$0.1268 \leqq x \leqq 0.2156$	$0.115 \leqq \emptyset \leqq 0.225$	.01973704	.94900275	-.59872593	1.0791514	-.77037815
$0.2156 \leqq x \leqq 0.88$	$0.225 \leqq \emptyset \leqq 1.05$	.035	.81	0	0	0

Continued

β_0	β_1	β_2	β_3	β_4	β_5
0	39.794878	71.373905	-37698.06	967820.68	-8055491.6
-.7586	55.5	-1222.74	15310.324	-101552.94	273254.8
.58034	12.719	-94.949	253.07	0	0
.93789	3.3253945	-13.5813	20.012511	0	0
1.09941	1.0128348	-2.62257	3.129756	-1.45936	0

TABLE 4. NUMERICAL VALUES OF THE INDIVIDUAL TERMS IN A PARTIAL SUM OF (16) FOR THE ELLIPTIC CYLINDER (FIGURE 14)

	Expansion (16) $x = 0.7151$ $y^* = 1.830$
$A_1\ y^*$	0.87662
$A_2\ y^{*2}/2$	0.14866
$A_3\ y^{*3}/3!$	0
$A_4\ y^{*4}/4!$	-0.29075
$A_5\ y^{*5}/5!$	0.14806
$A_6\ y^{*6}/6!$	0.83699×10^{-2}
$A_7\ y^{*7}/7!$	-9.6007×10^{-2}
$A_8\ y^{*8}/8!$	7.1677×10^{-2}
$A_9\ y^{*9}/9!$	0.35023×10^{-2}
$u(x, y^*)/u_e(x)$	0.6986

TABLE 5. AUXILIARY FUNCTIONS FOR MASS TRANSFER AT THE CIRCULAR CYLINDER

Case	$u_w(x)$	$v_w(x)$
1	0	0
2	0	M(x)
3	0	-M(x)
4	M(x)	M(x)
5	M(x)	0
6	M(x)	-M(x)

See equation (43).

The subregions H_I, etc., are defined in Section II. Heavy lines refer to the boundaries of subregions. The subscript α takes the values 0, 1, and 2 before separation, $x = x_s$, is reached.

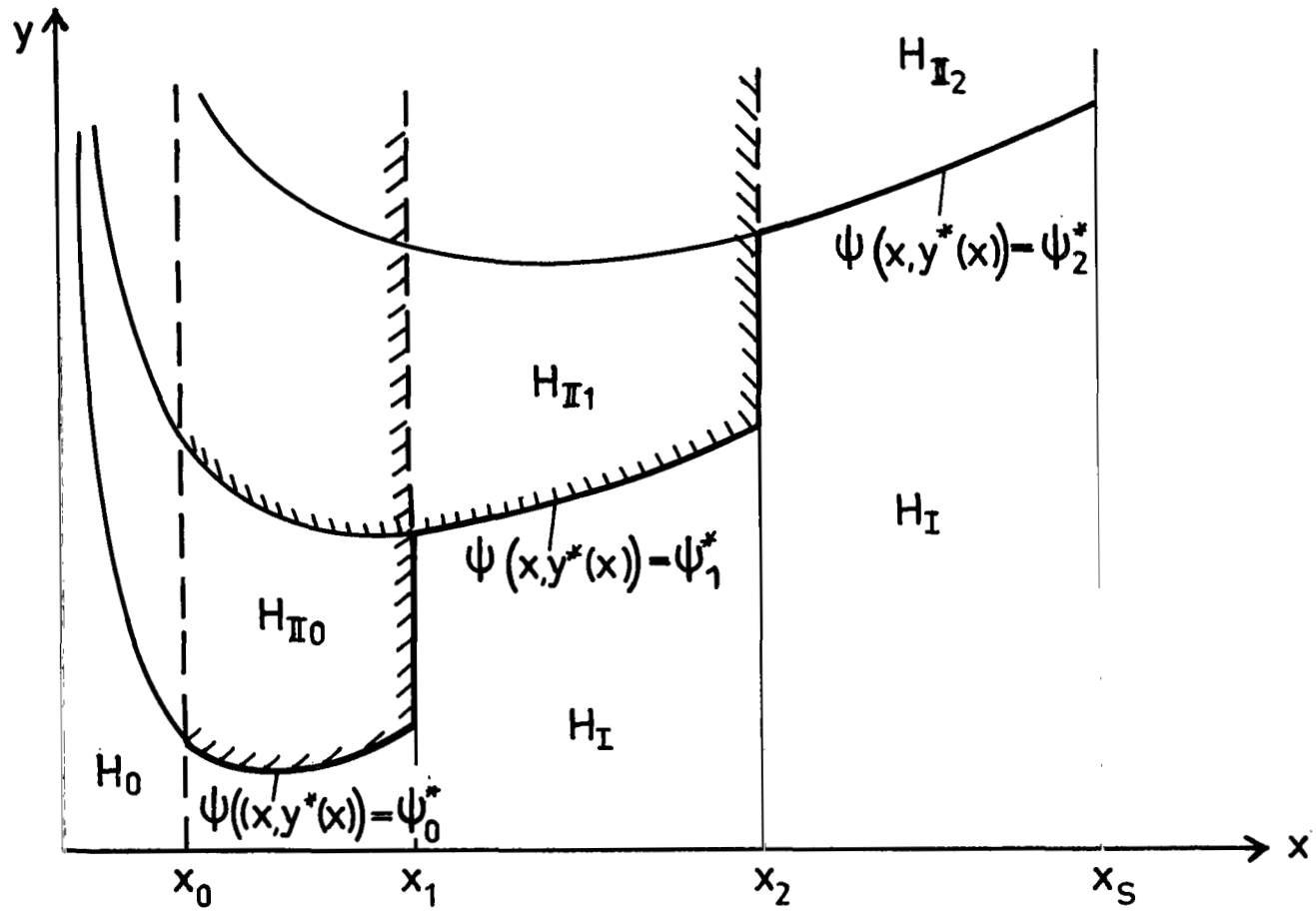

FIGURE 1. FLOW PLANE AND NOTATIONS

B refers to the available six-term partial sum of Blasius' expansion (27). The numbers at the curves refer to the number of terms in partial sums of (16). The coefficients of (16) have been evaluated by use of the general formulas (19) and (20) for the coefficients and backward difference quotients for their derivatives.

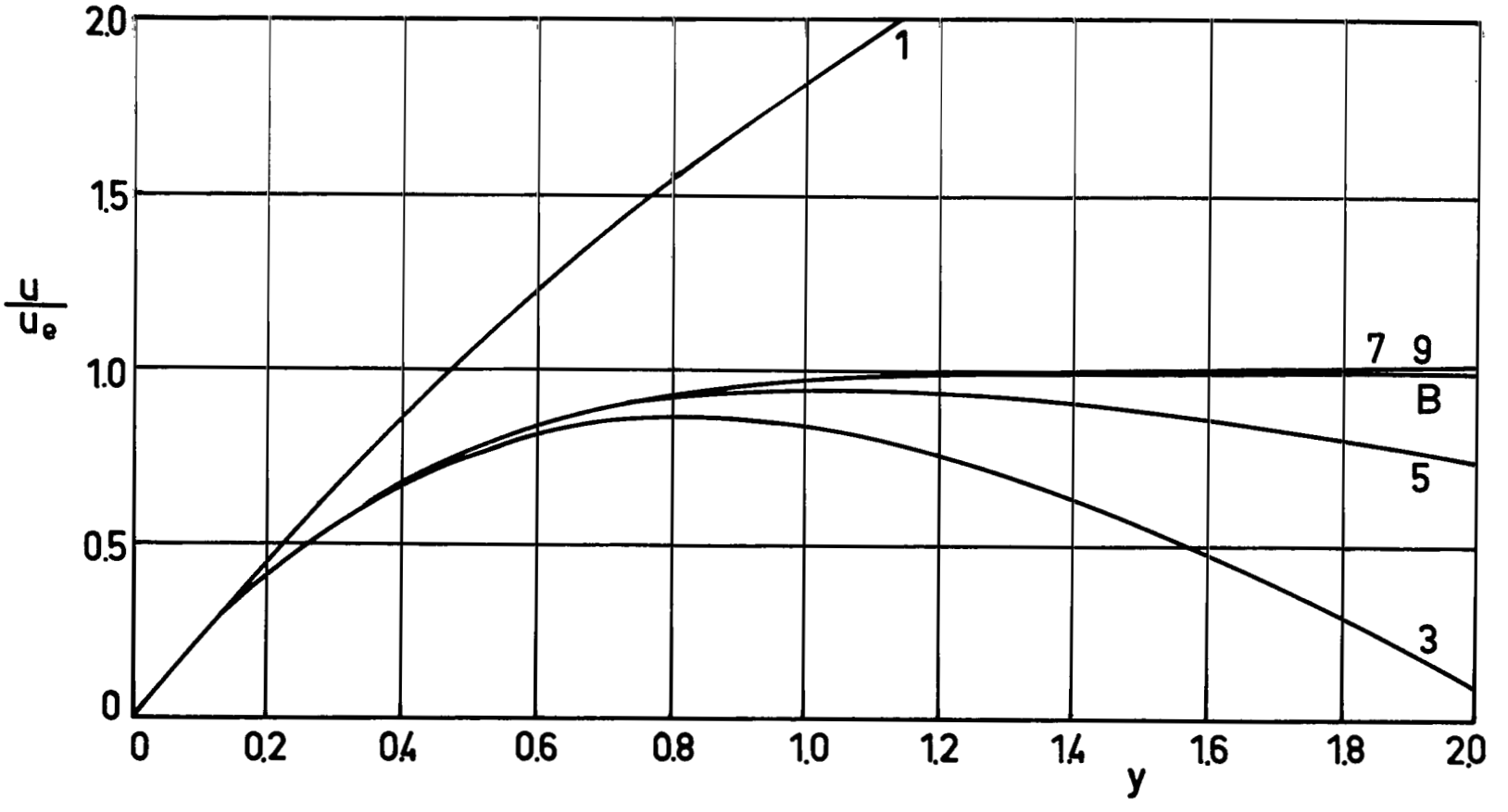

FIGURE 2. $u(x, y)/u_e(x)$ AT $x = 0.1$ ($\varphi = 11.5°$) FOR THE CIRCULAR CYLINDER

B refers to the available six-term partial sum of Blasius' expansion (27). The numbers at the curves refer to the number of terms in partial sums of (16). The coefficients of (16) have been evaluated by use of the general formulas (19) and (20) for the coefficients and backward difference quotients for their derivatives.

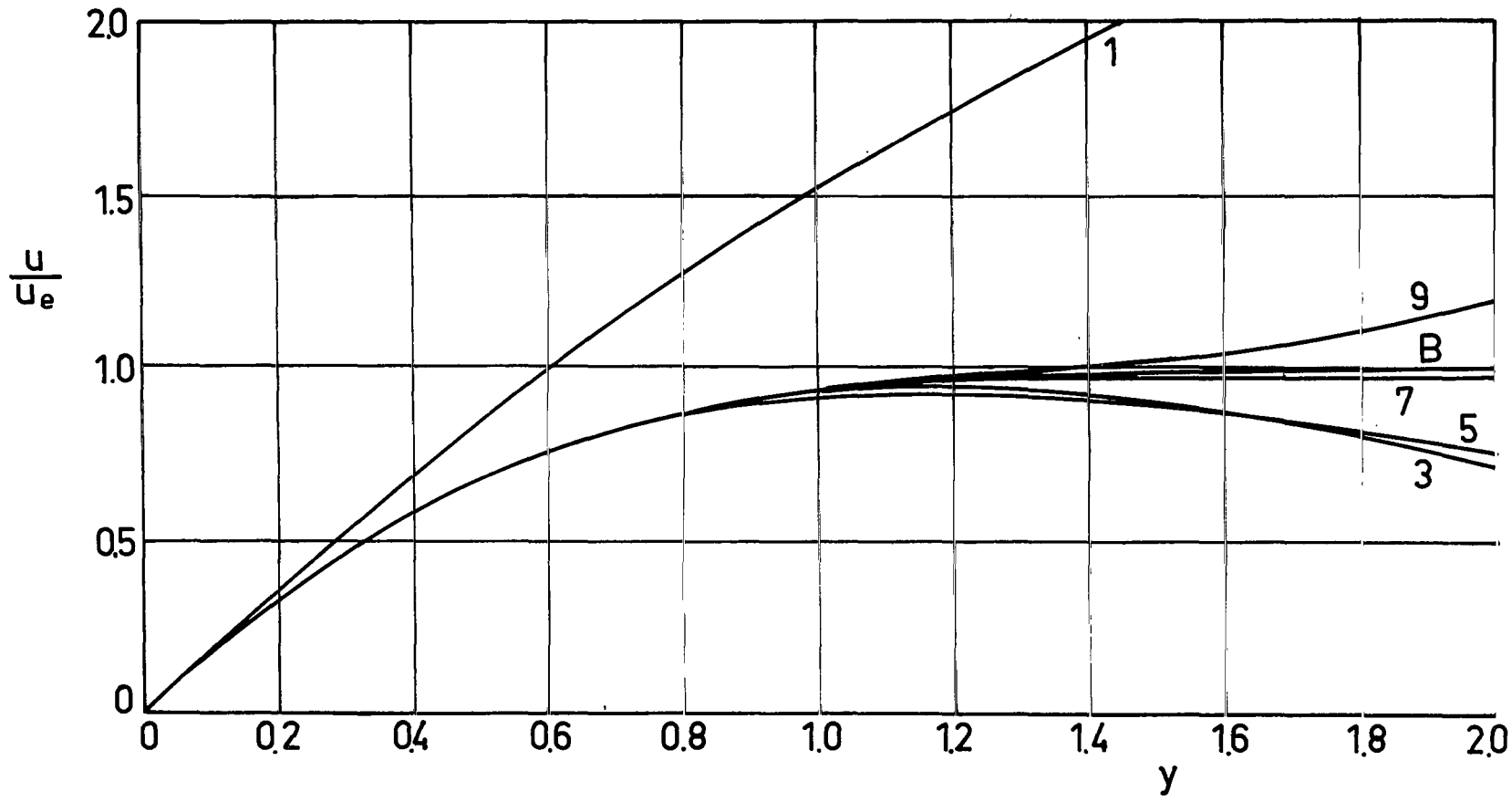

FIGURE 3. $u(x, y)/u_e(x)$ AT $x = 0.5$ ($\varphi = 57.2°$) FOR THE CIRCULAR CYLINDER

B refers to the available six-term partial sum of Blasius' expansion (27). The numbers at the curves refer to the number of terms in partial sums of (16). The coefficients of (16) have been evaluated by use of the general formulas (19) and (20) for the coefficients and backward difference quotients for their derivatives.

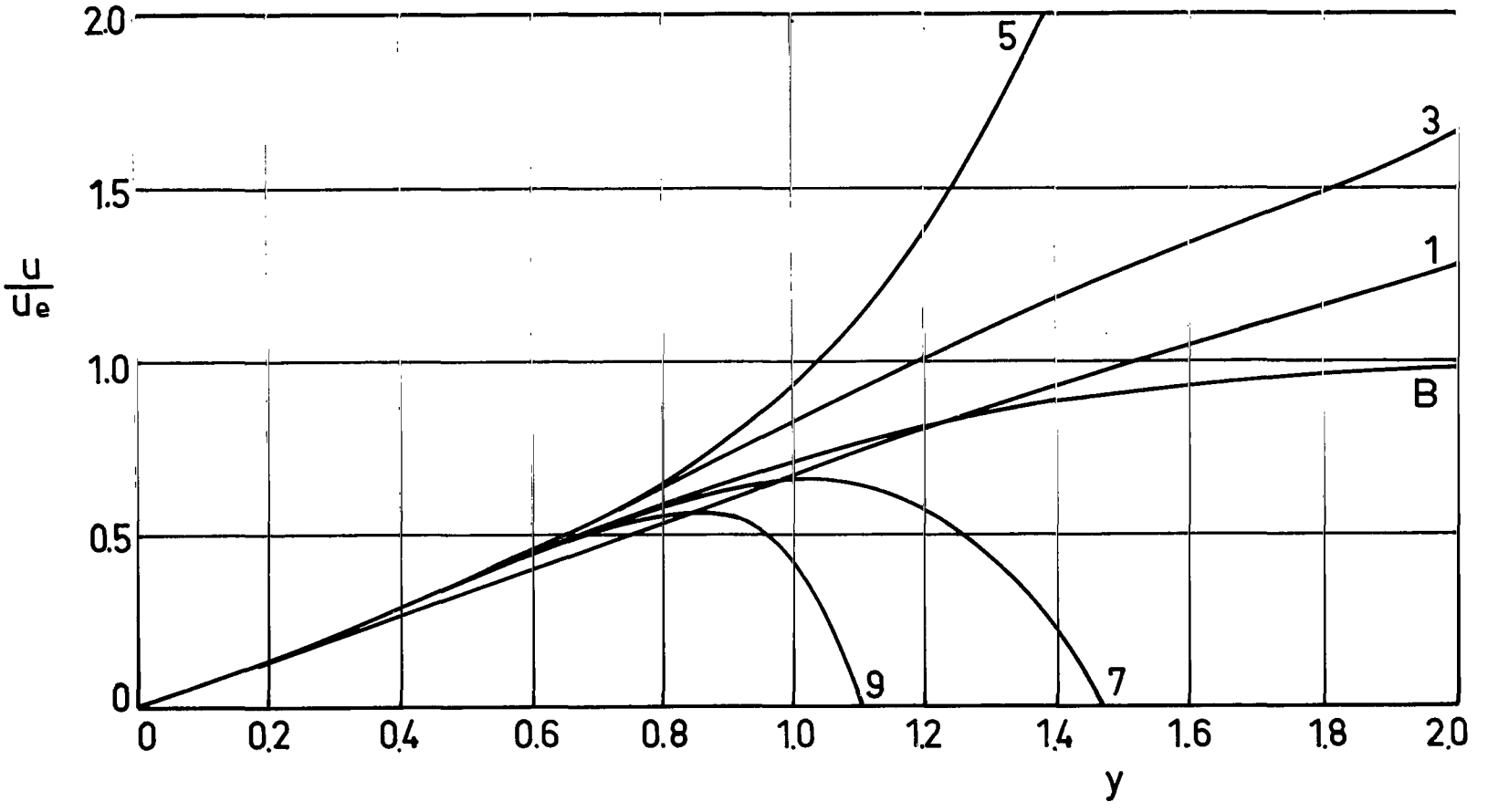

FIGURE 4. $u(x, y)/u_e(x)$ AT $x = 0.85$ ($\varphi = 97.4°$) FOR THE CIRCULAR CYLINDER

B refers to the available six-term partial sum of Blasius' expansion (27). The numbers at the curves refer to the number of terms in partial sums of (16). The coefficients of (16) have been evaluated by use of the special formulas (21) for the coefficients and the unsymmetric finite expressions (37) for their derivatives.

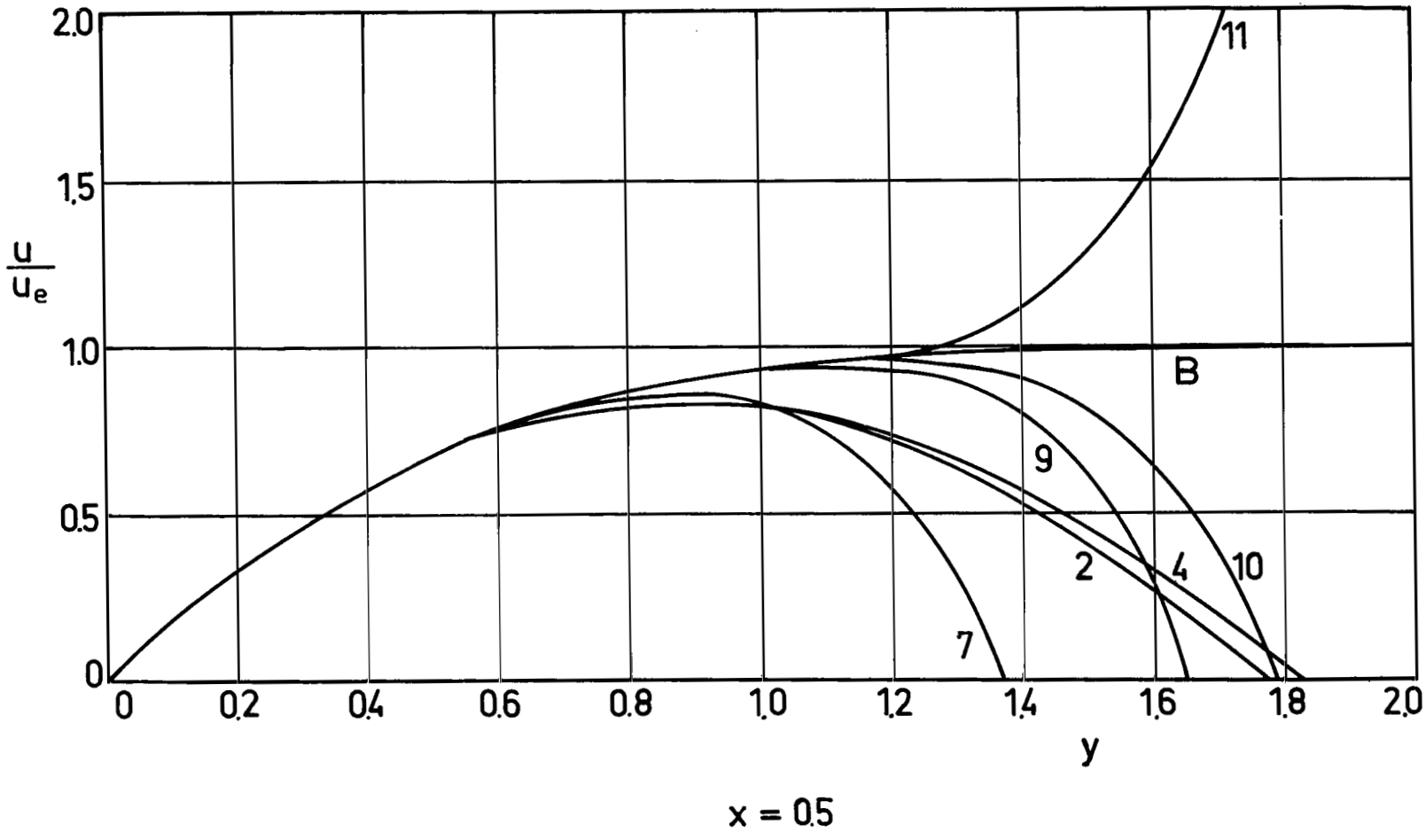

FIGURE 5. $u(x, y)/u_e(x)$ AT $x = 0.5$ ($\varphi = 57.2°$) FOR THE CIRCULAR CYLINDER

B refers to the available six-term partial sum of Blasius' expansion (27). The numbers at the curves refer to the number of terms in partial sums of (16). The coefficients of (16) have been evaluated by use of the special formulas (21) for the coefficients and the unsymmetric finite expressions (37) for their derivatives.

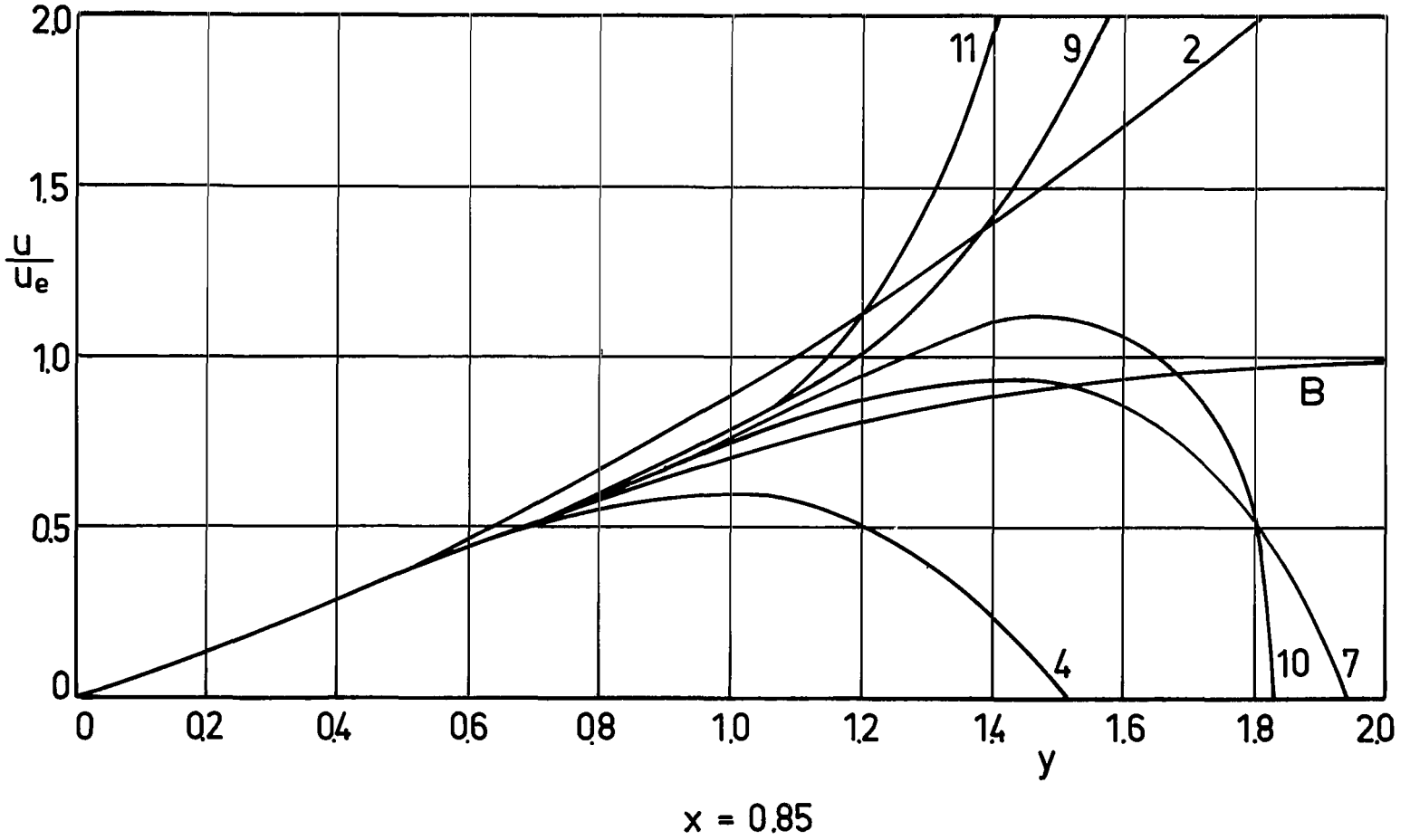

FIGURE 6. $u(x, y)/u_e(x)$ AT $x = 0.85$ ($\varphi = 97.4°$) FOR THE CIRCULAR CYLINDER

B refers to the available six-term partial sum of Blasius' expansion (27). The numbers at the curves refer to the number of terms in partial sums of (22). The coefficients of (22) have been evaluated by use of the general formulas (24) - (26) for the coefficients and backward difference quotients for their derivatives.

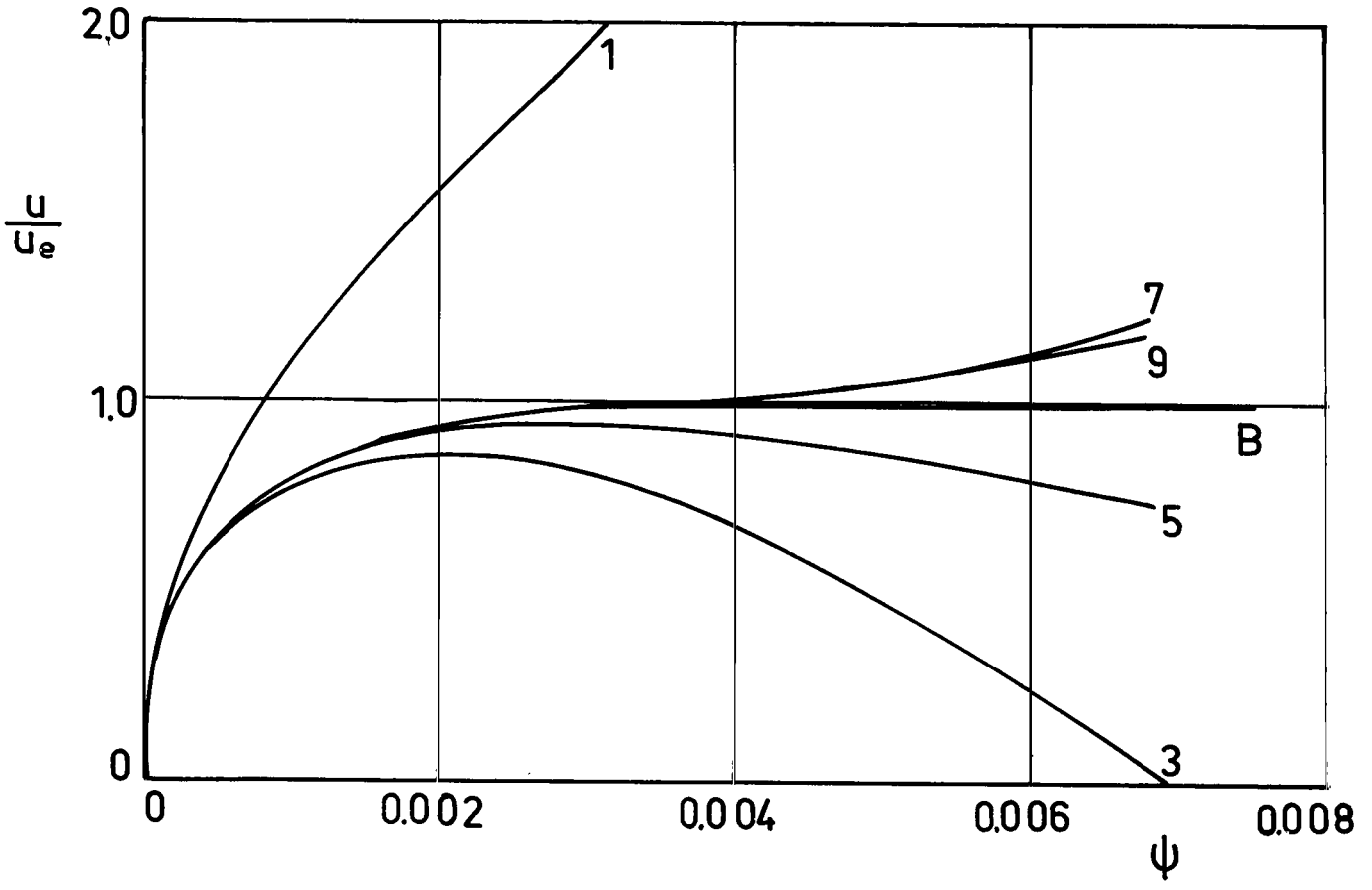

FIGURE 7. $u(x, y)/u_e(x)$ AT $x = 0.1$ ($\varphi = 11.5°$) FOR THE CIRCULAR CYLINDER

B refers to the available six-term partial sum of Blasius' expansion (27). The numbers of the curves refer to the number of terms in partial sums of (22). The coefficients of (22) have been evaluated by use of the general formulas (24) - (26) for the coefficients and backward difference quotients for their derivatives.

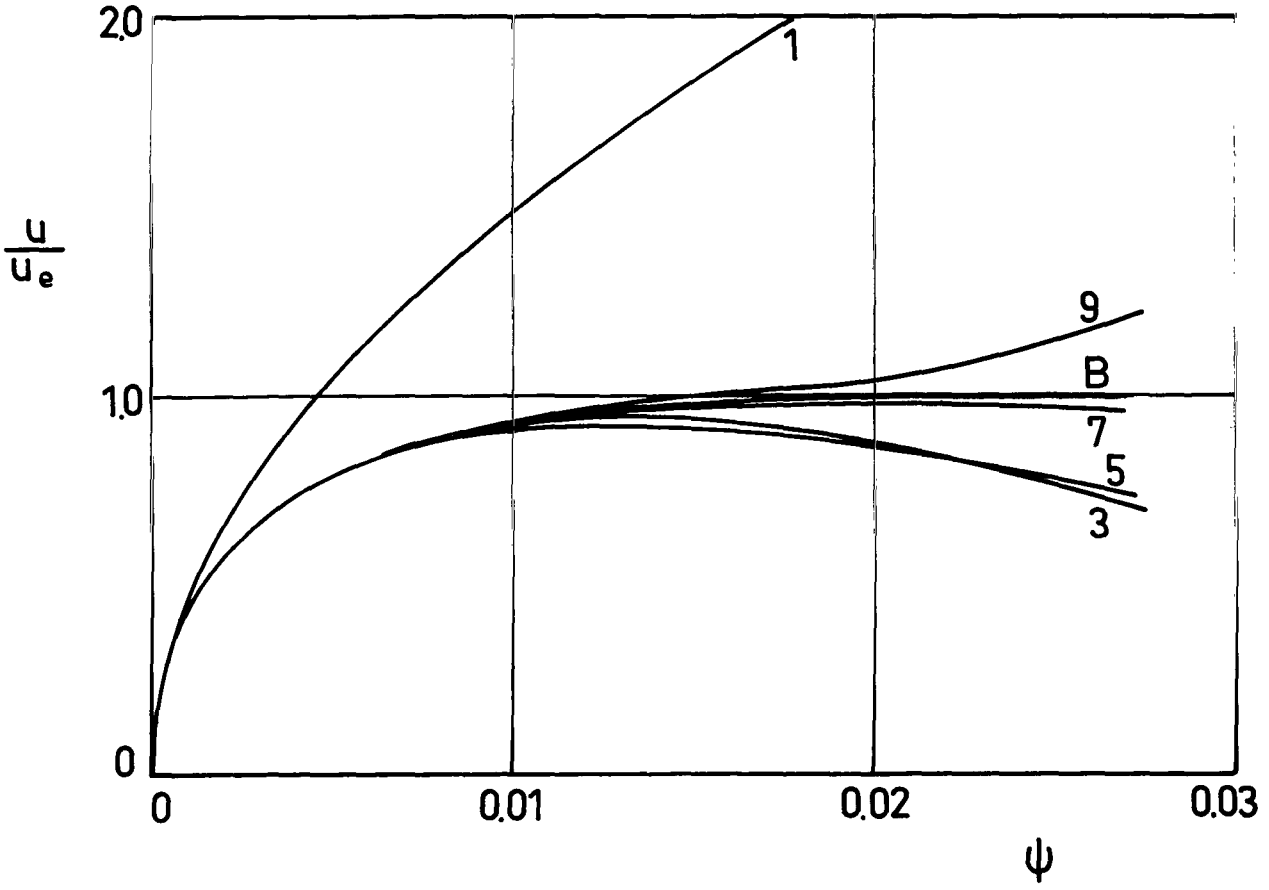

FIGURE 8. $u(x, y)/u_e(x)$ AT $x = 0.5$ ($\varphi = 57.2°$) FOR THE CIRCULAR CYLINDER

B refers to the available six-term partial sum of Blasius' expansion (27). The numbers at the curves refer to the number of terms in partial sums of (22). The coefficients of (22) have been evaluated by use of the general formulas (24) - (26) for the coefficients and backward difference quotients for their derivatives.

FIGURE 9. $u(x, y)/u_e(x)$ AT $x = 0.85$ ($\varphi = 97.4°$) FOR THE CIRCULAR CYLINDER

The solid line represents (28) following from a six-term partial sum of Blasius' expansion (27). The dashed line represents (34), which is a result of employing the outer solution for the entire boundary layer.

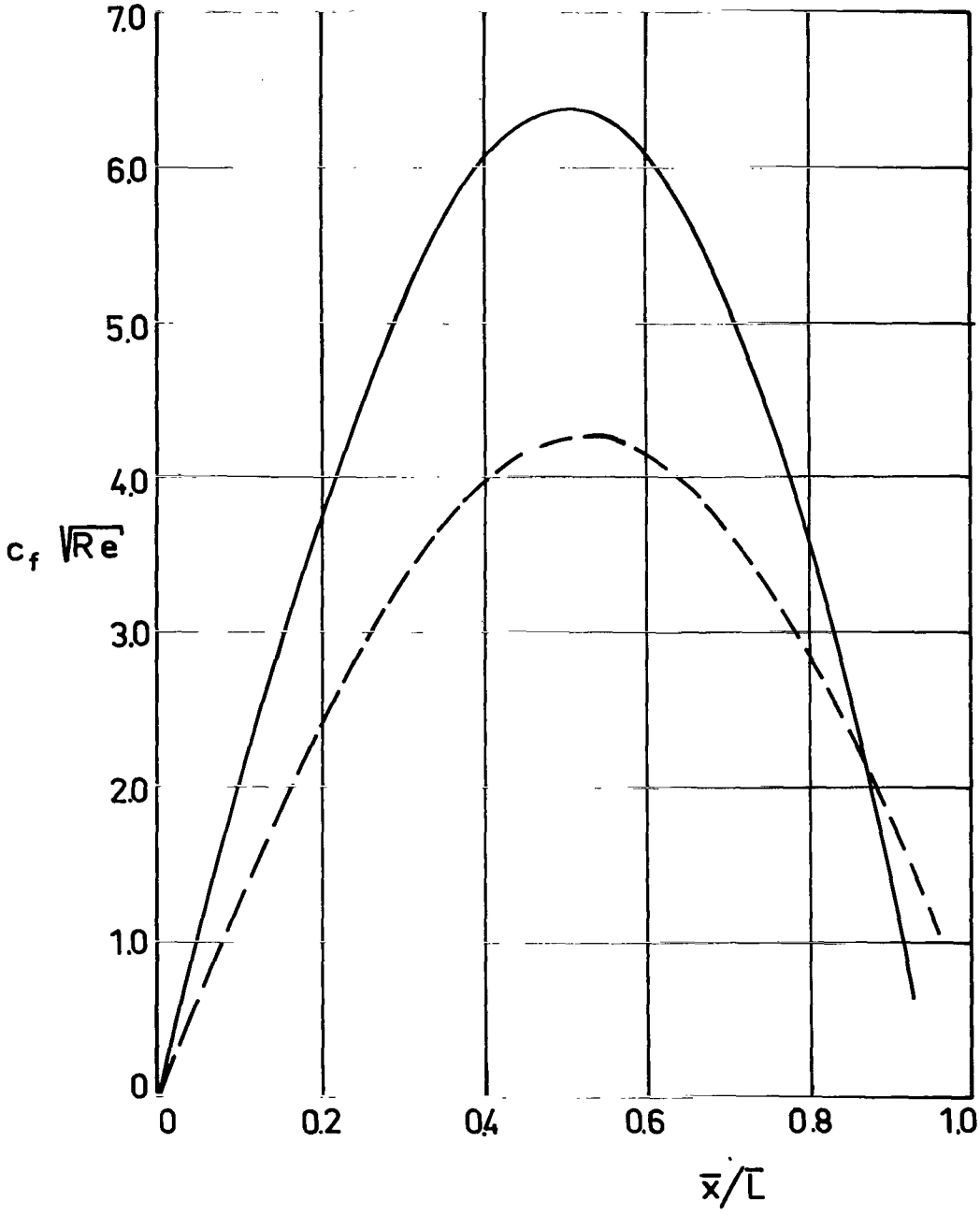

FIGURE 10. $c_f(x)\ Re^{1/2}$ FOR THE CIRCULAR CYLINDER, FROM BLASIUS' EXPANSION (28) AND FROM THE APPROXIMATION (34)

The solid line represents (28) following from a six-term partial sum of Blasius' expansion (27). The dashed line represents (34), which is a result of employing the outer solution for the entire boundary layer.

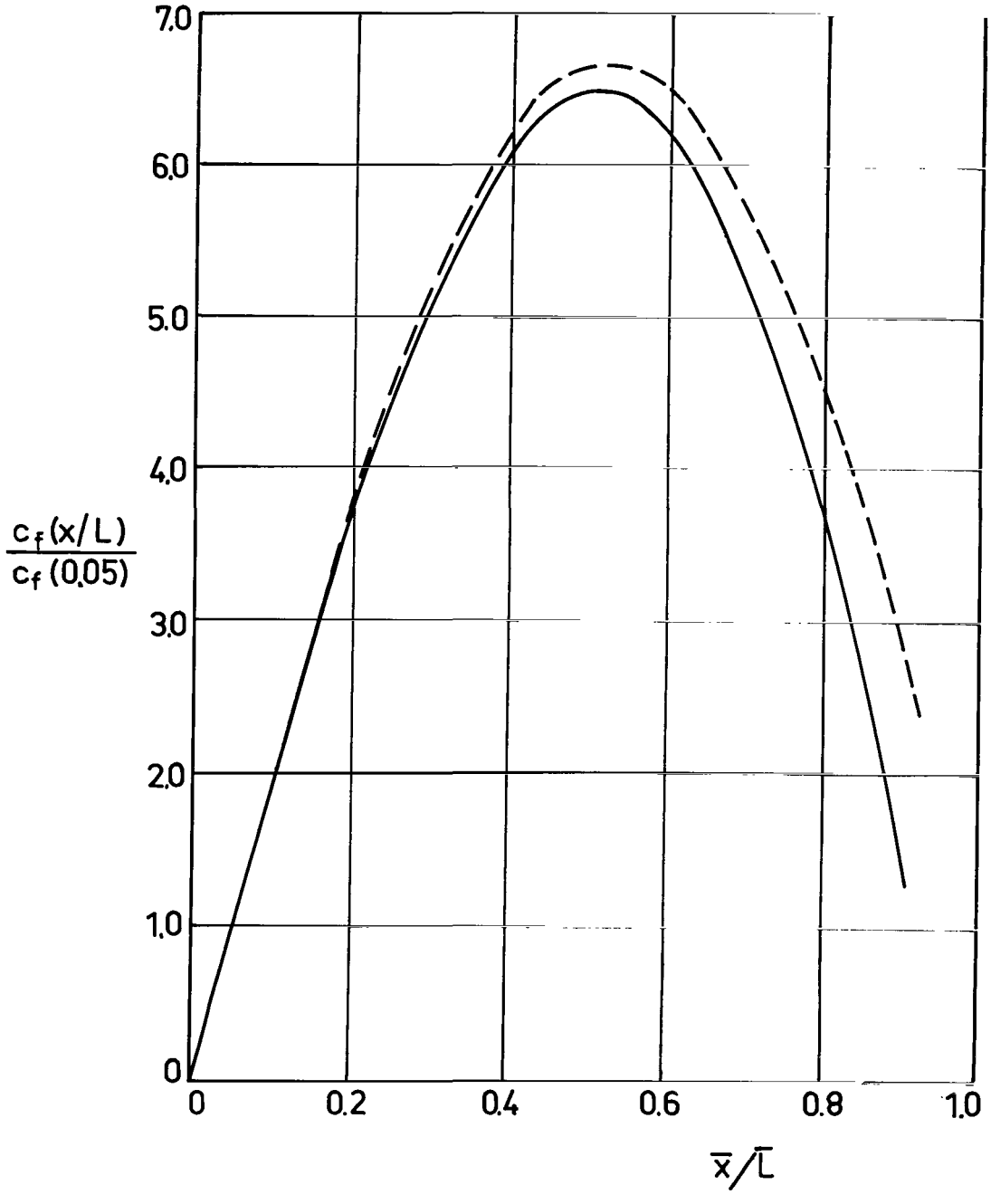

FIGURE 11. $c_f(x)/c_f(0.05)$ FOR THE CIRCULAR CYLINDER, FROM BLASIUS' EXPANSION (28) AND FROM THE APPROXIMATION (34)

The solid line represents (28) following from a six-term partial sum of Blasius' expansion (27). The dashed line represents partial sums of (22).

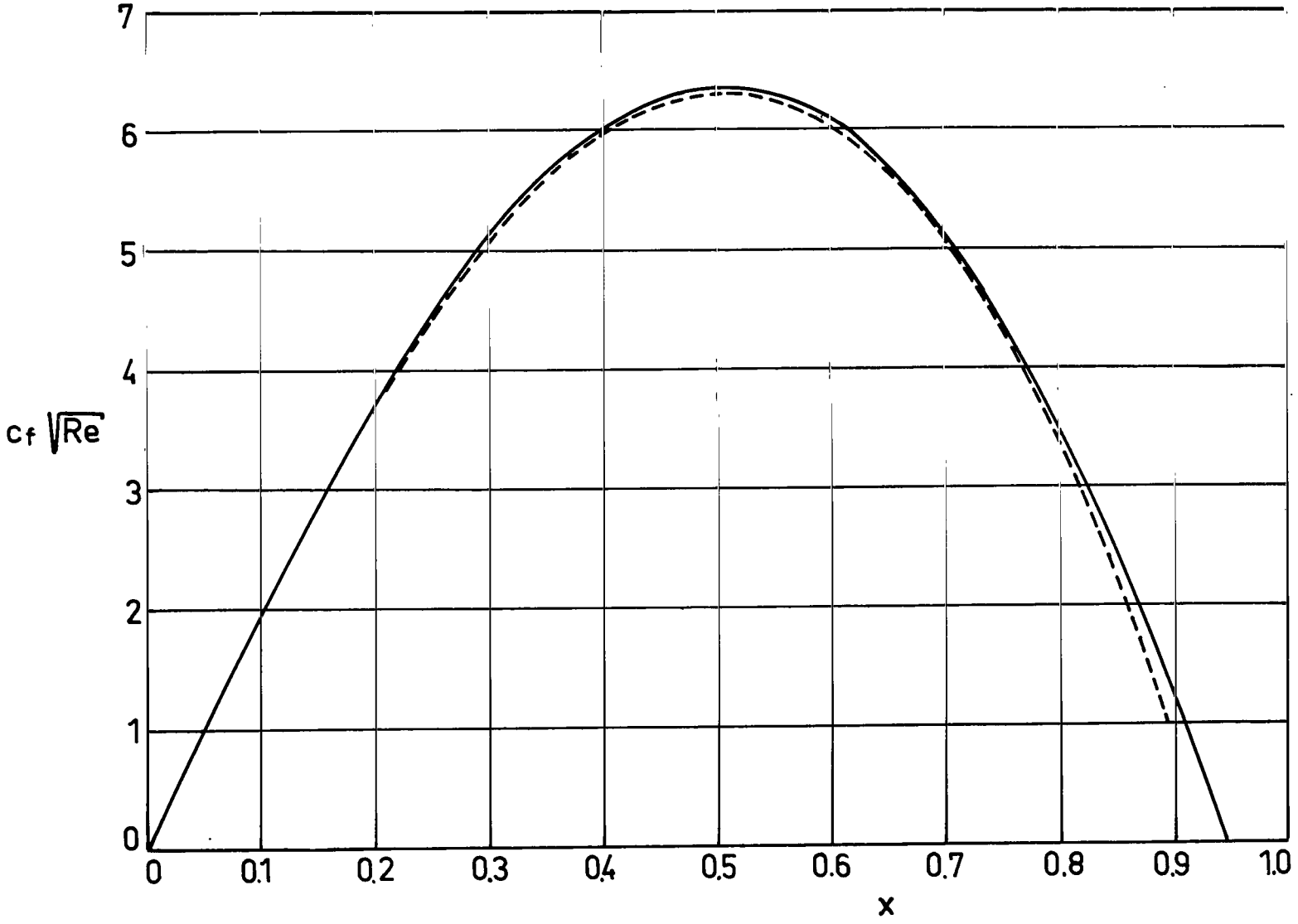

FIGURE 12. $c_f(x)\ Re^{1/2}$ FOR THE CIRCULAR CYLINDER, FROM BLASIUS' EXPANSION AND FROM (16)

The solid line represents (28) following from a six-term partial sum of Blasius' expansion (27). The dashed line represents partial sums of (22) which are continued by use of partial sums of (16).

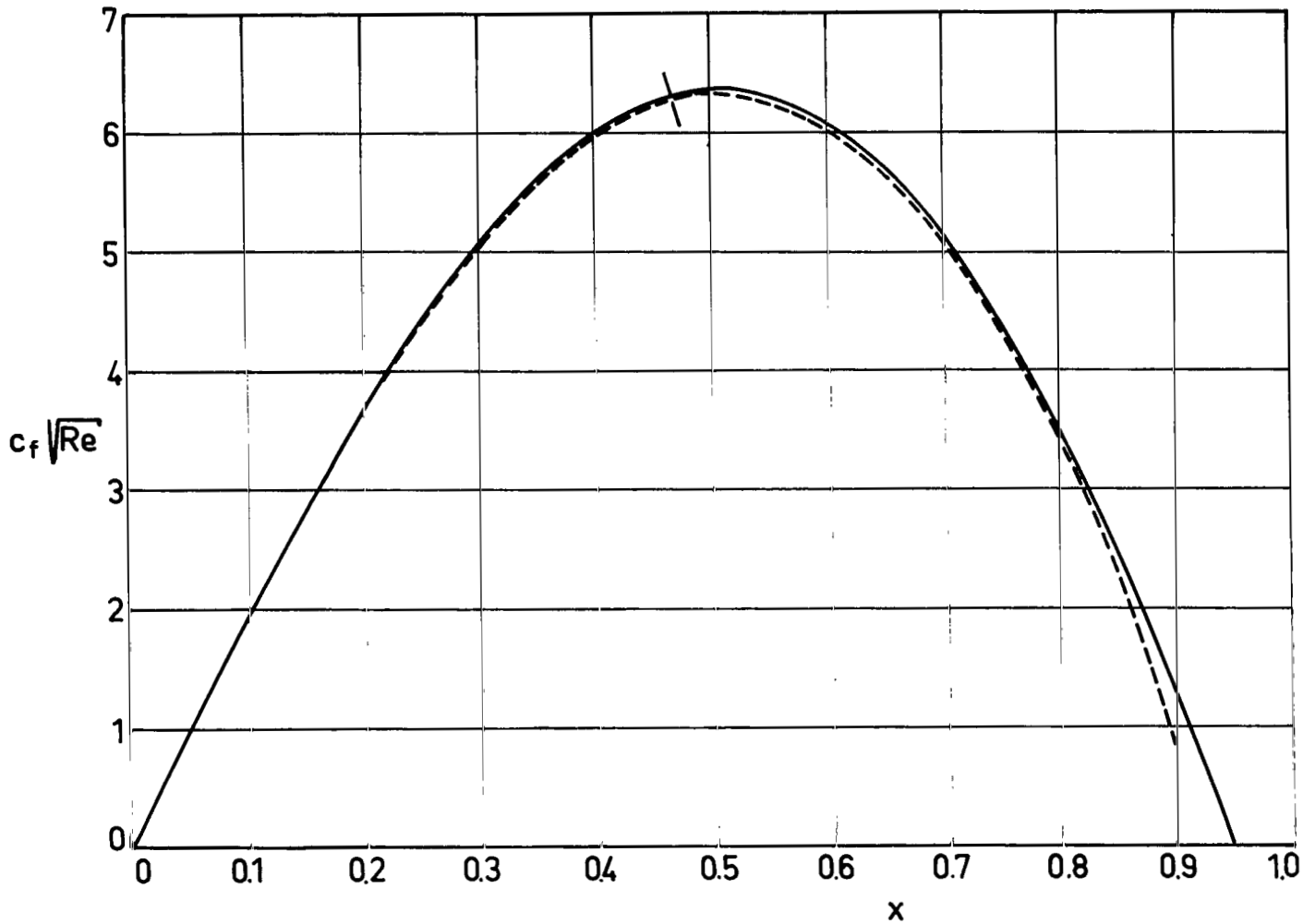

FIGURE 13. $c_f(x)\ Re^{1/2}$ FOR THE CIRCULAR CYLINDER, FROM BLASIUS' EXPANSION AND FROM (22) WITH CONTINUATION BY USE OF (16)

The solid line represents (16) and the dashed line (22).

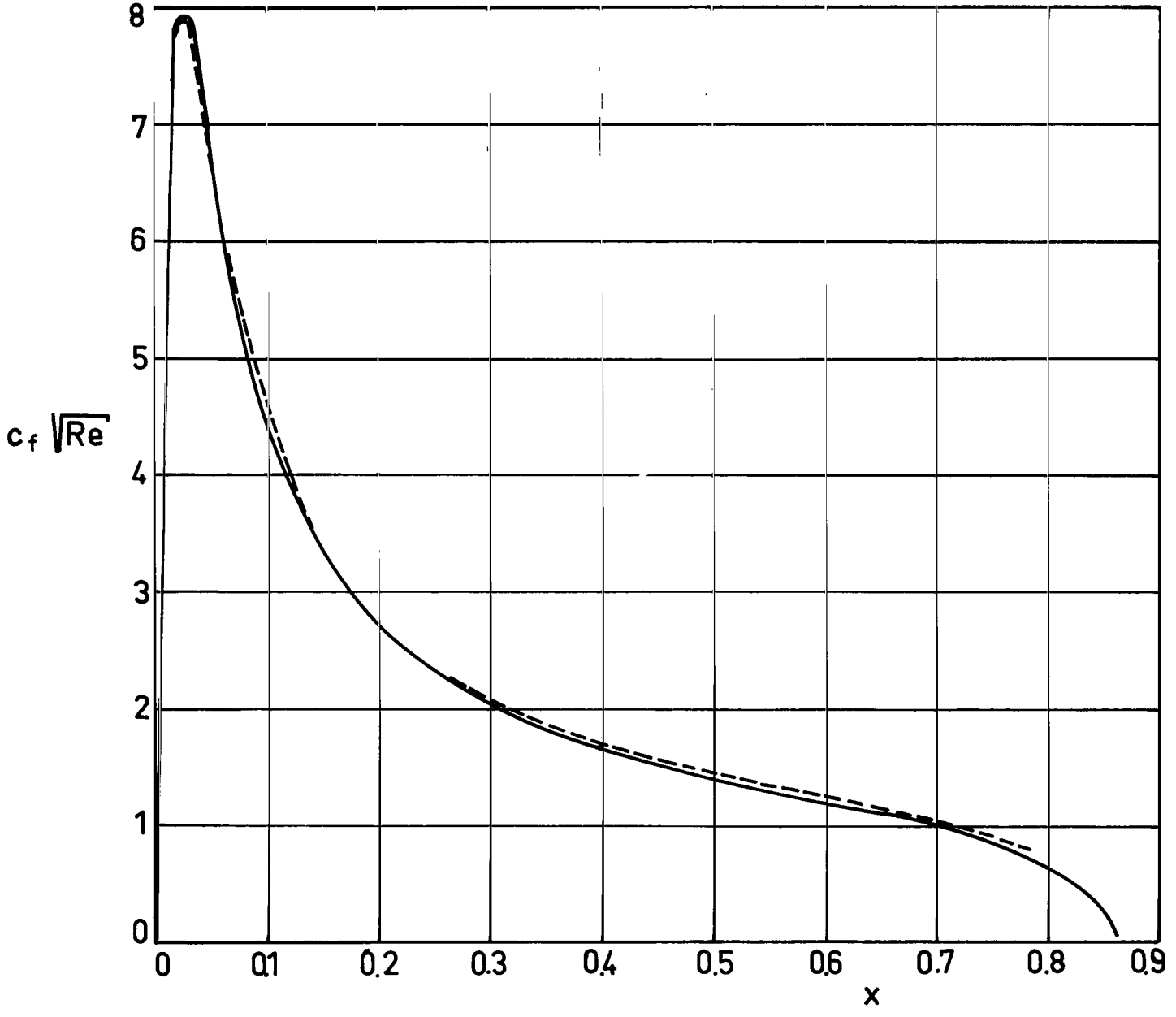

FIGURE 14. $c_f(x)\ Re^{1/2}$ FOR THE ELLIPTIC CYLINDER, FROM (16) AND FROM (22)

Cases 1, 2, and 3 are defined in equation (43) and Table 5.

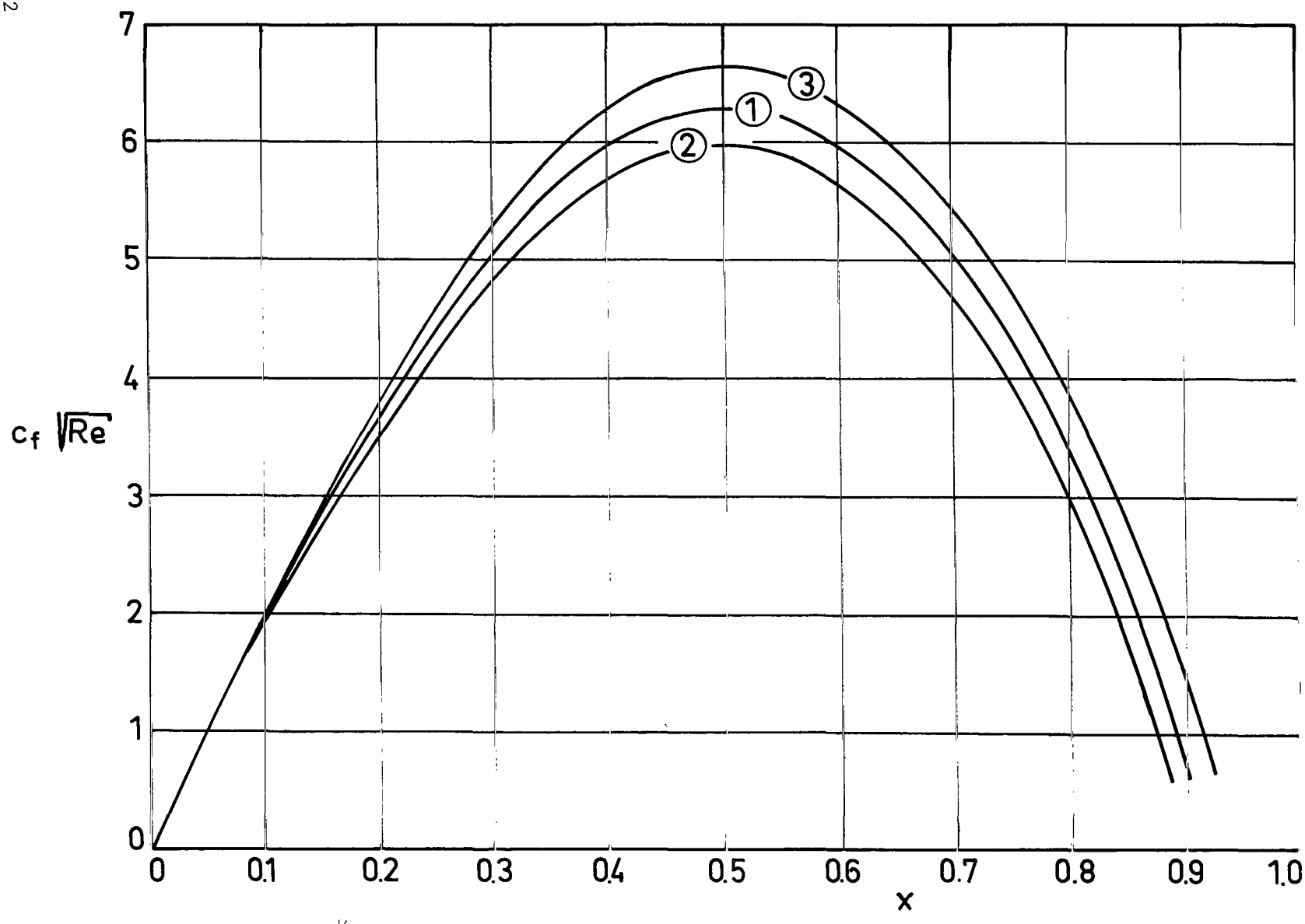

FIGURE 15. $c_f(x)\ Re^{1/2}$ FOR THE CIRCULAR CYLINDER, FROM (16): NORMAL BLOWING AND SUCTION VECTORS

Cases 4, 5, and 6 are defined in equation (43) and Table 5.

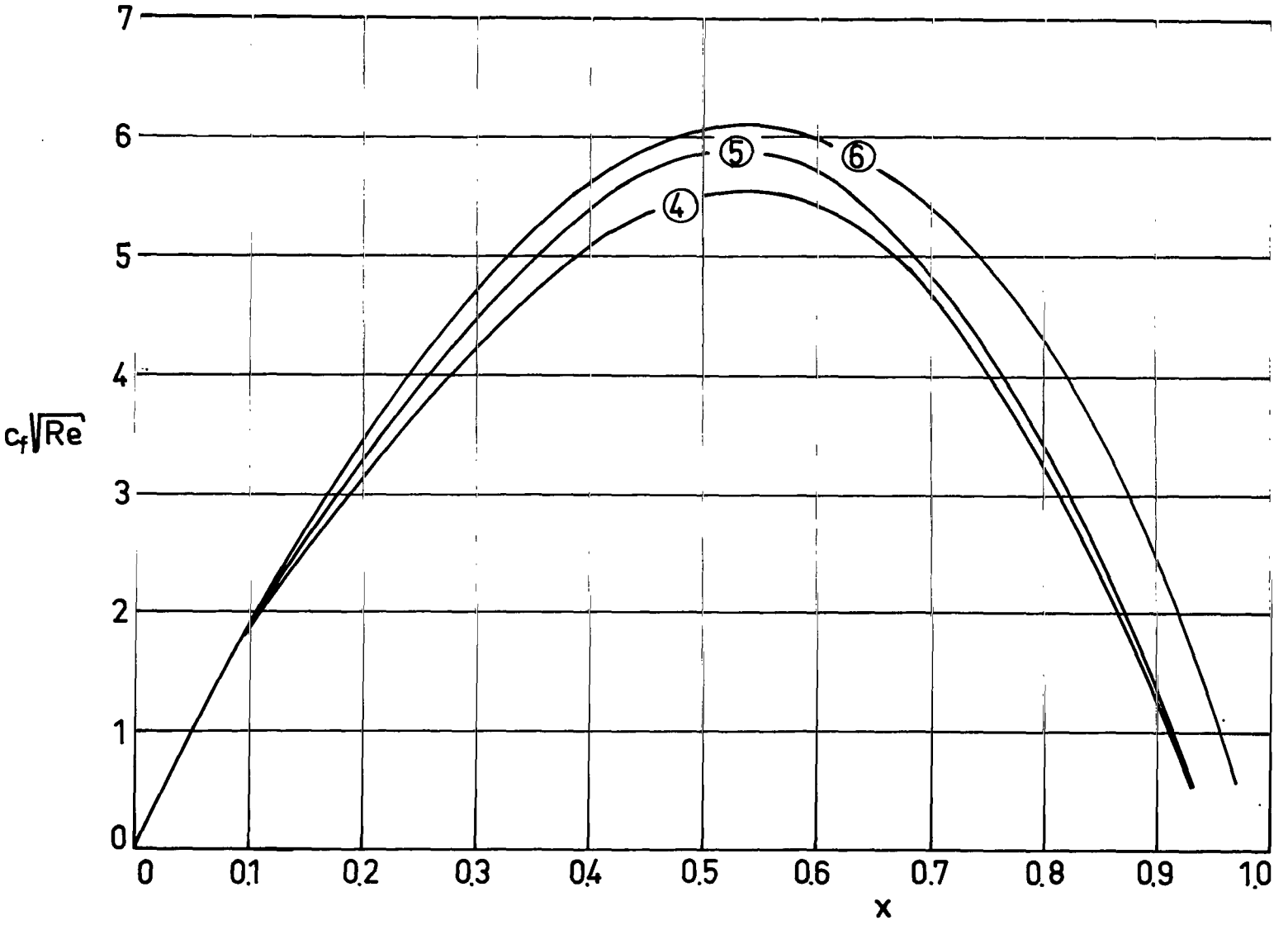

FIGURE 16. $c_f(x)\ Re^{1/2}$ FOR THE CIRCULAR CYLINDER, FROM (16): INCLINED BLOWING AND SUCTION VECTORS

Cases 1, 2, and 4 are defined in equation (43) and Table 5.

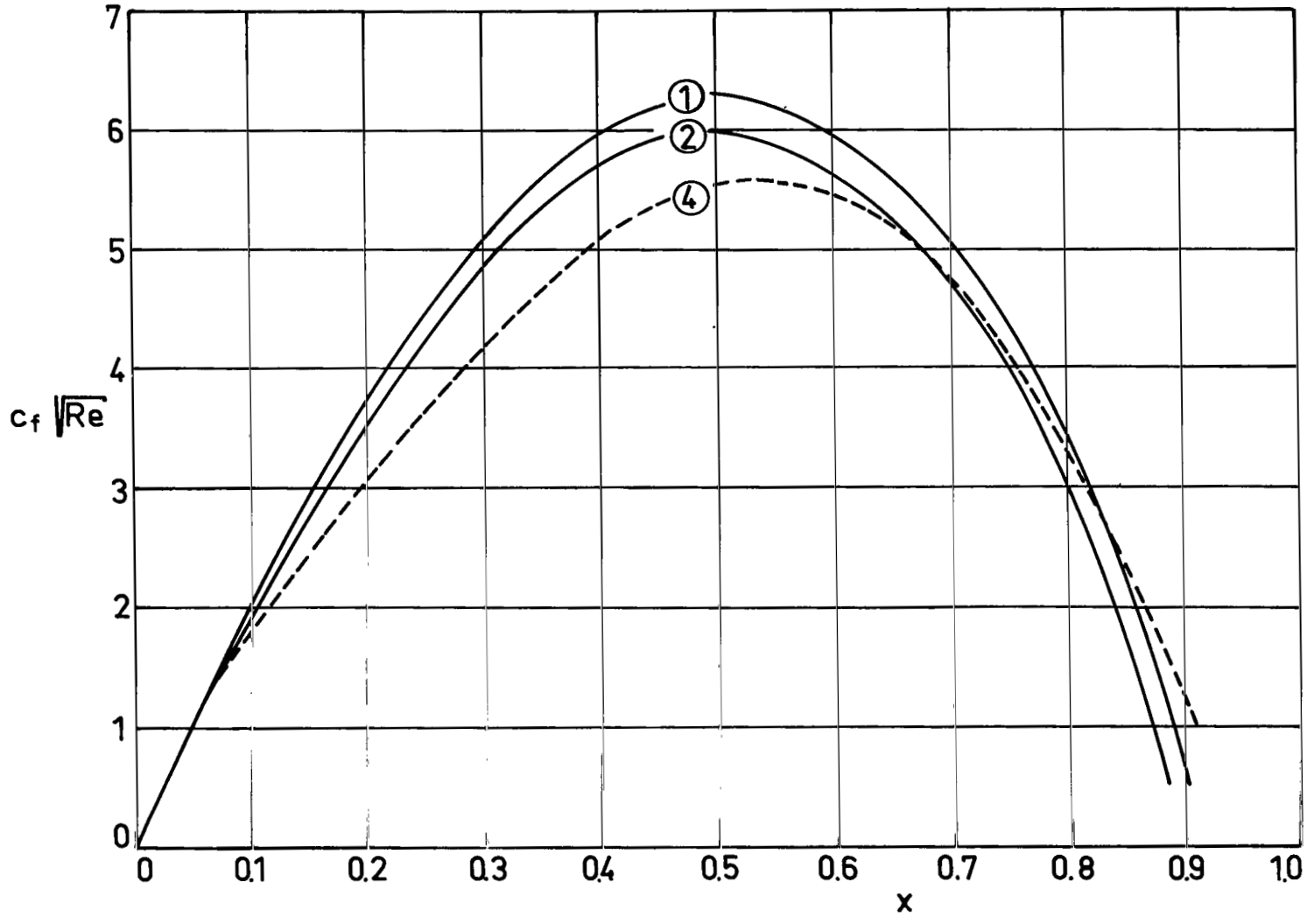

FIGURE 17. $c_f(x)\ Re^{1/2}$ FOR THE CIRCULAR CYLINDER, FROM (16): INFLUENCE OF THE INCLINATION OF THE BLOWING VECTOR

The solid line represents zero mass transfer and the dashed line $u_w(x) \equiv 0$ and $v_w(x) \equiv -0.2$.

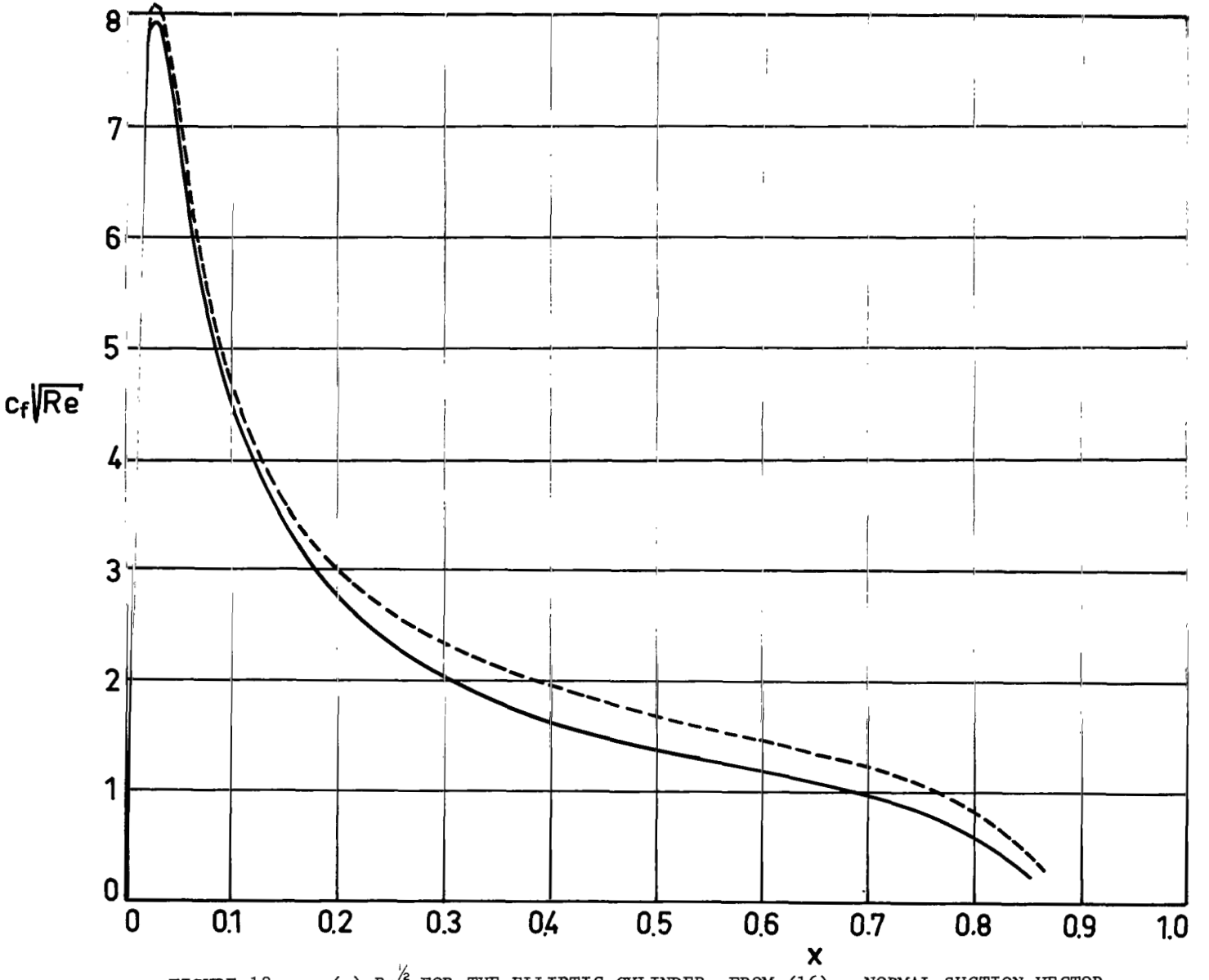

FIGURE 18. $c_f(x)\ Re^{1/2}$ FOR THE ELLIPTIC CYLINDER, FROM (16): NORMAL SUCTION VECTOR

APPENDIX A

VALIDITY OF BLASIUS' EXPANSION

For the flow past a symmetrical cylinder of arbitrary cross section with a blunt leading edge, the velocity distribution at the outer edge of the boundary layer can be expressed in the form

$$\bar{u}_e(\bar{x}) = \sum_{n=0} \bar{u}_{2n-1}\, \bar{x}^{2n-1}.$$

Blasius has shown in Reference 6 that $\bar{u}(x, y)$ can be represented by

$$\bar{u} = -\bar{u}_1 f_1' \bar{x} + \sum_{n=0} 2n\, \bar{u}_{2n-1} f_{2n-1}'(\eta)\, \bar{x}^{2n-1}.$$

For the circular cylinder, this expansion takes the form of equation (27). The functions $f_{2n-1}'(\eta)$ are solutions of ordinary differential equations which for $n \geq 3$ depend on the numbers $\bar{u}_i$. Howarth [22] has replaced each one of the functions f_5', f_7' and f_9' by universal functions independent of the coefficients $\bar{u}_i$ of the particular profile under consideration. Tifford [59] has calculated the function f_{11}'. According to Reference 28, the momentum integral of the boundary layer is not satisfied by the available terms in Blasius' expansion if the flow region of increasing pressure is considered in the boundary layer at the circular cylinder with $u_e = 2 \sin \varphi$. According to Reference 14, the friction coefficient varies proportionally to $(x_s - x)^{1/2}$ as $x \to x_s$. Figure 12 shows that the available terms in Blasius' expansion (28) for $c_f(x)\, Re^{1/2}$ do not satisfy the consequent condition $c_f'(x_s)\, Re^{1/2} = -\infty$. This situation indicates that a higher order partial sum is required to approximate the infinite series for $u(x, y)$ in the region of decelerated boundary layer flow past the circular cylinder.

In addition to this deficiency in case of the circular cylinder, Blasius' expansion exhibits serious shortcomings for profiles less blunt than the circle. For example, a sequence of elliptic cylinders with ratio λ of minor and major axes is considered, with the major axis of length $\bar{L}$ aligned with free stream. Conformal representation of these ellipses on the circle yields $\bar{u}_e(\bar{x}, \lambda)/\bar{u}_\infty$ according to Section X. Obviously, accurate approximations by use of Blasius' expansion may be expected only if the polynomial

$$\bar{u}_e(\bar{x}) = \sum_{n=0} \bar{u}_{2n-1}\, \bar{x}^{2n-1}$$

yields less than, say, 5 percent error as compared to the results of the conformal representation. In dependence on the ratio λ of the axes, the following table gives the station x at which this 5 percent error is reached.

λ	0.98	0.95	0.90	0.50
x	0.90	0.55	0.35	0.05

It is seen that Blasius' expansion solves Prandtl's boundary layer problem only for profiles of considerable bluntness.

APPENDIX B

HISTORICAL NOTES ON THE INNER AND THE OUTER SOLUTIONS

The asymptotic transition of the boundary layer to the inviscid irrotational outer flow suggests the subdivision of the boundary layer into an inner and an outer region. This approach seems to have been used for the first time by Blasius (Reference 45, 1908) in order to solve the "flat plate" boundary layer with $u_e(x) \equiv \text{const}$. In similarity variables

$$\eta = \bar{y}\sqrt{\bar{u}_\infty/\bar{\nu}\bar{x}} \quad \text{and} \quad f(\eta) = \bar{\psi}/\sqrt{\bar{\nu}\bar{x}\bar{u}_\infty},$$

this problem is governed by the differential equation $ff'' + 2f''' = 0$, e.g., Ch. VII of Reference 48. Blasius obtained the solution of this equation in the form of a power series expansion about $\eta = 0$ and an asymptotic expansion for $\eta = \infty$, the two solutions being joined at a suitable point in the boundary layer. The usefulness of the matching method is shown, e.g., by the agreement between Blasius' solution and a Runge-Kutta solution presented in Reference 61.

Blasius' matching method was applied again in 1934 by von Kármán and Millikan [27]. According to Reference 28, these authors obtained their outer solution from the linearized differential equation (29). By use of the expansion

$$\bar{p}(\bar{\varphi}) = \sum_{m=0}^{M} \bar{a}_m \, \bar{\varphi}^{\,m/2}, \tag{B-1}$$

they presented the outer solution for even values of m in the following form:

$$\bar{g} - \bar{g}_o \operatorname{erf} z = \sum_{m=0}^{M} \bar{a}_m \, \Gamma\left(\frac{m}{2} + 1\right) (4\bar{\varphi})^{m/2} \, (i^m \operatorname{erfc} z); \tag{B-2}$$

here $z = \bar{\psi}/2\sqrt{\bar{\nu}\bar{\varphi}}$, Γ denotes the Γ-function, erf the error function, and i^m erfc represents the m-th repeated integral of the complementary error function, e.g., Reference 7. According to Reference 28, von Kármán and Millikan obtained a closed-form inner solution from the linearized momentum equation

$$\partial^2\bar{u}/\partial\bar{y}^2 + (\bar{k}\bar{u}/\bar{A}) = \bar{k},$$

where

$$\bar{k} = (1/\bar{\mu})\ d\bar{p}/d\bar{x}$$

and $\bar{A}$ denotes the velocity component at the inflection point (defined by $\partial^2\bar{u}/\partial\bar{y}^2 = 0$). In the region where $u_e'(x) > 0$, the outer solution is used by these authors for the entire width of the boundary layer. This yields rather poor results for blunt bodies as is seen in Figure 10 for the case of the circular cylinder. For slender bodies, though, the outer solution yields more accurate answers for $c_f(x)\ Re^{1/2}$ as is shown by pertinent results in References 1 and 2. *Von Kármán and Millikan employed their inner solution* only between the wall and the point of inflection, i.e., in the region where $u_e'(x) < 0$. It is pointed out in Reference 28 that although this method "seems to be more reliable than the Pohlhausen method in predicting separation, it errs in setting the separation point too far forward and in predicting too rapid a boundary layer growth."

In Reference 60 (1945), Tollmien studied the asymptotic transition $\bar{y}/\sqrt{\bar{\nu}} \to \infty$ by employing solutions of the linearized differential equation (29) *as they are given in treatises on heat conduction, e.g., Ch. II of Reference 7.* The solution consists of two integrals, the first accounting for the initial distribution $g(0, \psi)$ at $\emptyset = 0$ and the second representing the influence of a free boundary function $g(\emptyset, 0)$ at the wall $\psi = 0$. This function $g(\emptyset, 0)$ is equivalent to $G(\emptyset)$ in (32). Tollmien has shown that the first integral may be omitted for both a boundary layer beginning at a stagnation point and the boundary layer past a flat plate with a sharp leading edge and aligned with the free stream. The asymptotic transition of the boundary layer toward the outer potential flow is represented in each one of these two cases by the first term of an asymptotic expansion in powers of $\bar{\psi}/2\sqrt{\bar{\nu}\bar{\emptyset}}$ of the remaining second integral. The first terms of both expansions depend on one free constant each, c_1 and c_2, which are determined by the asymptotic behavior of the initial velocity profile as $\psi \to \infty$. This situation again stresses the importance of the upstream history according to discussions in the Introduction and in Section V.

For the similarity cases defined by $\bar{u}_e = \bar{c}\ \bar{x}^m$ and $\bar{u}_w = \bar{v}_w = 0$, Riegels and Zaat [46, 1947] have solved a linearized version of Prandtl's momentum equation which is asymptotically valid as $\bar{y}/\sqrt{\bar{\nu}'} \to \infty$. The solution depends on a free parameter $A = A(m)$ which is determined by matching with numerical solutions derived for small and medium values of $\bar{y}/\sqrt{\bar{\nu}'}$.

Betz [5, 1955] has derived a differential equation of a form similar to (29). The convolution-type integral of this equation is used in the range $\bar{\delta}^*(x) \leq \bar{y} < \infty$, where $\bar{\delta}^*$ is the displacement thickness of the boundary layer. This integral, which depends on a boundary function $\bar{X}(\bar{\nu}\bar{\emptyset})$ comparable to $\bar{G}'(\emptyset)$ in (32), is expanded in a series by use of universal functions $\bar{G}_n(\xi)$ and a Taylor series for $\bar{u}_e^2\ \bar{X}$ as a function of $\bar{\nu}\bar{\emptyset}$; here

$$\xi = (\bar{y} - \bar{\delta}^*(\bar{x}))\ \bar{u}_e(\bar{x})/2\sqrt{\bar{\nu}\bar{\emptyset}(\bar{x})}$$

is essentially the variable used in Görtler's expansion [18, 19]. In Reference 5, Betz has tabulated universal functions $\bar{G}_n(\xi)$ and evaluated his expansion for the case of similarity solutions with $\bar{u}_e = \bar{c}\ \bar{x}^m$ and $\bar{u}_w = \bar{v}_w = 0$. The applicability of Betz's solution depends critically on the convergence of the Taylor expansion for $\bar{u}_e^2\ \bar{X}$. A comparison with Blasius' series discussed in Appendix A shows that this problem may impose severe limitations upon a series evaluation of the convolution-type integral of (29).

The calculation procedure proposed by Kosson in Reference 28 (1963) is a major modification of the method of von Kármán and Millikan. The factor u/u_e in equation (10b) is replaced by a constant number C, which then also appears in the solution. Kosson determines C by use of some approximately valid relations and points out that in general $C \cong 0.8$. The inner solution is represented by the polynomial

$$\bar{u} = \sum_{n=1}^{4} \bar{a}_n\ \bar{y}^n;$$

in exceptional cases, though, Kosson uses the inner solution given by von Kármán and Millikan in Reference 27. Kosson presents a closed-form generalization of (B-2) which is due to replacing (B-1) by

$$\bar{p}(\bar{\varphi}) = \sum_{m=0}^{M} \bar{a}_m\ \bar{\varphi}^{m/2} + \sum_{n=0}^{N} \bar{b}_n\ e^{\bar{\lambda}_n \bar{\varphi}}\ , \qquad \text{(B-3)}$$

where m and n are integers and $\bar{\lambda}_n > 0$. Since considerable difficulty may be encountered in approximating a given $\bar{p}(\bar{\varphi})$ distribution by (B-3) (see Appendix A), Kosson in lieu recommends a closed-form expression for $(\bar{g} - \bar{g}_o\ \mathrm{erfz})$ which follows from replacing the given $\bar{p}(\bar{\varphi})$ distribution by a step curve. Kosson applied his method to the following cases in Reference 28: (a) a constant or a linear variation in $\bar{u}_e(\bar{x})$, (b) the circular cylinder with the velocity distribution $\bar{u}_e(x) = 2 \sin \varphi$ as given by potential theory, (c) the circular cylinder with $\bar{u}_e(\bar{x})$ following from the measured pressure distribution [13], and (d) Schubauer's ellipse of Reference 21. Kosson remarks in his paper [28] that his method "occupies a middle ground between the integral method and numerical methods, with respect to accuracy and computing time. A typical problem, ..., takes from 2 to 5 minutes on an IBM 7090 digital computer." The calculation method presented in this paper is a more refined version of Kosson's application of the matching principle. The authors of this paper were not aware of Reference 28 before its publication and they completed their paper before Reference 28 came out in May 1963.

APPENDIX C

SOLUTIONS OF THE LINEARIZED VON MISES EQUATION

Both the complementary error integral

$$F(\varnothing - \eta, \psi - \psi_\alpha^*) = \frac{2}{\sqrt{\pi}} \int_{\frac{\psi-\psi_\alpha^*}{2\sqrt{\varnothing-\eta}}}^{\infty} e^{-\beta^2} \, d\beta \tag{C-1}$$

and the expression

$$g(\varnothing, \psi) - 1 = \int_{\eta=0}^{\eta=\varnothing} [G(\eta) - 1] \frac{\partial}{\partial \varnothing} F(\varnothing - \eta, \psi - \psi_\alpha^*) \, d\eta \tag{C-2}$$

satisfy the differential equation (29) of the outer solution for $\psi > \psi_\alpha^*$. Expression (C-2) fulfills the first and third one of the pertinent initial and boundary conditions (31), i.e.,

$$g(0, \psi) = \lim_{\psi \to \infty} g(\varnothing, \psi) = 1.$$

It will be shown now that the second one of the conditions (31) is also satisfied by (C-2), i.e.,

$$\lim_{\psi \to \psi_\alpha^*} g(\varnothing, \psi) = G(\varnothing).$$

The coordinate transformation

$$\mu = \frac{\psi - \psi_\alpha^*}{2\sqrt{\varnothing - \eta}} \tag{C-3}$$

relates η and μ at fixed values of both $\varphi > 0$ and $\psi - \psi^*_\alpha > 0$. Upon this transformation, (C-2) can be written as follows:

$$g(\varphi, \psi) - 1 = \frac{2}{\sqrt{\pi}} \int_{\frac{\psi-\psi^*_\alpha}{2\sqrt{\varphi}}}^{\frac{\psi-\psi^*_\alpha}{2\sqrt{\varphi}} + \sqrt{\psi-\psi^*_\alpha}} e^{-\mu^2} \left[G\left(\varphi - \frac{(\psi - \psi^*_\alpha)^2}{4\mu^2} \right) - 1 \right] d\mu \qquad (C\text{-}4)$$

$$+ \frac{2}{\sqrt{\pi}} \int_{\frac{\psi-\psi^*_\alpha}{2\sqrt{\varphi}} + \sqrt{\psi-\psi^*_\alpha}}^{\infty} e^{-\mu^2} \left[G\left(\varphi - \frac{(\psi - \psi^*_\alpha)^2}{4\mu^2} \right) - 1 \right] d\mu.$$

Since its integrand is bounded, the first integral in (C-4) tends to zero together with $(\psi - \psi^*_\alpha)$. Evidently, the integration variable μ of the second integral in (C-4) fulfills the inequality

$$\mu > \sqrt{\psi - \psi^*_\alpha}$$

since $\psi > \psi^*_\alpha$. If $G(\varphi - (\psi - \psi^*_\alpha)^2/4\mu^2)$ is defined to take on the value $G(\varphi)$ when both $\psi - \psi^*_\alpha$ and μ are zero, the second integral is a continuous function of $\psi - \psi^*_\alpha$ in the entire range of variation $0 \leq \psi - \psi^*_\alpha < \infty$. As $\psi \to \psi^*_\alpha$, therefore, the second integral in (C-4) tends towards

$$\frac{2}{\sqrt{\pi}} \left[G(\varphi) - 1 \right] \int_{\frac{\psi-\psi^*_\alpha}{2\sqrt{\varphi}} + \sqrt{\psi-\psi^*_\alpha}}^{\infty} e^{-\mu^2} \, d\mu = G(\varphi) - 1. \qquad (C\text{-}5)$$

The right-hand side of (C-2) may be integrated by parts because both F and G possess continuous derivatives with respect to $\emptyset$ (e.g., p. 65 of Reference 69),

$$g(\emptyset, \psi) - 1 = \int_0^{\emptyset} F(\emptyset - \eta, \psi - \psi_\alpha^*) \frac{dG(\eta)}{d\eta} d\eta. \tag{C-6}$$

Here, the relations $G(0) \equiv g(0, \psi_\alpha^*) = 1$ and $F(0, \psi - \psi_\alpha^*) = 0$ have been employed. Since F possesses a Riemann integral with respect to $\emptyset$ and $\partial F/\partial\psi$ is a continuous function of both $\emptyset - \eta$ and $\psi - \psi_\alpha^*$, equation (C-9) may be differentiated with respect to ψ (e.g., p. 67 of Reference 69),

$$\frac{\partial g(\emptyset, \psi)}{\partial \psi} = - \frac{2}{\sqrt{\pi}} \int_0^{\emptyset} \frac{dG(\eta)}{d\eta} \frac{\exp\left[- \frac{(\psi - \psi_\alpha^*)^2}{4(\emptyset - \eta)} \right]}{2\sqrt{\emptyset - \eta}} d\eta. \tag{C-7}$$

If $|dG/d\eta| \leq M$, this integral exists for any value of ψ in $0 \leq \psi - \psi_\alpha^* < \infty$ since

$$\left| \frac{\partial g(\emptyset, \psi)}{\partial \psi} \right| \leq \frac{2}{\sqrt{\pi}} M \int_0^{\emptyset} \frac{d\eta}{2\sqrt{\emptyset - \eta}} = \frac{2}{\sqrt{\pi}} M \sqrt{\emptyset}. \tag{C-8}$$

Therefore, as $\psi \to \psi_\alpha^*$, the right-hand side of (C-7) tends towards

$$\frac{\partial g(\emptyset, \psi_\alpha^*)}{\partial \psi} = - \frac{1}{\sqrt{\pi}} \int_0^{\emptyset} \frac{dG(\eta)}{d\eta} \frac{d\eta}{\sqrt{\emptyset - \eta}}. \tag{C-9}$$

Equation (C-9) is multiplied by $(\omega - \emptyset)^{1/2}$ and subsequently integrated over $\emptyset$ in the limits $\emptyset = 0$ and $\emptyset = \omega$. Because of $G(\emptyset) = g(\emptyset, \psi_\alpha^*)$ and

$$\int_{\phi=0}^{\phi=\omega} \frac{1}{\sqrt{\omega-\phi}} \left[\int_{\eta=0}^{\eta=\phi} \frac{dG(\eta)}{d\eta} \frac{d\eta}{\sqrt{\phi - \eta}} \right] d\phi = \int_{\eta=0}^{\eta=\omega} \frac{dG(\eta)}{d\eta} \left[\int_{\phi=\eta}^{\phi=\omega} \frac{d\phi}{\sqrt{(\omega - \phi)(\phi - \eta)}} \right] d\eta =$$

$$= \pi \int_{\eta=0}^{\eta=\omega} \frac{dG(\eta)}{d\eta} d\eta = \pi \left[g(\omega, \psi_\alpha^*) - 1 \right], \tag{C-10}$$

the relation

$$- \sqrt{\pi} \left[g(\phi, \psi_\alpha^*) - 1 \right] = \int_0^{\phi} \frac{\partial g(\eta, \psi_\alpha^*)}{\partial \psi} \frac{d\eta}{\sqrt{\phi - \eta}} \tag{C-11}$$

is obtained finally after a suitable change of notations has been carried out.

Regions $H_{m,n}$ are introduced

$$\phi_{n-1} < \phi < \phi_n, \quad \psi_{m-1} < \psi < \psi_m, \tag{C-12}$$

referring to a suitably selected grid in the ϕ - ψ plane. Approximate solutions of von Mises' boundary layer equations (10b) may be obtained by employing the linearized differential equation

$$\frac{\partial g_{m,n}}{\partial \phi} = U_{m,n} \frac{\partial^2 g_{m,n}}{\partial \psi^2} \text{ (with } U_{m,n} = \text{const.) in } H_{m,n}. \tag{C-13}$$

If $g(\phi, \psi)$ is known for $0 \leq \phi \leq \phi_{n-1}$, $0 < \psi < \infty$ and for $\phi_{n-1} \leq \phi \leq \phi_n$, $0 < \psi < \psi_{m-1}$, the following initial and boundary conditions can be prescribed on the parabolic boundary of $H_{m,n}$:

$$\begin{cases} g_{m,n}(\phi_{n-1}, \psi) = \gamma_1(\psi) & \text{for} \quad \psi_{m-1} \leq \psi \leq \psi_m, \\ g_{m,n}(\phi_{n-1}, \psi) \equiv 0 & \text{for} \quad \psi < \psi_{m-1} \text{ and } \psi > \psi_m \\ g_{m,n}(\phi, \psi_{m-1}) = \gamma_2(\psi), & \text{and} \\ \dfrac{\partial g_{m,n}(\phi, \psi_{m-1})}{\partial \psi} = \gamma_0(\psi). \end{cases} \tag{C-14}$$

The solution $g_{m,n}(\emptyset, \psi)$ of (C-13) may be represented by the sum

$$g_{m,n}(\emptyset, \psi) = g_1(\emptyset, \psi) + g_2(\emptyset, \psi) + g_3(\emptyset, \psi) \tag{C-15}$$

of the three "influence integrals" (e.g., Ch. II of Reference 7)

$$g_1(\emptyset, \psi) = \frac{\int_{\psi_{m-1}}^{\psi_m} G_1(\emptyset_{n-1}, \beta) \exp\left[-(\psi - \beta)^2/4U_{m,n}(\emptyset - \emptyset_{n-1})\right] d\beta}{2\sqrt{\pi U_{m,n}(\emptyset - \emptyset_{n-1})}}, \tag{C-16}$$

$$g_2(\emptyset, \psi) = \int_{\emptyset_{n-1}}^{\emptyset} G_2(\eta, \psi_{m-1}) \frac{\partial}{\partial \emptyset} F(\emptyset - \eta, \psi - \psi_{m-1})\, d\eta, \tag{C-17}$$

and

$$g_3(\emptyset, \psi) = \int_{\emptyset_{n-1}}^{\emptyset} G_3(\eta, \psi_m) \frac{\partial}{\partial \emptyset} F(\emptyset - \eta, \psi_m - \psi)\, d\eta. \tag{C-18}$$

These three integrals depend on the unknown functions $G_1(\emptyset_{n-1}, \psi)$, $G_2(\emptyset, \psi_{m-1})$, and $G_3(\emptyset, \psi_m)$. Comparison to (C-2) shows that $g_2(\emptyset_{n-1}, \psi) = g_3(\emptyset_{n-1}, \psi) = 0$. According to Ch. II of Reference 7, therefore, $G_1(\emptyset_{n-1}, \psi) = \gamma_1(\psi)$. The functions $G_2(\emptyset, \psi_{m-1})$ and $G_3(\emptyset, \psi_m)$ can be determined by requiring that (C-15) take on the prescribed boundary functions $\gamma_0(\psi)$ and $\gamma_2(\psi)$ on the boundary

$$\psi = \psi_{m-1}, \quad \emptyset_{n-1} \leq \emptyset \leq \emptyset_n \text{ of } H_{m,n}.$$

In this way, the solution (C-15) of (C-13) is obtained in $H_{m,n}$.

In the subregion $H_{Io}\varnothing(x_o) < \varnothing < \varnothing(x_s)$, $\psi_w < \psi < \psi_o$ with $\psi_o < \psi^*_\alpha$, the inner solution is represented by partial sums of (16) or (22). If $c_f(\varnothing)\ Re^{1/2}$ is already known for $\varnothing(x_o) \leqq \varnothing \leqq \varnothing_{n-1}$, the numerical procedure of Section VII is employed to determine $c_f(\varnothing_n)\ Re^{1/2}$ with the following pertinent additions: Within each iteration cycle for $c_f(\varnothing_n)\ Re^{1/2}$, partial sums of (16) or (22) are evaluated on the boundary line $\psi = \psi_o$, $\varnothing_{n-1} \leqq \varnothing \leqq \varnothing_n$ of H_{Io}. From $g(\varnothing_{n-1}, \psi)$, $g(\varnothing, \psi_o)$ and $\partial g(\varnothing, \psi_o)/\partial\psi$, there follows the solution $g_{o,n}(\varnothing, \psi)$ of (C-13) for $H_{o,n}$. Subsequently, $g_{1,n}(\varnothing, \psi)$, $g_{2}(\varnothing, \psi)$, etc. are determined. If $\psi_M = \psi^*_\alpha$, both $g(\varnothing, \psi_M)$ and $\partial g(\varnothing, \psi_M)/\partial\psi$, as following from $g_{M,n}(\varnothing, \psi)$, are substituted in the boundary relation (36) of the outer solution. The constant number $U_{m,n}$ is chosen in such a way that $U_{m,n}$ represents an average of the initial and boundary distributions $u(\varnothing_{n-1}, \psi)$ and $u(\varnothing, \psi_{m-1})$.

APPENDIX D

BOUNDS OF THE RIGOROUS SOLUTION

With reference to discussions of approximate solution methods in the Introduction, it is desirable to determine rigorously valid bounds of exact boundary layer solutions. These bounds can be constructed by use of Nickel's modified version [37-39] of the lemma of Nagumo [36] and Westphal [68] for nonlinear parabolic differential operators. According to Reference 39, the region H_P and its parabolic boundary Γ_P are introduced,

$$\begin{cases} H_P: & 0 < x < x_1 < x_s, \qquad 0 < y < \infty; \\ \Gamma_P: & x = 0, \quad 0 < y < \infty; \qquad y = 0, \quad 0 \leqq x < x_1; \\ & y = \infty, \quad 0 \leqq x < x_1. \end{cases} \tag{D-1}$$

The "admissible" functions as defined in Reference 39 are subjected to conditions on continuity, differentiability, and signs. From the point of view of engineering applications, the most important ones of these conditions are $u(x, y) > 0$ and $\partial u(x, y)/\partial y > 0$ in H_P and $\partial u(x, 0)/\partial y > 0$ in $0 < x \leqq x_1$. In sections $x = \text{const.}$, the admissible function $u(x, y)$ then increases monotonically wity y, as is true for exact solutions $u(x, y)$ according to theorem (Ia) in Section II. The subscripts L and U denote lower and upper bounds, respectively. At the wall $y = 0$, it is assumed that $u_{wL}(x) = u_{wU}(x) = u_w(x) \equiv 0$. The following theorem then holds true according to Reference 39:

(III). Both the exact solution $u(x, y)$ of Prandtl's boundary layer problem and the admissible functions $u_L(x, y)$ and $u_U(x, y)$ are assumed to satisfy the initial and boundary conditions (11a) - (14a) on Γ_P with $u_w = u_{Lw} = u_{Uw} \equiv 0$. If

$$P_P\, u_L(x, y) \leqq P_P\, u(x, y) = 0 \leqq P_P\, u_U(x, y) \text{ in } H_P, \tag{D-2}$$

where the operator P_P is defined in (5),

$$u_L(x, y) \leqq u(x, y) \leqq u_U(x, y) \text{ in } H_P + \Gamma_P. \tag{D-3}$$

Von Mises' transformation (6) and (7) relates H_P and Γ_P to H_M and Γ_M,

$$\begin{cases} H_M: \quad 0 < \varphi < \varphi(x_1), & \psi_w < \psi < \infty; \\ \Gamma_M: \quad \varphi = 0, \quad \psi_w < \psi < \infty, \text{ etc.} \end{cases} \tag{D-4}$$

Since the Jakobian (8) is nonzero in H_P, the inverse, x_M and y_M, of von Mises' transformation can be determined in H_P,

$$x_M(\varphi) = \int_0^{\varphi} \frac{dt}{u_e(t)} \quad \text{and} \quad y_M(\varphi, \psi, u) = \int_{\psi_w}^{\psi} \frac{dt}{u(\varphi, t)} . \tag{D-5}$$

According to Reference 39, $u(\varphi, \psi)$ and $u_L(\varphi, \psi)$ are defined with reference to the corresponding *stream line distributions*,

$$\begin{cases} u(\varphi, \psi) \equiv u\Big(x_M(\varphi), \quad y_M(\varphi, \psi, u)\Big) \\ \text{and} \\ u_L(\varphi, \psi) \equiv u_L\Big(x_M(\varphi), \quad y_M(\varphi, \psi, u_L)\Big) \end{cases} \tag{D-6}$$

In terms of von Mises' boundary layer operator

$$P_M\, u(\varphi, \psi) \equiv \frac{\partial u}{\partial \varphi} - \frac{u_e\, u'_e}{u} - \frac{\partial}{\partial \psi}\left(u \frac{\partial u}{\partial \psi}\right) . \tag{D-7}$$

Prandtl's momentum equation (5) can be written as follows:

$$P_P u(x, y) = u(\varphi, \psi)\; P_M u(\varphi, \psi) \quad \text{in } H_M. \tag{D-8}$$

Application of (9) transforms $u\, P_M\, u = 0$ into von Mises' differential equation (10). Because of (D-2), (D-4) and (D-8),

$$P_M\, u_L(\emptyset,\ \psi) \leqq P_M\, u(\emptyset,\ \psi) = 0 \leqq P_M\, u_U(\emptyset,\ \psi) \text{ in } H_M. \tag{D-9}$$

From this relation there follows according to Reference 39

$$u_L(\emptyset,\ \psi) \leqq u(\emptyset,\ \psi) \leqq u_U \quad \text{in } H_M + \Gamma_M. \tag{D-10}$$

Because of (D-5) and (D-10)

$$y_M(\emptyset,\ \psi,\ u) = \int_{\psi_w}^{\psi} \frac{dt}{u(\emptyset,\ t)} \leqq \int_{\psi_w}^{\psi} \frac{dt}{u_L(\emptyset,\ t)} = y_M(\emptyset,\ \psi,\ u_L). \tag{D-11}$$

Theorem (Ia) in Section II, (D-6), and (D-11) yield

$$\begin{aligned} &u_L\Big(x_M(\emptyset),\ y_M(\emptyset,\ \psi,\ u_L)\Big) = u_L(\emptyset,\ \psi) \leqq u(\emptyset,\ \psi) = \\ &= u\Big(x_M(\emptyset),\ y_M(\emptyset,\ \psi,\ u)\Big) \leqq u\Big(x_M(\emptyset),\ y_M(\emptyset,\ \psi,\ u_L)\Big) \text{ in } H_M + \Gamma_M. \end{aligned} \tag{D-12}$$

Since H_M and Γ_M correspond H_p Γ_p,

$$u_L(x,\ y) \leqq u(x,\ y) \quad \text{in} \quad H_P + \Gamma_P \tag{D-13}$$

with the equivalent relation holding true between u_U and u. It is thus seen that (D-3) in theorem (III) is valid regardless of whether the differential relations (D-2) in Cartesian coordinates or (D-9) in von Mises' coordinates have been used to determine u_L and u_U. This conclusion obviously is still valid if (D-9) is employed in part of the boundary layer flow plane under consideration and (D-2) in the remaining part.

The bounds will be constructed separately in H_I and H_{II}, employing Cartesian coordinates in H_I and von Mises coordinates in H_{II}. For simplicity, the brief outline to be given here will be restricted to one stream line $\psi = \psi_o^*$ separating H_I and H_{IIo}. A sufficiently large value of ψ_o^* is assumed

so that both $\partial^2 g_L/\partial\psi^2$ and $\partial^2 g_U/\partial\psi^2$ are negative in $0 < \varphi \leqq \varphi(x_1)$, $\psi_o^* \leqq \psi < \infty$; i.e., any points of inflection of u_U and u_L in sections x = const. are restricted to H_I. The lower bounds are assumed to satisfy the following conditions on the boundaries of H_I and H_{II}, respectively:

$$g_L(0, y) = 1, \quad g_L(x, 0) = 1 - u_e^2(x), \quad g_L\Big(x, \psi_o^*(x, y)\Big) = G_L\Big(\varphi(x)\Big), \tag{D-14}$$

and

$$g_L(0, \psi) = 1, \quad \lim_{\psi \to \infty} g_L(\varphi, \psi) = 1, \quad \text{and} \quad g_L(\varphi, \psi_o^*) = G_L(\varphi). \tag{D-15}$$

These conditions also apply to the upper bounds after the subscript L has been replaced by U. With reference to (39), u_L and u_U are assumed to satisfy the linear differential equations

$$\frac{\partial g_L}{\partial \varphi} = \frac{\partial^2 g_L}{\partial \psi^2} \tag{D-16a}$$

and

$$\frac{\partial g_U}{\partial \varphi} = U_2 \frac{\partial^2 g_U}{\partial \psi^2} \tag{D-16b}$$

in H_{IIo}. Because of $\partial^2 g_L/\partial\psi^2 < 0$, $\partial^2 g_U/\partial\psi^2 < 0$, equations (39) and (D-16), and theorem (Ia) in Section II,

$$\frac{\partial g_L}{\partial \varphi} - \frac{u_L}{u_e}\frac{\partial^2 g_L}{\partial \psi^2} \leqq \frac{\partial g}{\partial \varphi} - \frac{u}{u_e}\frac{\partial^2 g}{\partial \psi^2} = 0 \leqq \frac{\partial g_U}{\partial \varphi} - \frac{u_U}{u_e}\frac{\partial^2 g_U}{\partial \psi^2} \quad \text{in } H_{IIo}. \tag{D-17}$$

To facilitate the discussions with regard to H_I, only the construction of the lower bound will be outlined here. This bound u_L is expressed by a partial sum of

$$u_L = \sum_{n=1}^{\infty} A_{nL} \frac{y^n}{n!} \quad \text{in } H_I, \tag{D-18}$$

which is to satisfy the following differential equation

$$P_P\, u_L(x, y) = F_L(x, y) + B_L(x). \tag{D-19}$$

The "discrepancy term" $F_L(x, y)$ appears in (D-19) because any partial sum of (D-18) in general does not fulfill the differential equation $P_P u(x, y) = 0$. The free function B_L of x is determined in such a way that

$$P_P u_L(x, y) - F_L(x, y) \leqq P_P u(x, y) = 0 \quad \text{in} \quad H_I + \psi_o^*. \tag{D-20}$$

Because of (D-14), (D-15), (D-17), and (D-20), the conditions of theorem (III) are satisfied, i.e.,

$$u_L(x, y) \leqq u(x, y) \quad \text{in} \quad H_I + \psi_o^* + H_{IIo}. \tag{D-21}$$

Here, the equivalence of determining the bounds in Cartesian coordinates and in von Mises coordinates has been employed. The admissible functions employed in theorem (III) are supposed to be continuous and to possess continuous first derivatives with respect to y in $0 \leqq x \leqq x_1$, $0 < y < \infty$; regarding the second derivative of admissible functions with respect to y, only the existence in this region is assumed in Reference 39. While these conditions on u_L and $\partial u_L/\partial y$ are fulfilled in H_I and H_{II}, the functional values of u_L and $2\partial u_L/\partial y = \partial g_L/\partial \psi$ as following from the individual representations in H_I and H_{II} have to be matched along the curve $\psi = \psi_o^*$ separating H_I and H_{II}. For this purpose, the matching procedure of the inner and the outer solution as presented in Sections VI and VII may be employed. In addition to the stepwise numerical solution of the integro-differential equation (36) for $c_{fL}(x)$, the functional values of $B_L(x)$ have to be determined at every grid point $\varnothing_n$ in such a way that (D-17) is satisfied in $\varnothing_{n-1} < \varnothing \leqq \varnothing_n$, $0 < y \leqq y^*(x)$. The double iteration procedure thus required at every step for $c_{fL}(\varnothing_n)$ and $B_L(\varnothing_n)$ is facilitated by the fact that any number $B_L(\varnothing_n)$ will do which satisfies the inequality sign in (D-18).

The relationship (D-21), its equivalent $u \leqq u_U$, and $g_L(x, 0) = g_U(x, 0) = g(x, 0) = 1 - u_e^2(x)$ according to (D-14) show that $A_{1L}(x) \leqq A_1(x) \leqq A_{1U}(x)$; i.e.,

$$c_{fL}(x) \leqq c_f(x) \leqq c_{fU}(x) \quad \text{for } 0 < x < x_1 \tag{D-22}$$

because of (18). These bounds for the exact friction coefficient $c_f(x)$ enable one to determine bounds of the separation point,

$$x_{sL} \leqq x_s \leqq x_{sU} \tag{D-23}$$

from $c_{fL}(x_{sL}) = c_{fU}(x_{sU}) = 0$, respectively. Details of this calculation procedure for the bounds and numerical applications will be presented in a forthcoming paper by the first author.

The outer solution of Section V satisfies the differential equation (D-16a) for the lower bound in H_{II}. The condition (D-2) in theorem (III) is satisfied by solutions of (D-16a) provided $\partial^2 g_L/\partial\psi^2 < 0$. If, in addition,

$$g_L(\emptyset, \psi_o^*) = g(\emptyset, \psi_o^*) = g_U(\emptyset, \psi_o^*) \tag{D-24}$$

and

$$\lim_{\psi \to \infty} g_L(\emptyset, \psi) = \lim_{\psi \to \infty} g_U(\emptyset, \psi) = g_L(0, \psi) = g_U(0, \psi) = 1, \tag{D-25}$$

the outer solution represents a lower bound in H_{IIo}. The conditions (D-24) can be satisfied, e.g., if the outer solution is applied for the entire boundary layer, i.e., $\psi_o^* = \psi_w$. This yields equation (34) whose evaluation for the boundary layer past the circular cylinder is compared in Figure 10 to a supposedly rigorous solution. It is seen in this figure that $c_{fa}(x)\ Re^{1/2}$ from (34) actually represents a lower bound of $c_f(x)\ Re^{1/2}$ if $u_e'(x) > 0$. Past the point of minimum pressure, $x_m = 0.787$, however, equation (34), ceases to represent a rigorously valid lower bound of $c_f(x)\ Re^{1/2}$ since $g(\emptyset, \psi)$ possesses a point of inflection in sections $\emptyset$ = const. for $\emptyset > \emptyset(x_m)$.

Upon the transformation

$$\psi_U - \psi_o^* = \sqrt{U_2}\ (\psi_L - \psi_o^*), \tag{D-26}$$

the differential equations (D-16a) and (D-16b) and their solutions become identical because of (D-24) and (D-25),

$$g_L(\emptyset, \psi_L) = g_U(\emptyset, \sqrt{U_2}\ \psi_L). \tag{D-27}$$

Because of theorem (III),

$$0 < \frac{\partial g_L(\emptyset,\ \psi_o^*)}{\partial \psi_L} \leqq \frac{\partial g(\emptyset,\ \psi_o^*)}{\partial \psi} \leqq \frac{\partial g(\emptyset,\ \psi_o^*)}{\partial \psi_U} = U_2^{-\frac{1}{2}} \frac{\partial g_L(\emptyset,\ \psi_o^*)}{\partial \psi_L} \ . \qquad \text{(D-28)}$$

According to Section VI, the constant number U_2 may be chosen arbitrarily within the bounds zero and one, see (39). Because of this reason, (D-27) represents an a priori estimate of the linearization error incurred by the outer solution.

LIST OF REFERENCES

1. Adams, E. W., "The Low and the High Prandtl Number Approaches for Heat Transfer in Laminar Flows of Incompressible Fluids with Constant Material Properties," Proc. Fourth U. S. Nat. Congr. Appl. Mech., ASME, 1962.

2. Adams, E. W., "Heat Transfer in Laminar Flow of Incompressible Fluids with $Pr \to 0$ and $Pr \to \infty$," NASA TN D-1527, 1963.

3. Adams, E. W., "A Class of Similar Solutions for the Velocity and the Temperature Boundary Layer in Planar or Axially Symmetric Channel Flow," Zeitsch.f.Flugwissensch., Vol. 11, 316-322, 1963.

4. Adams, E. W., "Gestaltaussagen für laminare, ebene, instationäre Mehrkomponenten-Grenzschichten mit veränderlichen Stoffeigenschaften," to be published.

5. Betz, A., "Zur Berechnung des Übergangs laminarer Grenzschichten in die Aussenströmung," 50 Jahre Grenzschichtforschung, 63-70, edit.H.Görtler and W. Tollmien, Braunschweig, 1955.

6. Blasius, H., "Grenzschichten in Flüssigkeiten mit kleiner Reibung," Z. Math.u. Phys., Vol. 56, 1, 1908, also NACA Tech. Memo. No. 1256.

7. Carslaw, H. S., and J. C. Jaeger, "Conduction of Heat in Solids," Oxford University Press, London, 2nd edit., 1959.

8. Collatz, L., "The Numerical Treatment of Differential Equations," Springer, 3rd edit., Berlin, 1959.

9. Donoughe, P. L. and J. N. B. Livingood, "Exact Solutions of Laminar-Boundary-Layer Equations with Constant Property Values for Porous Walls with Variable Temperature," NACA Tech. Rep. 1229, 1955.

10. Falkner, V. M., and S. W. Skan, "Some Approximate Solutions of the Boundary Layer Equations," Phil. Mag., Vol. 12, 865, 1931.

11. Fried, H., "Einige Verallgemeinerungen des Nagumo Westphal Abschätzungssatzes," Diplomarbeit, Universität Freiburg, 1964.

12. Geropp, D., "Näherungstheorie für kompressible laminare Grenzschichten mit zwei Formparametern für das Geschwindigkeitsprofil," Dissertation Techn. Hochschule Karlsruhe, 1963; also DVL Bericht 288, 1963.

13. Goldstein, S., "Modern Developments in Fluid Dynamics," Oxford University Press, London, Vol. 1, p. 150, 1938.

REFERENCES (Continued)

14. Goldstein, S., "On Laminar Boundary Layer Flow Near a Point of Separation," Quart. J. Mech. Appl. Math., Vol. 1, 43, 1948.

15. Goldstein, S. and J. M. Burgers, "Lectures on Fluid Mechanics," Interscience Publ., London and New York, 1960.

16. Görtler, H., "Ein Differenzenverfahren zur Berechnung laminarer Grenzschichten," Ing. Archiv, Vol. 16, 173-187, 1948.

17. Görtler, H., "Über die Lösung nichtlinearer partieller Differentialgleichungen vom Reibungsschichttypus," ZAMM, Vol. 30, 265-267, 1950.

18. Görtler, H., "A New Series for the Calculation of Steady Laminar Boundary Layer Flows," J. Math. Mech., Vol. 6, 1, 1957.

19. Görtler, H., "Zahlentafeln universeller Funktionen zur neuen Reihe für die Berechnung laminarer Grenzschichten," DVL Bericht 34, 1957.

20. Hartree, D. R. and J. R. Womersley, "A Method for the Numberical or Mechanical Solution of Certain Types of Partial Differential Equations," Proc. Roy. Soc. London, Series A., Vol. 101, 353-366, 1937.

21. Hartree, D. R., "The Solution of the Equation of the Laminar Boundary Layer for Schubauer's Observed Pressure Distribution for an Elliptic Cylinder," Brit. Aeron. Res. Council, R.u.M. 2427, 1949.

22. Howarth, L., "On the Calculation of Steady Flow in the Boundary Layer near the Surface of a Cylinder in a Stream," Brit. Aeron. Res. Council, ARC Rep. 1632, 1935.

23. Howarth, L., "Concerning the Effect of Compressibility on Laminar Boundary Layers and Their Separation," Proc. Roy. Soc. London, Series A, Vol. 194, 16-42, 1948.

24. Howarth, L., "Laminar Boundary Layers," Encyclopedia of Physics, Vol. VIII/1, 264-350, Springer, Berlin 1959.

25. Illingworth, C. R., "Steady Flow in the Laminar Boundary Layer of a Gas," Proc. Roy. Soc. London, Series A, Vol.199, 533-558, 1949.

26. von Kármán, T., "Über laminare und turbulente Reibung," ZAMM, Vol. 1, 233-252, 1921, also NACA Tech. Memo 1092, 1946.

27. von Kármán, T., and C. B. Millikan, "On the Theory of Laminar Boundary Layers Involving Separation," NACA Rep. 504, 1934.

28. Kosson, R. L., "An Approximate Solution for Laminar Boundary Layer Flow," AIAA Journal, Vol. 1, 1088-1096, 1963.

29. Krawczyk, R., "Über Differenzenverfahren bei parabolischen Differentialgleichungen," Arch. Rat. Mech. Anal., Vol. 13, 81-121, 1963.

30. Kwang-Tzu-Yang, "An Improved Integral Procedure for Compressible Laminar Boundary-Layer Analysis," J. Appl. Mech., Vol. 38, 9-20, 1961.

31. Kwang-Tzu-Yang, "On the Calculation of Unsteady Incompressible Laminar Boundary Layers over Arbitrary Cylinders," Dep. Mech. Engin., Univ. of Notre Dame, Tech. Note 62-21, 1962.

32. Lighthill, M. J., "Contributions to the Theory of Heat Transfer Through a Laminar Boundary Layer," Proc. Roy. Soc. London, Vol. 202, 359-377, 1950.

33. Mangler, W., "Ein Verfahren zur Berechnung der laminaren Reibungsschicht," Jahrb. d. deutschen Luftfahrtforsch., I, 18, 1941.

34. Mangler, W., "Die 'ähnlichen' Lösungen der Prandtlschen Grenzschichtgleichungen," ZAMM, Vol. 23, 241-251, 1943.

35. Mangler, W., "Zusammenhang zwischen ebenen und rotationssymmetrischen Grenzschichten in kompressiblen Flüssigkeiten," ZAMM, Vol. 28, 97-103, 1948.

36. Nagumo, M., "Note in Kansū Hōteisiki," No. 15, 1939 (in Japanese).

37. Nickel, K., "Einige Eigenschaften von Lösungen der Prandtlschen Grenzschicht Differentialgleichungen," Arch. Rat. Mech. Anal., Vol. 2, 1-31, 1958.

38. Nickel, K., "Parabolic Equations with Applications to Boundary Layer Theory, Partial Differential Equations and Continuum Mechanics," 319-330, edit. E. Langer, Univ. of Wisconsin Press, 1961.

39. Nickel, K., "Eine einfache Abschätzung für Grenzschichten," Ing. Arch., Vol. 31, 85-100, 1962.

40. Nickel, K., "Gestaltaussagen über Lösungen parabolischer Differentialgleichungen," Journal für die reine und angew. Math., Vol. 211, 78-94, 1962.

41. Nickel, K., "Die Prandtlschen Grenzschichtdifferentialgleichungen als asymptotischer Grenzfall der Navier-Stokesschen und der Eulerschen Differentialgleichungen," Arch. Rat. Mech. and Anal., Vol. 13, 1-14, 1963.

42. Nirenberg, L., "A Strong Maximum Principle for Parabolic Equations," Comm. Pure Appl. Math., Vol. 6, 167-177, 1953.

43. Pohlhausen, K., "Zur näherungsweisen Integration der Differentialgleichung der laminaren Reibungsschicht," ZAMM, Vol. 1, 252-268, 1921.

44. Prandtl, L., "Über Flüssigkeitsbewegungen bei sehr kleiner Reibung," Proc. Third Internat. Math. Congr., Heidelberg, 1904, also NACA Tech. Memo 452, 1928.

45. Prandtl., L., "The Mechanics of Viscous Fluids," Aerod. Theory III, 85, edit. W. F. Durand.

46. Riegels, F., and J. A. Zatt, "Zum Übergang von Grenzschichten in die ungestörte Strömung," Nachr. Akad. Wissensch. Göttingen, Math. Phys. Klasse, Heft 2, 1947.

47. Rheinboldt, W., "Über die äussere Randbedingung bei den Grenzschichtgleichungen," 50 Jahre Grenzschichtforschung, 328-333, edit. H. Görtler and W. Tollmien, Braunschweig, 1955.

48. Schlichting, H., "Boundary Layer Theory," McGraw-Hill Book Co. 4th edit., New York, 1960.

49. Schlichting H. and E. Truckenbrodt, "Aerodynamik des Flugzeugs," Vol. 1, Springer, Berlin 1959.

50. Smith, A. M. O., "Rapid Laminar Boundary-Layer Calculations by Piecewise Application of Similar Solutions," J. Aero. Sci., vol. 23, 901-912, 1956.

51. Smith, A. M. O., "Solution of Prandtl's Boundary-Layer Equations," Douglas Aircraft Co., Inc. Engin. Paper 1530, 1963.

52. Smith, A. M. O., and D. W. Clutter, "Solution of the Incompressible Laminar Boundary-Layer Equations," AIAA Journal, Vol. 1, 2062-2071, 1963.

53. Schönauer, W., "Die Lösung der Crocco'schen Grenzschichtdifferentialgleichung mit dem Differenzenverfahren für stationäre, laminare, inkompressible Strömungen, Dissertation," Tech. Hochsch. Karlsruhe, 1963.

54. Schönauer, W., "Ein Differenzenverfahren zur Lösung der Grenzschichtgleichung für stationäre, laminare, inkompressible Strömung," Ing. Arch., Vol. 33, 173-189, 1964.

55. Schröder, K., "Verwendung der Differenzenrechnung zur Berechnung der laminaren Grenzschicht," Math. Nachr., Vol. 4, 439, 1951.

56. Stewartson, K., "Correlated Incompressible and Compressible Boundary Layers," Proc. Roy. Soc. London, Series A, Vol. 200, 84-100, 1950.

57. Terrill, R. M., "Laminar Boundary-Layer Flow Near Separation with and Without Suction," Phil. Trans. Roy. Soc. London, Series A, No. 1022, Vol. 253, 55-100, 1960.

58. Terrill, R. M., "Comment on 'An Approximate Solution for Laminar Boundary Layer Flow'," AIAA Journal, Vol. 2, 587-588, 1964.

59. Tifford, A. N., "Heat Transfer and Frictional Effects in Laminar Boundary Layers, Part 4, Universal Series Solution," WADC Tech. Rep. 53-288, Part 4, 1954.

60. Tollmien, W., "Über das Verhalten einer Strömung längs einer Wand am äusseren Rand ihrer Reibungsschicht," Festschrift zum 60. Geburtstag von Albert Betz, AVA Göttingen, 218-224, 1945.

61. Töpfer, C., "Bemerkingen zu dem Aufsatz von H. Blasius, 'Grenzschichten in Flüssigkeiten mit kleiner Reibung'," Z.Math. Phys. vol. 60, 397, 1912.

62. Velte, W., "Eine Anwendung des Nirenbergschen Maximumprinzips für parabolische Differentialgleichungen in der Grenzschichttheorie," Arch. Rat. Mech. Anal., Vol. 5, 420-431, 1960.

63. Velte, W., "Bemerkungen über Randmaxima bei parabolischen Differentialoperatoren," ZAMM, Vol. 43, 421-423, 1963.

64. Velte, W., "Maximumneigenschaften temperaturabhängiger Grenzschichten," ZAMM, Vol., 43, 424-428, 1963.

65. Walz, A., "Anwehdungen des Energiesatzes von Wieghardt auf einparametrize Geschwindigkeitsprofile in laminaren Grenzschichten," Ing., Arch., Vol. 16, 243-248, 1948.

66. Walz, A., "Theorie und Praxis der Berechnung von Strömungsgrenzschichten," Habilitationsschrift Tech. Hochsch. Karlsruhe, 1957.

67. Walz, A., "Neue Anwendung des Prinzips der gemittelten Grenzschichtbedingunge nach von Kármán und Pohlhausen," Grenzschichtforschung, 368-376, edit. H. Görtler, Springer, 1958.

68. Westphal, H., "Zur Abschätzung der Lösungen nichtlinearer parabolischer Differentialgleichungen," Math.Z., Vol. 51, 690-695, 1949.

69. Whittaker, E. T. and G. N. Watson, "A Course of Modern Analysis," Cambridge Univ. Press, 4th edit., 1946.

70. Wieghardt, K., "Über einen Energiesatz zur Berechnung laminarer Grenzschichten," Ing. Arch., Vol. 16, 231-242, 1948.

71. Witting, H., "Verbesserung des Differenzenverfahrens von H. Görtler zur Berechnung laminarer Grenzschichten," ZAMP, Vol. 3, 376-397, 1953.

72. Witting, H., "Über die Instabilitäten der Prandtlschen Grenzschichtgleichungen, 50 Jahre Grenzschichtforschung," 334-342, edit. H. Görtler and W. Tollmien, Braunschweig, 1955.

"The aeronautical and space activities of the United States shall be conducted so as to contribute . . . to the expansion of human knowledge of phenomena in the atmosphere and space. The Administration shall provide for the widest practicable and appropriate dissemination of information concerning its activities and the results thereof."

—NATIONAL AERONAUTICS AND SPACE ACT OF 1958

NASA SCIENTIFIC AND TECHNICAL PUBLICATIONS

TECHNICAL REPORTS: Scientific and technical information considered important, complete, and a lasting contribution to existing knowledge.

TECHNICAL NOTES: Information less broad in scope but nevertheless of importance as a contribution to existing knowledge.

TECHNICAL MEMORANDUMS: Information receiving limited distribution because of preliminary data, security classification, or other reasons.

CONTRACTOR REPORTS: Technical information generated in connection with a NASA contract or grant and released under NASA auspices.

TECHNICAL TRANSLATIONS: Information published in a foreign language considered to merit NASA distribution in English.

TECHNICAL REPRINTS: Information derived from NASA activities and initially published in the form of journal articles.

SPECIAL PUBLICATIONS: Information derived from or of value to NASA activities but not necessarily reporting the results of individual NASA-programmed scientific efforts. Publications include conference proceedings, monographs, data compilations, handbooks, sourcebooks, and special bibliographies.

Details on the availability of these publications may be obtained from:

SCIENTIFIC AND TECHNICAL INFORMATION DIVISION

NATIONAL AERONAUTICS AND SPACE ADMINISTRATION

Washington, D.C. 20546